NASA TECHNICAL TRANSLATION NASA TT F-16626

A MATHEMATICAL MODEL FOR HEAT AND MATERIAL EXCHANGE IN BUBBLES

K. Kovansky

Translation of "Ein mathematisches Modell fuer den Waerme- und Stoffaustausch bei Blasen," Zurich, Eidgenoessische Technische Hochschule, 1968, 134 pages.

(NASA-TT-F-16626) A MATHEMATICAL MODEL FOR HEAT AND MATERIAL EXCHANGE IN BUBBLES (Kanner (Leo) Associates) 103 p HC $5.50 CSCI 20M

N76-11370

G3/34 Unclas 01528

NOV 1975
RECEIVED
NASA STI FACILITY
INPUT BRANCH

NATIONAL AERONAUTICS AND SPACE ADMINISTRATION
WASHINGTON, D.C. 20546 OCTOBER 1975

STANDARD TITLE PAGE

1. Report No. NASA TT F-16626	2. Government Accession No.	3. Recipient's Catalog No
4. Title and Subtitle A MATHEMATICAL MODEL FOR HEAT AND MATERIAL EXCHANGE IN BUBBLES		5. Report Date October 1975 6. Performing Organization Code
7. Author(s) K. Kovasky Eidgenoessische Technische Hochschule		8. Performing Organization Report No. 10. Work Unit No 11. Contract or Grant No. NASw-2790
9. Performing Organization Name and Address Leo Kanner Associates Redwood City, California 94063		13. Type of Report and Period Covered Translation
12. Sponsoring Agency Name and Address National Aeronautics and Space Administration, Washington, D.C. 20546		14. Sponsoring Agency Code

15. Supplementary Notes

Translation of "Ein mathematisches Modell fuer den Waerme- und Stoffaustausch bei Blasen," Zurich, Eidgenoessische Technische Hochschule, 1968, 134 pages.

16. Abstract

A mathematical model is formulated for heat and material exchange in bubbles which form at a nozzle and then rise in an otherwise still liquid. The hydrodynamics of the flow are assumed to be known, and their effect as a result of combined laminar and turbulent surface renewal is taken into account. The exchange process is considered in three stages: (1) bubble formation, (2) transition period, and (3) quasi-stationary bubble rise. A mathematical solution is derived for the first and third stage on the basis of similar assumptions, and indications as to how to estimate the exchange process in the transition period are presented. In the absence of theoretical or experimental results regarding bubble formation with which this theory might be compared, and in view of the fact that a numerical solution would involve complicated computer programming, [cont.]

17. Key Words (Selected by Author(s))	18. Distribution Statement Unclassified-Unlimited		
19. Security Classif. (of this report) Unclassified	20. Security Classif. (of this page) Unclassified	21. No. of Pages	22. Price

NASA-HQ

TITLE PAGE [cont.]

16. solutions for rising bubbles are worked out only for the following cases: ellipsoids of revolution in potential flow, spherical bubbles rising in tubes, and large spherical caps. Results are compared with experimental results established in the literature for the absorption of carbon dioxide bubbles in water, and with theoretical solutions for rotationally symmetrical bodies in laminar flow. The proposed model is considered especially suitable for the description of surface turbulence, which is known to be capable of significantly increasing material exchange. Two theoretical possibilities are suggested for determining the intensity of the surface renewal caused by surface turbulence by means of this theory.

To my parents,
in gratitude for the
many sacrifices which
they made for us.

FOREWORD

I conducted this study as the Institute for Caloric Apparatus, Low-Temperature Technology and Research Techniques. I wish to express my sincere thanks to the director of the Institute, Prof. Dr. P. Grassmann, for his support. His extensive supervision and his wealth of experience in scientific research made my work a great deal easier.

I wish particularly to acknowledge the efforts of my co-advisor, Prof. Dr. H. Thomann, whose critical comments stimulated me to make several valuable additions to the text.

I am also grateful to Prof. O. Zweifel for his support and Dr. J. Waldvogel, who greatly aided me in solving a number of mathematical problems, as well as to my colleagues at the Eidgenoessische Technische Hochschule for their very helpful discussions and encouragement.

Finally, I wish to thank Mrs. D. Szerenyi for her help in preparing the manuscript.

TABLE OF CONTENTS

		Page
1.	Introduction	1
1.1.	Purpose of Study	1
1.2.	Problem	1
1.3.	Note on the Contents of Each Chapter	2
1.4.	Simplifying Assumptions	2
1.5.	Model of Laminar and Turbulent Surface Renewal	4
Part I:	Derivation of the Theoretical Relationships	11
2.	Bubble Formation	11
2.1.	The Age Distribution Function of Turbulent Vortices	11
2.2.	Age Distribution Function of Laminar Surface Renewal in Bubble Formation	14
2.3.	Calculation of the Mass Transfer Coefficient for Bubble Formation as a Function of Time	16
3.	Bubble Rise	19
3.1.	Age Distribution Function of Laminar Surface Renewal for Bubble Rise	19
3.2.	Calculation of the Mass Transfer Coefficient for Bubble Rise as a Function of Location on the Bubble Surface	23
4.	Comparison of the Relationships Derived for Bubble Rise with Other Theoretical Solutions	27
Part II:	Calculation and Comparison of Results with Other Theoretical and Experimental Results	32
5.	Ellipsoidal and Spherical Bubbles	32
5.1.	Spheroids in Potential Flow	32
5.2.	Spherical or Spheroidal Bubbles and Drops with Complete Internal Circulation	35
6.	Cylindrical Bubbles Rising in Vertical Tubes ("Tube Bubbles")	40
7.	Large Spherical Cap Bubbles	42
8.	Comparison of Results Derived in This Study for Bubbles in Steady-State Rise with Some Experimental Results Known from the Literature and with Other Theoretical Solutions	45

Page

9. Theoretical Results Concerning the Influence of Turbulence on Mass Transfer for Bubbles in Steady-State Rise 49

10. Appendix 55

10.1. Some Properties of the System of Equations (3.2-14) 55
10.2. An Approximation Formula for $B(S,\omega)$ for Small Values of S 58
10.3. Identity of the Theoretical Solutions Given b Beek and Kramers [18] and by Lochiel and Calderbank [19] for Mass Transfer at a Sliding Boundary Surface 62

11. A Comment on Surface Turbulence 63

Summary 65

Diagrams and Tables 67

References 87

About the Author 91

LIST OF SYMBOLS

For simplicity, the dimensions are given in cm, sec, grams (mass) and °C. The equations used are uniform in terms of dimension so that a different system of measurement could also be used.

Symbol	Definition	Dimension
a	1.) The semiaxis of a spheroid parallel to the direction of flow	cm
	2.) Tube diameter	cm
B	Dimensionless mass-transfer parameter ($Sh/Pe^{\frac{1}{2}}$)	--
$\overline{B}$	Value of B averaged over the bubble surface	--
b	1.) Semiaxis of a spheroid normal to the direction of flow	cm
	2.) Cross-sectional diameter of a spherical cap bubble	cm
c	Concentration	$g\ cm^{-3}$
Δc	Difference in concentration between the interface and the liquid core (liquid outside the concentration boundary layer)	$g\ cm^{-3}$
D	Diffusivity	$cm^2\ s^{-1}$
d_B	Diameter of a sphere of equal volume (equivalent diameter)	cm
d_B^*	d_B in dimensionless form (d_B/l_c)	--
E	Eccentricity of a spheroid (b/a) or a spherical cap (b/h)	--
F	Bubble surface area	cm^2
F*	Dimensionless bubble surface area (F/l_c^2)	--
F'	Derivative of F after time t	$cm^2\ s^{-1}$
$\dot{f}$	Surface current density defined by eqn. (3.1-2)	s^{-1}
F_D	Cross-section of nozzle	cm^2

Symbol	Definition	Dimension
Fr	Froud's number ($v_c^2/g.l_c$)	--
g	Gravitational acceleration	$cm.s^{-2}$
h	Height of a spherical cap	cm
I	Quantity defined by eqn. (3.2-2)	s
Int	Function defined by eqn. (2.3-7)	$s^{-\frac{1}{2}}$
J	I in dimensionless form ($I.v_c/l_c$)	--
k	Factor used in calculating the velocity distribution of a spheroid in potential flow (see eqn. 5.1-2)	--
l	Length of a bubble rising in a tube	cm
l_c	Characteristic length	cm
M	Dimensionless quantity defined by eqn. (7-1)	--
$\dot{m}$	Material flow of the gas streaming through a nozzle	$g\ s^{-1}$
Nu	Nusselt number ($\alpha.l_c/\lambda$); λ = thermal conductivity	--
Pe	Peclet number ($v_c.l_c/D$) = Re.Sc	--
Pr	Prandtl number (ν/a); a = diffusivity	--
R	Dimensionless radius in spherical coordinates (r/l_c)	--
Re	Reynolds number ($v_c.l_c/\nu$)	--
r	1.) Radius in spherical coordinates	cm
	2.) Radius of curvature of a spherical cap or the upper part of a tube bubble	cm
S	1.) Dimensionless arc length (σ/l_c)	--
	2.) Function defined by eqn. (2.3-2)	--
s	Surface current density for turbulent surface renewal (surface renewal rate)	s^{-1}

Symbol	Definition	Dimension
Sh	Sherwood number ($\beta l_c/D$)	--
Sc	Schmidt number (ν/D)	--
t	Time (measured from the start of bubble formation)	s
t*	Point in time at which a "large surface element" is formed (cf. Fig. 1.5-1)	s
t_c	Characteristic time	s
t_B	Time of bubble formation	s
u	Mathematical auxiliary variable defined by eqn. (2.3-5)	$s^{\frac{1}{2}}$
V	1.) Dimensionless velocity (v/v_c)	--
	2.) Volume	cm^3
V*	Dimensionless volume (V/l_c^3)	--
v	Velocity	$cm\ s^{-1}$
v_B	Velocity of the rise or fall of a bubble or drop	$cm\ s^{-1}$
v_c	Characteristic velocity	$cm\ s^{-1}$
X	x in dimensionless form (x/l_c)	--
x	Cylindrical ccordinate (parallel to the axis)	cm
Y	y in dimensionless form (y/l_c)	--
y	Cylindrical coordinate (normal to the axis)	cm
α	1.) Heat transfer coefficient	$g\ s^{-3}\ {}^oC^{-1}$
	2.) Factor in eqn. (5.2-2)	--
β	Mass transfer coefficient (relative to Δc)	$cm\ s^{-1}$
$\bar{\beta}$	Mass transfer coefficient averaged over the bubble surface (relative to Δc)	$cm\ s^{-1}$

Symbol	Definition	Dimension
δ	Dirac function	--
δ_c	Thickness of concentration boundary layer	cm
ζ	Age distribution function of laminar surface renewal for bubbles in steady-state rise	s^{-1}
θ	1.) Semi-front clearance angle of a spherical cap	--
	2.) Angle of a spheroid acc. to Fig. 5.1-1	--
	3.) τ^* in dimensionless form ($\tau^* \cdot v_\infty / l_c$)	--
ϑ	Temperature	^oC
μ	Viscosity	$g\ cm^{-1} s^{-1}$
ν	Kinematic viscosity	$cm^2\ s^{-1}$
ξ	Mathematical auxiliary variable defined by eqn. (2.3-4)	$s^{\frac{1}{2}}$
ρ	Density	$g\ cm^{-3}$
σ	1.) Arc length	cm
	2.) Surface tension	$g\ s^{-2}$
τ	Age of a small surface element (cf. Fig. 1.5-1)	s
τ^*	Age of a large surface element (cf. Fig. 1.5-1)	s
ϕ	Age distribution function of turbulent vortices	s^{-1}
ϕ^*	Continuous portion of ϕ	s^{-1}
φ	Polar angle in spherical coordinates	--
ψ	Age distribution function of laminar surface renewal in bubble formation	s^{-1}
Ω	s in dimensionless form in bubble formation ($s \cdot t_c$)	--

Symbol	Definition	Dimension
ω	s in dimensionless form in bubble rise ($s \cdot l_c / v_c$)	--

Subscripts

g	gas phase
fl	liquid phase
i	within the bubble or drop
a	outside the bubble or drop
B	"bubble"
D	"nozzle"
1	indicates that a variable is dimensionless (only in Chap. 2.3 and 4)

A MATHEMATICAL MODEL FOR HEAT AND MATERIAL EXCHANGE IN BUBBLES

K. Kovansky
Eidgenoessische Technische Hochschule

1. Introduction

1.1. Purpose of Study

/9*

Numerous types of contact apparatus in which gas bubbles are made to rise through a liquid medium (e.g. sieve trays, bubble trays) are used in the chemical industry. Many factors which influence mass and heat transfer in such apparatus are quite complicated and are often difficult to deal with in theoretical terms. In most cases, an exact theoretical solution is rendered impossible by the extremely unsteady-state and irregular nature of the process, and the researcher must resort to simplified computational methods based on suitable mean values. Since such methods are, by their very natures, uncertain, it is vital that they be supported experimentally, which is why experiments in this field will always play a decisive role. On the other hand, it is desirable in such cases to tentatively construct idealized theoretical models, for they often provide information which is helpful in clarifying complex relationships and identifying the factors which influence a particular phenomenon. This paper deals with an experiment of this type, the primary object being to determine how heat and mass transfer are affected by hydrodynamic conditions. The hydrodynamics are assumed to be known, and no attempt is made to determine the factors which influence them.

1.2. Problem

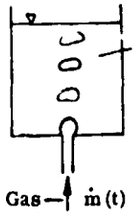

A simple contact apparatus is assumed, consisting of a vessle filled with a liquid, into which the gas phase is infected through a nozzle (see Figure). Bubbles are formed which rise in succession through the liquid. The object is to determine mass and heat transfer relative to time during the "lifetime" of the bubble. Since Prof. Grassmann[1] has already directed several experimental research studies in which apparatus of this type was used [46-50], this investigation can be considered a theoretical supplement to these

/10

1) Director of the Institute for Caloric Apparatus, Low-Temperature Technology and Research Techniques. ETH Zurich.

* Numbers in the margin indicate pagination in the foreign text.

studies, although it is completely independent of them, and the measuring instruments and idealizations employed do not permit a direct comparison of the results.

1.3. Note on the Contents of Each Caapter

The Chapters and Sub-Chapters are numbered by the decimal system and are always referred to with the word "Chapter" and the appropriate decimal number. Equations and Figures bear the Chapter number and a sequential number set off by a hyphen; the sequential numbers begin again from one with each new Chapter (e.g. eqn. (5.2-4)). Within a Chapter, only the last number is cited; otherwise the complete number is given. The results of computer calculations are given in 20 diagrams and tables at the end of the paper. They are also numbered consecutively and are referred to with circled numbers (e.g. "Diagram (16)").

Fundamental assumptions and the mathematical structure of the model are explained in Chapters 1.4 and 1.5, which follow. Chapter 1.5 also presents the most important results of the mathematical derivations in broad outline, and organizes them in such a way that their physical significance becomes clear. The mathematical derivations themselves are given in Chapters 2 and 3. The reader who is less interested in the mathematical aspects than in the actual results may skip these Chapters; he should not, /11
however, omit the relatively short Chapter 4, since in this Chapter the solution proposed for a bubble in steady-state rise is compared with other known theoretical solutions, and several characteristic features of such solutions emerge. A discussion is also presented in this Chapter of the conditions under which the assumptions made are valid. Therefore, anyone who takes the trouble to follow the often complicated mathematical operations need not spend time wondering under what conditions the assumptions are true when he encounters an apparently unsubstantiated hypothesis. But if the reader wishes to begin with a clear picture of the physical reality "hidden" behind the mathematical formulae, he is encouraged to read Chapter 4 immediately after the Introduction.

In the second part of the paper (Chapters 5-9), the results of the computations are presented and compared with other theoretical and experimental results. Occasionally, concrete computational examples are given in place of dimensionless functions in order to better illustrate the physical significance of theoretical results. Because the comparisons and discussions are often speculative and rather long, the reader who is interested primarily in the results of the computer calculations should note that these results are discussed in Chapters 5.1, 6 and 7.

1.4. Simplifying Assumptions

It is assumed that the bubbles form periodically at the nozzle

and neither coalesce nor under go radical, irregular changes in shape while rising[2]. It is also assumed that they are axially symmetrical when rising and that the transfer process during this period is quasi-steady state, i.e. can be calculated as if the instantaneous shape, velocity profile and concentration distribution were steady-state. /12

It is further assumed that the time functions (Fig. 1) describing the hydrodynamic conditions are known. In the diagram, m represents the material flow of the gas injected through the nozzle, F is the surface area of the bubble and s_g and s_{fl} the surface renewal rate (dimension $cm^2/(cm^2 \cdot s) = s^{-1}$, which is intended to characterize the gas and liquid turbulance, respectively)[3]. The lifetime of the bubble is divided into three stages: (1) bubble formation, (2) transition period, and (3) bubble rise. /13

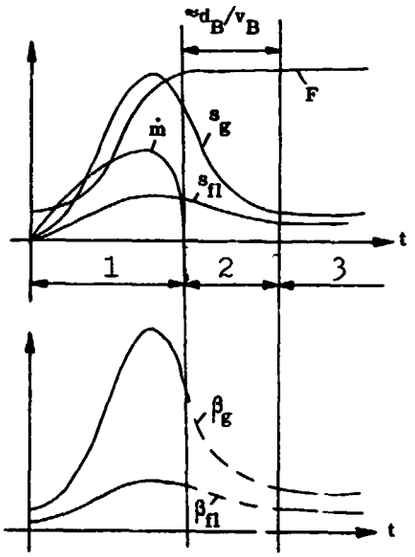

Fig. 1.4-1. Curves of some important parameters during bubble lifetime.
1 - bubble formation
2 - transition period
3 - bubble rise

The transition period is the time required after the bubble leaves the nozzle for the velocity profile, the turbulence surrounding and within the bubble, and mass transfer to attain the steady-state and quasi-steady state value. This corresponds roughly to the time required for the bubble to rise to the height of its own equivalent diameter d_B [51].

Besides the time function shown in the Figure, the bubble shape and the velocity profile at the interface must be known for each moment of the bubble rise. These parameters may, for example, be supplied by the functions

$$y(\delta) \text{ and } v(\delta)$$

(cf. Fig. 2), where δ represents the arc length measured from the front stagnation point. The bubble surface is thus assumed to slip freely through the liquid medium.

It is the object of the calculation to determine the gas and liquid heat- and mass-transfer coefficients $\alpha_g, \alpha_{fl}, \beta_g$, and β_{fl} as /14

2) For large gas quantitites $\dot{m}(t)$, bubbles are irregular, fluctuate in shape and often coalesce (viz. [4, 46, 48, 50]).

3) We shall not delve into when and to what ex nt this turbulence can be a factor. But it is known that in es when the resistance is from the gas phase, turbulence from the vorticity of the inflowing gas increases transfer so greatly that most transfer is during bubble formation (up to 85%, according to [22]); therefore turbulence must be considered.

functions of time . If these values are known, the entire transfer process can be calculated from the temperature and concentration of the liquid (assumed to be constant with respect to time and place) and the known temperature and concentration of the gas flowing through the nozzle.

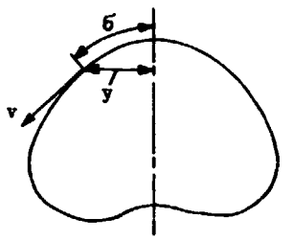

Fig. 1.4-2. Schematized shape of a bubble in steady-state rise.

From now on we shall consider only mass transfer, since Sh and Sc can be readily replaced by Nu and Pr in the equations derived. Also, because the equations are valid for both the gas and liquid phase, when the appropriate diffusivity and surface renewal rate are inserted, the phase in question need no longer be specified, and the symbols D, s and β need no subscripts.

Another simplifying assumption is that mass transfer is accompanied by the exchange of only one component and no chemical reactions[4].

A computational technique is derived only for bubble formation and bubble rise; the mass-transfer coefficient profile during the transition period can be easily calculated by taking the length of this period as d_B/v_B (cf. broken lines in Fig. 1, below).

1.5. Model of Laminar and Turbulent Surface Renewal /15

We speak of surface renewal when a new surface is produced by the movement of the bubble surface or by turbulent vortices. The first case is called "laminar," the second case "turbulent" surface renewal.

Taking a spherical bubble as an example, it is easy to see that laminar renewal can be by two means: (a) the sphere can grow with no displacement of the center, or (b) the sphere can be displaced with no growth, as it glides smoothly through the liquid. In this case new surface is continuously produced on the upper part and "old" surface is continuously lost from the lower.

While in the general case, both factors will operate at the same time (the sphere grows as it is displaced), we make the following simplifying assumption for our calculations:

---

4) It is not necessary that this restriction be observed. It is necessary only that chemical reactions or the transfer of other components have no appreciable effect on the transfer of the component of interest. The question of when this is true and when it is not is not within the scope of this study.

For laminar surface renewal, only the growth of the surface is taken into consideration while the bubble is forming, but only the slipping of the surface through the medium while the bubble is rising[5].

Let us imagine turbulent surface renewal combined with this laminar surface renewal, caused by turbulent vortices advancing to the surface and replacing old liquid and gas components. According to this model, an element dF of the bubble surface will consist of smaller elements of age $\tau_1^*, \tau_2^*, \tau_3^*, \ldots$ (cf. Fig. 1) as a result of laminar surface renewal. If turbulent surface renewal is added to this, the effect might well be that each of the above elements will consist of still smaller elements of age $\tau_1, \tau_2, \tau_3, \ldots$. /16

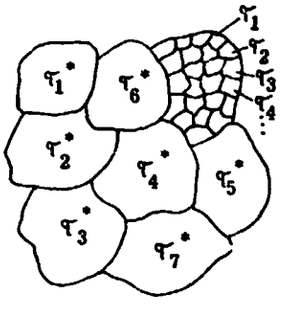

Fig. 1.5-1. An element dF of the bubble surface.

From now on, the small elements of age $\tau_1, \tau_2, \tau_3, \ldots$ will be designated as "smaller elements," "turbulent vortices," or simply as "vortices," while the elements of age $\tau_1^*, \tau_2^*, \tau_3^*, \ldots$ will be called "larger elements"[6] and the entire structure shown in Fig. 1 referred to as "surface element dF."

Within a larger element the inequality

$$\tau^* \geqslant \tau \qquad (1.5\text{-}1)$$

is true, since a larger element cannot be renewed by turbulent vortices until it has been "born"[6]. On the other hand, a larger element can never be older than the bubble itself, so

$$t \geqslant \tau^* \qquad (1.5\text{-}2)$$ /17

This inequality is meaningful only in the case of bubble formation, however, because t cannot be a factor in bubble rise, which is assumed to be steady-state.

---

5) Since the bubble rise is considered a quasi-steady state process, a slow growth or shrinking of the bubble would be entirely acceptable within the framework of our model.

6) The association of the larger elements with laminar renewal and the smaller elements with turbulent renewal is more or less arbitrary. The result should be the same if we imagined the situation as reversed, although we did not perform tests to make sure due to the complicated mathematical derivations involved.

We shall now summarize briefly the most important definitions and mathematical results so that the reader may better understand the structure of our model. The mathematical derivations themselves may be found in Chapters 2 and 3 as well as in the Appendix (Chapter 10).

Looking at Fig. 1, if we let the number of smaller elements within a larger element tend to infinity, the age distribution of the smaller elements can be characterized by an age distribution function ϕ, which is determined solely by the time curve of the turbulent surface renewal s(t). It is dependent on time t and the age of the larger element τ^*, as well as on τ, and is defined as follows (the dependence on t will be explained later in more detail):

$\phi(\tau, \tau^*, t)\, d\tau$ is the surface component of those turbulent vortices within a larger element (as in Fig. 1) which have an age between τ and $\tau + d\tau$.

From the derivations in Chapter 2.1, we have

$$\phi(\tau,\tau^*,t) = s(t-\tau)\cdot \exp\left\{-\int_{t-\tau}^{t} s(t)\,dt\right\} + \exp\left\{-\int_{t-\tau^*}^{t} s(t)\,dt\right\} \cdot \delta(\tau-\tau^*) \quad 7) \qquad (1.5\text{-}3)$$

where the range of validity is given by inequalities (1) and (2). /18
Of course, the property characteristic of any distribution function

$$\int_{\tau=0}^{\bar{\tau}^*} \phi(\tau,\tau^*,t)\,d\tau = 1 \qquad (1.5\text{-}3a)$$

is true, regardless of the values of τ^* and t. The Dirac break at the upper limit of this integral must be included in the integral. To better understand the rather complex function (3), it is helpful to regard ϕ as a function only of τ and t, where τ^* is only a parameter, since the dependence on τ^* is relatively simple. τ^* appears only in the second term, and this term is a break only

---

7) To clarify the meaning of $\delta(\tau-\tau^*)$: The Dirac function $\delta(\tau)$ indicates a break at $\tau = 0$, so $\delta(\tau-\tau^*)$ indicates a break at the point where $\tau - \tau^* = 0$, i.e. where $\tau = \tau^*$. This condition should be met along a straight line in the τ-t coordinate system when τ and t are the independent variables and τ^* is regarded as the parameter (see Fig. 2.1-1); but the meaning of the expression is better illustrated by eqn. (4).

when τ has its maximum value, i.e. when $\tau = \tau^*$, and encompasses that part of the larger element (see Fig. 1) which has not been renewed by turbulent vortices. This property is more apparent when s = const, because then (ignoring inequality (2)) ϕ is dependent on t and is expressed more simply as

$$\phi(\tau,\tau^*) = se^{-s\tau} + e^{-s\tau^*} \cdot \delta(\tau - \tau^*) \qquad (1.5\text{-}4)$$

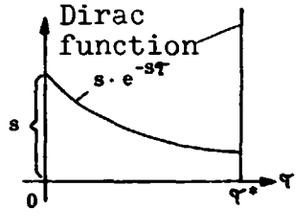

Fig. 1.5-2. The function $\phi(\tau,\tau^*)$.

This function is shown in Fig. 2 for a given τ^*. We can see at once that no clear picture could be obtained by representing $\phi(\tau,\tau^*)$ as an area on the $\tau - \tau^*$ plane due to its simple dependence on τ^*. /19

The dependence of the function ϕ on t is determined by the fact that the previous "renewal history" is the only decisive factor in the age distribution of the vortices at a given moment t; i.e. only that part of the given time function s(t') which lies between t' = 0 and t' = t. To economize on symbols, no distinction is made between t' as the consecutive variable and t as the given point in time, which is why, for example, t appears as both the variable of integration and the integration limit in eqn. (3).

The dependence of ϕ on τ^* is determined by the fact that surface renewal s(t') could affect the larger element only in the time interval $t - \tau^* \leqslant t' \leqslant t$.

It is interesting to note in eqn. (3) that the functional relationship between ϕ and τ^* is simpler than that between ϕ and t, since t influences the Dirac discontinuity only at the end of the spectrum. This property can be interpreted as follows: The effect of changes in s with time on the function ϕ is more clearly expressed in the dependence of ϕ on t than on τ^*. This can be seen in eqn. (4), where s does not change with time and ϕ is dependent on t in a very simple way, i.e. to the extent that τ^* can assume no value greater than t (age of entire bubble) in inequality (2).

As the bubble rises, t can play no further role since conditions were assumed to be steady-state. In this case bubble age must be considered infinite, i.e. t must be set equal to ∞ in inequality (2).

If we let the number of larger elements within surface element dF tend to infinity (cf. Fig. 1), their age distribution can also be characterized by an age distribution function. In the case of bubble formation, this function is determined by the function

F(t) (cf. Fig. 1.4-2) and is designated as $\Psi(t,\tau^*)$. In the case of bubble rise, however, it is given only by the functions $y(\delta)$ and $v(\delta)$ (cf. Fig. 1.4-2) and is designated as $\zeta(\delta,\tau^*)$. As these notations show, Ψ will be a function of place, and ζ a function of time. The mathematical formulae for $\Psi(t,\tau^*)$ are derived in Chapter 2.2, those for $\zeta(\delta,\tau^*)$ in Chap. 3.1; only the definitions of the two functions will be given here: /20

$\Psi(t,\tau^*)$ or $\zeta(\delta,\tau^*)\,d\tau^*$ is the surface component of those larger elements within dF (as in Fig. 1) with an age between τ^* and $\tau^* + d\tau^*$.

Of course, the equation characteristic of distribution functions still applies:

$$\int_0^t \psi(t,\tau^*)\,d\tau^* \equiv \int_{\tau_0^*}^{\infty} \zeta(\delta,\tau^*) \equiv 1 \qquad (1.5\text{-}4a)$$

The reader may not yet entirely understand the limits of these integrals, but they are given by the mathematical derivations in the aforementioned Chapters and encompass the area over which τ^* is distributed. (An additional comment on τ^* follows.) For reasons similar to those for the function ϕ, the function Ψ is also characterized by a Dirac break at the upper limit of the integral in eqn. (4a), which must be included in the integral (cf. eqn. (2.2-2)).

It is assumed that diffusion into a turbulent vortex occurs in the same manner as unidimensional unsteady-state diffusion into an infinite quiescent medium. In this case the diffusion equation assumes the form

$$\frac{\partial c}{\partial \tau} = D\,\frac{\partial^2 c}{\partial z^2} \qquad (1.5\text{-}4b)$$

where z designates the coordinate normal to the interface. The upper and lower limits are as follows: /21

$$\tau = 0 \quad \begin{cases} c = c_\infty & \text{für} \quad z \neq 0 \\ c = c_g & \text{für} \quad z = 0 \end{cases}$$

$$\tau > 0 \quad \begin{cases} c = c_\infty & \text{für} \quad z = \infty \\ c = c_g & \text{für} \quad z = 0 \end{cases}$$

where c_i and c_∞ are the constant concentrations of the diffusing component at the interface and at infinity, respectively. This problem is solved to yield the instantaneous mass transfer coefficient of the turbulent vortex (see Higbie [52]).

$$\beta' = \sqrt{\frac{D}{\pi\tau}} \qquad (1.5\text{-}5)$$

By taking the average of this expression first over all the vortices within a larger element and then over all the larger elements within the surface element dF (cf. Fig. 1), we obtain the mean mass transfer coefficient at surface element dF. This two-step operation yields the following expressions for bubble formation and bubble rise:

a) Bubble formation

$$\beta(t) = \int_{\tau^*=0}^{t} \left[\int_{\tau=0}^{\tau^*} \sqrt{\frac{D}{\pi\tau}}\, \phi(\tau, \tau^*, t)\, d\tau \right] \psi(t, \tau^*)\, d\tau^* \qquad (1.5\text{-}6)$$

b) Bubble rise

$$\beta(\sigma) = \int_{\tau^*=\tau_0^*}^{\infty} \left[\int_{\tau=0}^{\tau^*} \sqrt{\frac{D}{\pi\tau}}\, \phi(\tau, \tau^*)\, d\tau \right] \zeta(\sigma, \tau^*)\, d\tau^* \qquad (1.5\text{-}7)$$

The expressions enclosed by brackets correspond to the mean taken over all the smaller elements within a larger element of age τ^* (mean taken over τ), while bubble formation for ϕ requires eqn. (3) and bubble rise, eqn. (4)[8]. In both cases the outer integral corresponds to a mean taken over all larger elements within dF (cf. Fig. 1). /22

As these equations show, β is dependent only on bubble age t during bubble formation, and only on the location given by σ as the bubble rises. In eqn. (7) the lower limit of the outer integral is not zero, because at certain points on the bubble all the larger elements must have an age of at least τ^*, which can be determined for a given σ from the functions $y(\sigma)$ and $v(\sigma)$. In Chap. 2.3 and 3.2 it is shown how these equations can be evaluated when D, F(t), s(t), $y(\sigma)$ and $v(\sigma)$ are known. If we choose a characteristic time and a characteristic length for bubble formation, or a characteristic length and a characteristic velocity for bubble rise, then eqn. (6) and (7) lead to dimensionless functions with the following structure:

---

8) Mass transfer is steady-state during bubble rise (s = const.).

a) Bubble formation

$$B(\Theta') = \frac{Sh(\Theta')}{Pe^{1/2}} = \frac{\frac{\beta(t')\,l_c}{D}}{\left(\frac{l_c^2}{D \cdot t_c}\right)^{1/2}} = f\left\{ F^*(\Theta), \Omega(\Theta), \Theta' \right\} \qquad (1.5\text{-}8)$$

where $\Theta = t/t_c$; $\Theta' = t'/t_c$; t' = point in time for which β is calculated

$$F^*(\Theta) = \frac{F(t)}{l_c^2}$$

$$\Omega(\Theta) = t_c \cdot s(t) \qquad (1.5\text{-}9)$$

b) Bubble rise /23

$$B(S') = \frac{Sh(S')}{Pe^{1/2}} = \frac{\frac{\beta(\sigma')\,l_c}{D}}{\left(\frac{v_c\, l_c}{D}\right)^{1/2}} = f\left\{ Y(S), V(S), \omega, S' \right\} \qquad (1.5\text{-}10)$$

where $S = \sigma/l_c$; $Y = y/l_c$; $V = v/v_c$;

$S' = \sigma'/l_c$ σ' = place where β is calculated

$$\omega = \sqrt{\frac{s \cdot l_c}{v_c}} \qquad (1.5\text{-}11)$$

The functions on the right-hand side of eqn. (8) and (10) are very complicated integral expressions, which can be solved in general form only by computer. Since they are not particularly suitable for numerical evaluation, they call for rather extensive programming work and, under certain conditions, substantial calculating times[9]. Since neither theoretical nor experimental results could be found for bubble formation with which eqn. (8) could be compared, a program was formulated only for eqn. (10). This program is formulated in such a way that the dimensionless bubble shape and velocity distribution need not be entered as a function of arc length S -- which could be very inconvenient -- but either in polar or cylindrical coordinates. This is mentioned so that the reader will clearly understand the preparations for the calculation of special cases in Chap. 5.1, 6 and 7. From eqn. (10), it can also be proved that

9) Calculations were performed on a CDC 1064-A computer.

$$\left(\frac{\partial B(s)}{\partial \omega}\right)_{\omega=0} \equiv 0 \qquad (1.5\text{-}12)$$

(see proof in Chap. 10.1). The significance of this property is discussed in detail in Chap. 9.

Part I /25

Derivation of the Theoretical Relationships

2. Bubble Formation[1] /27

2.1. The Age Distribution Function of Turbulent Vortices

We are given the surface renewal rate as a function of time s(t) and the point in time t* at which a large element (cf. Fig. 1.5-1) is formed. The object is to find the age distribution function of the small surface elements at time t. In this case the age of the large element is

$$\tau^* = t - t^* \qquad (2.1\text{-}1)$$

At the instant of its "birth" ($t = t^*$), each small element is of zero age, i.e. the function ϕ must equal the Dirac function:

$$\phi(\tau, t^*, t=t^*) \equiv \delta(\tau) \qquad 2) \qquad (2.1\text{-}2)$$

It is clear that the Dirac function will form a part of the age distribution even when $t > t^*$, since a finite component a of the large element will always be of age τ^*, specifically that component which was not renewed by turbulent vortices by time t. But this component is continuously diminished by turbulent surface renewal, which can be described by the relation

$$da = - s(t)\, a\, dt \qquad (2.1\text{-}3)$$

Integrating this equation from t* to t, we have /28

$$a = \exp\left\{ - \int_{t^*}^{t} s(t)\, dt \right\} \qquad (2.1\text{-}4)$$

---

1) Although this study is not concerned with the hydrodynamics of bubble formation, reference is made to several papers dealing with this problem [4a, 22, 25].

2) $\phi(\tau, t^*, t)$ is used instead of $\phi(\tau, \tau^*, t)$ for clarity; regarding $\delta(\tau)$, cf. footnote to eqn. (1.5-3).

Designating the constant component of function ϕ as ϕ^*, we may write

$$\phi(\tau,\tau^*,t) = \phi^*(\tau,\tau^*,t) + \exp\left\{-\int_{t^*}^{t} s(t)\,dt\right\}\delta(\tau-\tau^*) \qquad 3)$$

(2.1-5)

If ϕ is integrated for given values of t* and t with respect to τ from 0 to t - t*, the result must by definition be one (the Dirac function for $\tau = \tau^* = t - t^*$ must be included in the integral). This yields the equation

$$\int_0^{t-t^*} \phi(\tau,t^*,t)\,d\tau = 1 - \exp\left\{-\int_{t^*}^{t} s(t)\,dt\right\} \qquad (2.1\text{-}6)$$

At time t the surface component of the vortices with age between τ and $\tau + d\tau$ is $\phi^*(\tau,t^*,t)\,d\tau$.

At time t - dt, the component of vortices with age between $\tau - d\tau$ and τ is $\phi^*(\tau - d\tau,t^*,t - dt)\,d\tau$.

If we now specify that $dt = d\tau$, an equal number of vortices are of age between τ and $\tau + d\tau$ at time t as between $\tau - d\tau$ and τ at time t - dt, minus those vortices which were replaced by new ones during the time elapsed. We may therefore write

$$\phi^*(\tau,t^*,t)d\tau = \phi^*(\tau-d\tau,t^*,t-dt)\,d\tau - s(t-dt)\left[\phi^*(\tau-d\tau,t^*,t-dt)d\tau\right]d\tau$$

/29

Using partial derivatives and dividing by $d\tau$, we have

$$\phi^*(\tau,t^*,t) = \phi^*(\tau,t^*,t) - \phi_t^*(\tau,t^*,t)d\tau - \phi_\tau^*(\tau,t^*,t)d\tau -$$

$$- \left[s(t) - s_t(t)d\tau\right]\left[\phi^*(\tau,t^*.t) - \phi_t^*(\tau,t^*,t)d\tau - \phi_\tau^*(\tau,t^*,t)d\tau\right]d\tau$$

which after the elimination of higher order terms and arguments can be reduced to the following simple form:

$$\boxed{\phi_t^* + \phi_\tau^* = -s(t)\,\phi^*} \qquad (2.1\text{-}7)$$

Using eqn. (6), the solution of this equation is found to be[4)]

---

3) Regarding $\delta(\tau - \tau^*)$, cf. footnote to eqn. (1.5-3).

4) The differential equation was solved by Dr. J. Waldvogel.

$$\phi(\tau, t^*, t) = s(t-\tau) \exp\left\{-\int_{t-\tau}^{t} s(t)\,dt\right\} \qquad (2.1\text{-}8)$$

Inserting this into eqn. (5) and substituting τ^* for t* according to eqn. (1), we obtain

$$\boxed{\phi(\tau, \tau^*, t) = s(t-\tau) \exp\left\{-\int_{t-\tau}^{t} s(t)\,dt\right\} + \exp\left\{-\int_{t-\tau^*}^{t} s(t)\,dt\right\} \delta(\tau-\tau^*)} \quad 5) \qquad (2.1\text{-}9)$$

As eqn. (8) shows, the function ϕ^* is independent of t* or τ^* and, seen in purely mathematical terms, would exist over the entire $t - \tau$ plane. But because only positive values are meaningful for t, τ^*, and τ, and inequalities (1.5-1) and (1.5-2) are valid, the physical validity range of ϕ^* can be given by the relation

$$0 \leqslant \tau \leqslant \tau^* \leqslant t \qquad (2.1\text{-}10)$$

which corresponds to the shaded area in Fig. 1. Of course, the age distribution function $\phi(\tau, \tau^*, t)$ has the same range of validity.

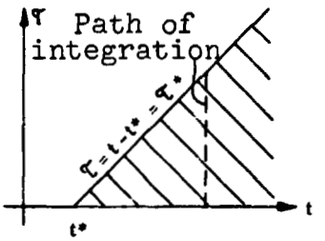

Fig. 2.1-1.

The path of the integration over ϕ^* in eqn. (6) is shown in Fig. 1 by a broken line.

For $\tau = 0$ and $\tau^* > 0$, the relation

$$\phi(\tau = 0, \tau^*, t) = s(t) \qquad (2.1\text{-}11)$$

follows from eqn. (9). The second term vanishes, since $\delta(\tau - \tau^*)$ is different from zero only if $\tau = \tau^*$ (cf. note to eqn. (1.5-3)). The physical significance of this result is plausible: At a given moment t, as many vortices are of age zero as have been carried to the surface at that moment by turbulent surface renewal (s = surface renewal rate).

If s(t) is a constant, eqn. (9) gives the relation

$$\phi(\tau, \tau^*, t) = \phi(\tau, \tau^*) = s\,e^{-s\cdot\tau} + e^{-s\cdot\tau^*} \cdot \delta(\tau - \tau^*) \qquad (2.1\text{-}12)$$

---

5) Regarding $\delta(\tau - \tau^*)$, cf. footnote to eqn. (1.5-3).

which is shown in Fig. 1.5-2.

If we let τ^* tend to infinity, the factor before the Dirac discontinuity becomes zero; integrated over τ, this term also yields zero, i.e. it makes no further contribution to the age distribution and can therefore be eliminated. In this way we arrive at the equation

$$\phi(\tau) = s\, e^{-s\tau} \tag{2.1-13}$$

It should be mentioned that eqn. (13) was previously derived by Danckwerts [25], and eqn. (12) by Teiriki Takaki and Siro Maeda [54]. Here they appear as special cases of the much more general eqn. (9).

2.2. Age Distribution Function of Laminar Surface Renewal in Bubble Formation

Since the bubble surface grows during bubble formation, new surface is continuously created, and the age distribution of the different elements can be characterized by an age distribution function $\Psi(\tau^*,t)$.

F(t), i.e. bubble surface as a function of time, was assumed to be known. A surface element dF which forms at time t* during dt is then

$$dF(t^*) = \frac{dF}{dt}(t^*)\, dt \tag{2.2-1}$$

If we assume that $dt = d\tau^*$, then using eqn. (2.1-1) and (1) we find that at time t the portion of the surface which has an age between τ^* and $\tau^* + d\tau^*$ is

$$\psi(\tau^*,t)\, d\tau^* = \frac{dF(t^*)}{F(t)} = \frac{dF(t-\tau^*)}{F(t)} = \frac{1}{F(t)} \frac{dF(t-\tau^*)}{dt} d\tau^* \qquad /32$$

Dividing this by $d\tau^*$, we obtain the function $\Psi(\tau^*,t)$, to which a Dirac discontinuity must be added since a bubble surface corresponding to the nozzle diameter F_D was suddenly formed at t = 0 (F(t) also contains F_D; cf. Fig. 1):

$$\boxed{\psi(\tau^*,t) = \frac{1}{F(t)} \left[\frac{dF(t-\tau^*)}{dt} + F_D \cdot \delta(\tau^* - t) \right]}\ ^{6)} \tag{2.2-2}$$

---

6) Regarding $\delta(\tau^* - t)$, cf. footnote to eqn. (1.5-3).

It is immediately apparent that this equation satisfies the condition

$$\int_0^t \psi(\tau^*, t)\, d\tau^* = 1 \qquad (2.2\text{-}3)$$

The age distribution function is somewhat more complicated if bubble surface growth is not uniform, i.e. if gas flows back into the nozzle while the bubble is forming. Such cases are possible for relatively small volume flows in the nozzle, as has been determined experimentally by L'Ecuyer and Murthy [22]. Such a case is shown schematically in Fig. 1. As long as the bubble surface grows (0 to t'), eqn. (2) is valid. Between t' and t" surface is "destroyed", and we make the assumption that all age classes are destroyed to the same degree. But this means that the shape of the age spectrum remains unchanged between t' and t"; the spectrum is merely shifted to the right along the τ^* axis, corresponding to the uniform ageing of all the surface elements (see Fig. 1). At time t_1 the age distribution will therefore have roughly the shape of the broken curve. The term dF/dt in eqn. (2) thus contributes nothing (provided it is less than zero) to age distribution; i.e. it behaves as if it were zero. Accordingly, the age distribution at time t_1 can be expressed with the following equations: /33

$$\psi(\tau^*, t_1) = \frac{1}{F(t)} \left[\frac{dF(t_1 - \tau^*)}{dt} + F_D \cdot \delta(\tau^* - t) \right] \qquad (2.2\text{-}4)$$

where $$dF/dt = 0 \text{ if } t_1 - \tau^* > t' \qquad (2.2\text{-}5)$$

The factor before the brackets must contain F(t') rather than $F(t_1)$, because no reduction in surface area is allowed for within the brackets due to eqn. (5), while eqn. (3) must be satisfied.

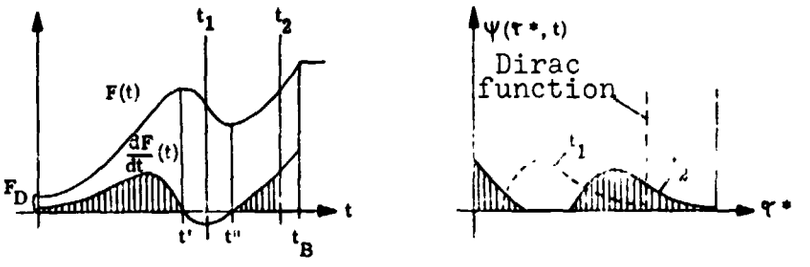

Fig. 2.2-1. Age distribution function of laminar surface renewal for non-uniform bubble growth.

Analogous considerations reveal that at time t_2 the age distribution must be something like the shaded region in the Figure, which can be described with the following equations:

$$\psi(\tau^*,t_2) = \frac{1}{F(t')+F(t)-F(t'')}\left[\frac{dF(t_2-\tau^*)}{dt} + F_D\cdot\delta(\tau^*-t_2)\right] \qquad (2.2\text{-}6)$$

where $$dF/dt = 0 \text{ if } t' < t_2 - \tau^* < t'' \qquad (2.2\text{-}7)$$

The sum in the denominator of the fraction before the brackets is the shaded area under the curve dF/dt plus F_D. We are thus proceeding as if the surface area of the bubble would only increase and never decrease.

2.3. Calculation of the Mass Transfer Coefficient for Bubble Formation as a Function of Time

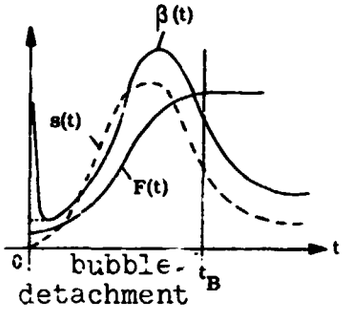

Fig. 2.3-1.

As was stated in Chap. 1.4, it is assumed that the functions F(t) and s(t) are known. To simplify calculations whereever possible, we further assume that F(t) is uniform. In this case the functions $\phi(\tau,\tau^*,t)$ and $\psi(\tau^*,t)$ can be inserted into eqn. (1.5-6) derived for bubble formation according to eqn. (2.1-9) and (2.2-2); this yields the following expression:

/35

$$\beta(t) = \sqrt{\frac{D}{\pi}}\int_{\tau^*=0}^{t}\left[\int_{\tau=0}^{\tau^*}\frac{1}{\sqrt{\tau}}\left\{s(t-\tau)\exp\left\{-\int_{t-\tau}^{t}s(t)dt\right\} + \exp\left\{-\int_{t-\tau^*}^{t}s(t)dt\right\}\right.\right.$$
$$\left.\left.\delta(\tau-\tau^*)\right\}d\tau\right]\cdot\frac{1}{F(t)}\left[\frac{dF(t-\tau^*)}{dt} + F_D\cdot\delta(\tau^*-t)\right]d\tau^* \qquad (2.3\text{-}1)$$

We will recall that the Dirac discontinuities which appear at the end of the region of integration in this formula must be included in the integral. From now on, for the sake of brevity, we shall employ the function

$$S(t) = \int_0^t s(t)\,dt \qquad (2.3\text{-}2)$$

and write simply F' instead of dF/dt. If we eliminate the braces and integrate the second member, we h[illegible] page):

$$\beta(t) = \sqrt{\frac{D}{q}} \int_{\tau^*=0}^{t} \left[\int_{\tau=0}^{\tau^*} \frac{s(t-\tau)}{\sqrt{\tau}} e^{-\left[S(t)-S(t-\tau)\right]} d\tau + \frac{1}{\sqrt{\tau^*}} e^{-\left[S(t)-S(t-\tau^*)\right]} \right]$$

$$\cdot \frac{1}{F(t)} \left[F(t-\tau^*) + F_D \cdot \delta(\tau^*-t) \right] d\tau^* \qquad (2.3\text{-}3)$$

With the substitutions

$$\tau = \xi^2 \qquad (2.3\text{-}4)$$

and

$$\tau^* = u^2 \qquad (2.3\text{-}5)$$

and after integrating the terms containing the Dirac discontinuity with respect to τ^*, we obtain from this equation

$$\beta(t) = \sqrt{\frac{D}{q}} \frac{1}{F(t)} \left\{ 2 \int_{u=0}^{\sqrt{t}} \left[2u \int_0^u s(t-\xi^2) e^{-\left[S(t)-S(t-\xi^2)\right]} d\xi + e^{-\left[S(t)-S(t-u^2)\right]} \right] \right.$$

$$\left. F'(t-u^2)du + F_D \left[2 \int_0^{\sqrt{t}} s(t-\xi^2) e^{-\left[S(t)-S(t-\xi^2)\right]} d\xi + \frac{1}{\sqrt{t}} e^{-S(t)} \right] \right\} \qquad (2.3\text{-}6)$$

/36

The above substitutions are useful because $\sqrt{\tau}$ or $\sqrt{\tau}^*$ appear in the denominator in eqn. (3); i.e., the integrand would have one pole at the lower limits of integration, which is very unfavorable for a numerical evaluation. This equation may be written in an even simpler form by using the following abbreviation:

$$\text{Int}(t,x) = \int_0^x s(t-\xi^2) e^{-\left[S(t)-S(t-\xi^2)\right]} d\xi \qquad (2.3\text{-}7)$$

$$\beta(t) = \sqrt{\frac{D}{q}} \frac{1}{F(t)} \left\{ 2 \int_{u=0}^{\sqrt{t}} \left[2u \, \text{Int}(t,u) + e^{-\left[S(t)-S(t-u^2)\right]} \right] F'(t-u^2)du + \right.$$

$$\left. + F_D \left[2 \, \text{Int}(t, x=\sqrt{t}) + \frac{1}{\sqrt{t}} e^{-S(t)} \right] \right\} \qquad (2.3\text{-}8)$$

We shall now introduce the following dimensionless variables

and dimensionless functions[7]:

$$t_1 = \frac{t}{t_c}; \quad \xi_1 = \frac{\xi}{\sqrt{t_c}}; \quad u_1 = \frac{u}{\sqrt{t_c}}; \quad x_1 = \frac{x}{\sqrt{t_c}} \tag{2.3-9}$$

$$s_1 = t_c \cdot s(t_c \cdot t_1) \tag{2.3-10}$$ /37

$$S_1(t_1) = S(t_c \cdot t_1) = \int_0^{t_1} s_1(t_1)\, dt_1 \tag{2.3-11}$$

$$Int_1(t_1, x_1) = \int_0^{x_1} s_1(t_1 - \xi_1^2)\, e^{-\left[S_1(t_1) - S_1(t_1 - \xi_1^2)\right]}\, d\xi_1 \tag{2.3-12}$$

$$F_1(t_1) = \frac{F(t_c \cdot t_1)}{l_c^2} \tag{2.3-13}$$

$$F'_1(t_1) = \frac{t_c}{l_c^2} \frac{dF(t_c \cdot t_1)}{dt} = \frac{dF_1}{dt_1} \tag{2.3-14}$$

$$F_{D1} = \frac{F_D}{l_c^2} \tag{2.3-15}$$

Using these equations, we can rewrite eqn. (7) in the form

$$Int(t,x) = \frac{1}{\sqrt{t_c}}\, Int_1(t_1, x_1) \tag{2.3-16}$$

and from eqn. (8) we obtain

$$B(t_1) = \beta(t_1)\sqrt{\frac{t_c}{D}} = \frac{Sh(t_1)}{Pe^{1/2}} = \sqrt{\frac{1}{\pi}}\,\frac{1}{F_1(t_1)} \left\{ 2\int_{u_1=0}^{\sqrt{t_1}} \left[2u_1 \cdot Int'_1(t_1, u_1) + e^{-\left[S_1(t_1) - S_1(t_1 - u_1^2)\right]} \right] \cdot F'(t_1 - u_1^2)\, du_1 + F_{D1} \left[2\, Int_1(t_1, x_1 = \sqrt{t_1}) + \frac{1}{\sqrt{t_1}} e^{-S_1(t_1)} \right] \right\} \tag{2.3-17}$$

Because of $t_1^{-\frac{1}{2}}$ in the last term, β is infinite for $t = 0$ (cf. Fig. 1). This is true because it was assumed that a new /38

7) The subscript 1 is added to all previous symbols.

surface of area F_D was suddenly formed at t = 0. In reality, however, this surface was already part of the previous bubble before it was released from the nozzle, so this pole cannot be present. The last term could simply be omitted, but then $\beta(t = 0) \equiv 0$, which cannot be true. Perhaps it is most appropriate to calculate $\beta(t)$ according to eqn. (17) and then substitute the broken horizontal line for the curve up to the minimum (see Fig. 1)[8].

There would seem to be no basic difficulties involved in calculating eqn. (17) with the aid of a computer. The functions $F_1(t_1)$ and $s_1(t_1)$ would presumably be stored in the machine as tables of supportive values. The program would first calculate $F_1'(t_1)$ and $S_1(t_1)$, which would probably also be stored as tables of supportive values. With suitable interpolation techniques the program could then quickly calculate these four functions for any argument desired. Only after these preliminary operations are completed should an effort be made to evaluate the integral expressions in eqn. (17); it would then be more advantageous to employ a subroutine for $Int_1(t_1, x_1)$.

3. Bubble Rise

/39

3.1. Age Distribution Function of Laminar Surface Renewal for Bubble Rise

It was assumed that the bubble is axially symmetrical and that its shape and velocity distribution at the interface are given by the functions $y(\sigma)$ and $v(\sigma)$ (cf. Fig. 1.4-2). To derive the age distribution function $\vartheta(\tau^*, \sigma)$, let us consider an annular cross-section of a rising bubble (Fig. 1). The surface current $2\pi yv$ is flowing toward the cross-section at point σ, and $2\pi(y + dy)(v + dv)$ is flowing away from the cross-section at point $\sigma + d\sigma$. The difference between these surface currents corresponds to the new surface produced on the annular cross-section during the unit of time in question. We assume that this new surface was supplied by the hypothetical surface-current density f (see Fig. 1) and write the continuity theorem as

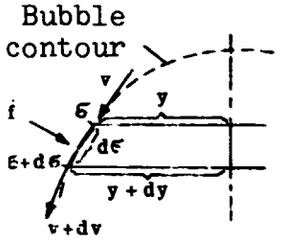

Fig. 3.1-1. An annular cross-section of the bubble.

$$2\pi (y + dy)(v + dv) - 2\pi yv = 2\pi y f d\sigma \qquad (3.1\text{-}1)$$

---

8) A better method may be to calculate the initial value of β from the equation

$$\beta(t=0) = \sqrt{\frac{D}{\pi t_D}}$$

and construct a line from this point tangent to the calculated
[cont. next page]

from

$$f = \frac{1}{v} \frac{d}{d\sigma}(vy) \tag{3.1-2}$$

The surface elements which are transported to the annular cross-section by f are of age $\tau^* = 0$ at the instant of their appearance. The elements which have age τ^* at point σ were transported to the bubble surface at some point σ_1 (cf. Fig. 2), where /40

$$\tau^* = \int_{\sigma_1}^{\sigma} \frac{d\sigma}{v(\sigma)} \tag{3.1-3}$$

i.e., the time required for the element to flow from σ_1 to σ. The surface current $2\pi y(\sigma)v(\sigma)$ consists of elements of varying age. Those elements having an age between τ^* and $\tau^* + d\tau^*$ must be transported by f to the bubble surface between σ_1 and $\sigma_1 - d\sigma_1$, where

$$d\sigma_1 = v(\sigma_1)\, d\tau^{*1)} \tag{3.1-4}$$

Accordingly, the number of elements within this age class at point σ must be equal to the ratio of the surface current $\dot{f}(\sigma_1) 2\pi y(\sigma_1)\, d\sigma_1$ to the surface current $2\pi y(\sigma)v(\sigma)$:

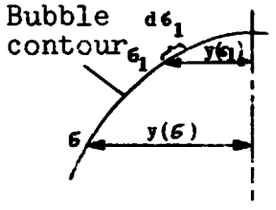

Fig. 3.1-2.

$$\zeta(\tau^*, \sigma)\, d\tau^* = \frac{\dot{f}(\sigma_1) 2\pi y(\sigma_1) d\sigma_1}{2\pi y(\sigma) v(\sigma)} \tag{3.1-5}$$

---

8) [cont.] curve (t_B = time of bubble formation). This approach would occasionally produce $\beta(t)$ curves with an initial drop; in physical terms this is entirely possible, especially if the boundary surface "swings back" into the orifice after the bubble is released — a phenomenon observed repeatedly at relatively low gas speeds.
In most cases, however, mass transfer in this initial period is negligible compared with the total mass transfer during bubble formation, and this question is of little significance.

1) The equation $d\tau^* = -d\sigma_1/v(\sigma_1)$ follows from eqn. (3) by differentiation, which appears to contradict equation (4) due to the minus sign. The reason for this is that in the subsequent derivation we regard the negatively measured $d\sigma_1$ as positive (cf. Fig. 2).

Substituting eqn. (4) for $d\sigma_1$, we obtain /41

$$\zeta(\tau^*, \sigma) = \frac{f(\sigma_1) y(\sigma_1) v(\sigma_1)}{y(\sigma) v(\sigma)} \tag{3.1-6}$$

or, from eqn. (2) by substitution,

$$\zeta(\tau^*, \sigma) = \frac{v(\sigma_1) \frac{d}{d\sigma}(y \cdot v)_{\sigma = \sigma_1}}{y(\sigma) v(\sigma)} \tag{3.1-7}$$

Together with eqn. (3), this equation determines the function $\zeta(\tau^*, \sigma)$ in implicit form; in principle, the variable σ_1 could be eliminated.

Since $\sigma_1 = \sigma$ for $\tau^* = 0$,

$$\zeta(\sigma, \tau^* = 0) = f(\sigma) \tag{3.1-8}$$

follows from eqn. (6). This is hardly surprising, because all elements which were produced at point σ by $f(\sigma)$ are of age $\tau^* = 0$. It can also be shown that the function $\zeta(\sigma, \tau^*)$ must satisfy the following differential equation:

$$\frac{\partial \zeta}{\partial \tau^*} + v \frac{\partial \zeta}{\partial \sigma} = -f \zeta \tag{3.1-9}$$

This equation is analogous to the differential equation (2.1-7), with f assuming the role of s. For the sake of completeness, the mathematical derivation is given in the next paragraph, although the equation has no further significance.

At point $\sigma - d\sigma$ the surface current component with age between $\tau^* - d\tau^*$ and τ^* is

$$2\pi y(\sigma - d\sigma) v(\sigma - d\sigma) \zeta(\sigma - d\sigma, \tau^* - d\tau^*) d\tau^*$$

At point σ the surface current component with age between τ^* and $\tau^* + d\tau^*$ is

$$2\pi y(\sigma) v(\sigma) \zeta(\sigma, \tau^*) d\tau^*$$

If we now specify that $d\tau^*$ be the time required for the current to flow from $\sigma - d\sigma$ to σ, then /42

$$d\tau^* = \frac{d\sigma}{v(\sigma)} \tag{3.1-10}$$

and the two expressions above must be equivalent:

$$2\pi y(\sigma - d\sigma)v(\sigma - d\sigma)\zeta(\sigma - d\sigma, \tau^* - d\tau^*)\,d\tau^* = 2\pi y(\sigma)v(\sigma)\zeta(\sigma, \tau^*)\,d\tau^*$$

If the functions at point $\sigma - d\sigma$ or $\tau^* - d\tau^*$ are expressed with the partial derivatives at point σ or τ^*, and the arguments are omitted, we obtain

$$(y - y'd\sigma)(v - v'd\sigma)(\zeta - \zeta_\sigma\, d\sigma - \zeta_\tau\, d\tau^*) = yv\zeta$$

Substituting eqn. (10) for $d\tau^*$ and eliminating the brackets and higher order terms:

$$\zeta_\tau + v\zeta_\sigma = -\zeta\frac{(yv)'}{y}$$

which leads to eqn. (9) after substitutions from eqn. (2).

Equation (7) is valid only as long as $\dot{f} \geq 0$, for eqn. (6) tells us that if f is negative, ϑ is also negative, which would not be meaningful. It can be seen from eqn. (2) that $\dot{f}$ goes negative at the point where (vy) attains its maximum. We designate this point as σ_o. From here on, surface is destroyed rather than produced, and as with the function $\psi(\tau^*, t)$ in Chap. 2.2, we make the assumption that surface elements of all age classes are lost to the same degree. In this case the age spectrum is shifted along the τ^* axis as σ increases, while its shape remains unchanged; this can be formulated mathematically as follows:

if $\sigma > \sigma_o$, then

$$\tilde{\vartheta}(\tau^*, \sigma) = \vartheta(\tau^* - \tau^*_{min}, \sigma_o)\ ^{2)} \qquad (3.1\text{-}11)$$

$$\text{for } \tau^* \geq \tau^*_{min}$$

and

$$\vartheta(\tau^*, \sigma) \equiv 0 \qquad (3.1\text{-}12)$$

$$\text{for } \tau^* \leq \tau^*_{min}$$

where

$$\tau^*_{min} = \int_{\sigma_o}^{\sigma} d\sigma / v(\sigma) \qquad (3.1\text{-}13)$$

If we now define τ^*_o as $\tau^*_o = \max[0, \tau^*_{min}]$ [3] (3.1-14)

---

2) The ~ sign over ϑ will be omitted later as a uniform system of notation is adopted.

3) See footnote to eqn. (3.2-14).

then the lower limit of the outer integral in eqn. (1.5-7) is correct in every case. The upper limit of integration is infinite because eqn. (3) always yields $\tau^* = \infty$ for $\sigma_1 = 0$ and $\sigma \neq 0$, provided $\left(\frac{dv}{d\sigma}\right)_{\sigma=0}$ is finite, which is usually the case.

3.2. Calculation of the Mass Transfer Coefficient for Bubble Rise as a Function of Location on the Bubble Surface

If eqn. (2.1-12) is inserted into eqn. (1.5-7) and internal integration is performed on the second term, we obtain

$$\beta(\sigma) = \sqrt{\frac{D}{\pi}} \int_{\tau_0^*}^{\infty} \left\{ \int_0^{\tau^*} \frac{s e^{-s\tau}}{\sqrt{\tau}} d\tau + \frac{e^{s\tau^*}}{\sqrt{\tau^*}} \right\} \zeta(\sigma, \tau^*) d\tau^* \tag{3.2-1}$$

If there is no separation of streamlines (wake), the functions $v(\sigma)$ and $y(\sigma)$ are more or less as shown in Fig. 1. In such a case it is always possible to find σ_0, the point at which (vy) attains a maximum. Cases may arise, however, when these functions are known only on a portion of the bubble, e.g. only up to σ'_{max} (see Fig. 1), and we will wish to perform the calculation for this portion only (for a "bubble cap").

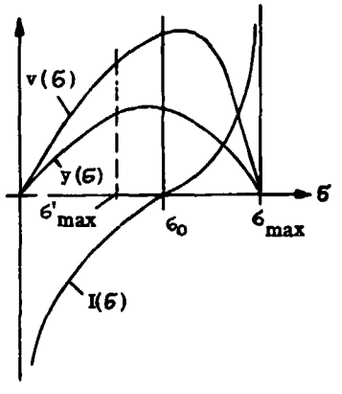

Fig. 3.2-1. Bubble without separation.

We shall now generalize the meaning of σ_0 such that in such a case σ'_{max} will be regarded as σ_0 and a value of σ_0 is defined in every case. We write /44

$$I(\sigma) = \int_{\sigma_0}^{\sigma} \frac{d\sigma}{v(\sigma)} \tag{3.2-2}$$

The function $I(\sigma)$ is also shown in Fig. 1. At $\sigma = 0$ and $\sigma = \sigma_{max}$, it exhibits logarithmic singularities provided $dv/d\sigma$ is finite at these points.

Differentiating eqn. (3.1-3) with respect to σ_1 and rearranging, we obtain

$$v(\sigma_1) \frac{d}{d\sigma_1} = -\frac{d}{d\tau^*} \tag{3.2-4}$$

which may be combined with eqn. (3.1-7) to yield

$$\zeta(\sigma, \tau^*) = -\frac{1}{v(\sigma) y(\sigma)} \frac{d}{d\tau^*} (v \cdot y)_{\sigma = \sigma_1} \tag{3.2-5}$$

This equation is valid only if $\sigma \leq \sigma_0$. According to eqn. (3.1-11), if $\sigma > \sigma_0$, the value of σ_0 must be substituted for σ in the old qualifying equations for ζ, and $\tau^* - \tau^*_{min}$ for τ^*. In this way the qualifying equations (5) and (3) assume the following form: /45

$$\tilde{\zeta}(\tau^*, \sigma) = \zeta(\tau^* - \tau^*_{min}, \sigma_0) = -\frac{1}{v(\sigma_0)y(\sigma_0)} \frac{d}{d\tau^*}(vy)_{\sigma=\sigma_1} \tag{3.2-6}$$

and

$$\tau^* - \tau^*_{min} = I(\sigma_0) - I(\sigma_1) \tag{3.2-7}$$

It follows from eqn. (2) and (3.1-13), however, that $\tau^*_{min} = I(\sigma)$ and $I(\sigma_0) = 0$, which may be inserted into eqn. (7) to yield

$$\tau^* = I(\sigma) - I(\sigma_1) \tag{3.2-8}$$

But this is identical to eqn. (3), so the qualifying equations for $\zeta(\sigma, \tau^*)$ (eqn. 3 and 5) and those for $\tilde{\zeta}(\sigma, \tau^*)$ (eqn. 8 and 6) can be written in the following unified form ($\sim$ sign omitted):

$$\begin{aligned} \zeta(\tau^*, \sigma) &= -\frac{1}{v(\sigma^*)y(\sigma^*)} \frac{d}{d\tau^*}(vy)_{\sigma=\sigma_1} \\ \sigma^* &= \min\left[\sigma, \sigma_0\right] \quad 4) \\ \tau^* &= I(\sigma) - I(\sigma_1) \end{aligned} \tag{3.2-9}$$

We now include equations (2), (1) and (3.1-14), again taking into consideration that $\tau^*_{min} = I(\sigma)$:

$$\begin{aligned} I(\sigma) &= \int_{\sigma_0}^{\sigma} \frac{d\sigma}{v(\sigma)} \\ \beta(\sigma) &= \sqrt{\frac{D}{\pi}} \int_{\tau^*_0}^{\infty} \left\{ \int_0^{\tau^*} \frac{e^{-s\tau}}{\sqrt{\tau}} d\tau + \frac{e^{-s\tau^*}}{\sqrt{\tau^*}} \right\} \zeta(\tau^*, \sigma) d\tau \\ \tau^*_0 &= \max\left[0, I(\sigma)\right] \quad 5) \end{aligned} \tag{3.2-10}$$ /46

4) See footnote to eqn. (3.2-14).

5) See footnote to eqn. (3.2-14).

Equations (9) and (10) now constitute a closed system, from which β can be calculated at any point σ on the bubble surface provided $v(\sigma)$, $y(\sigma)$ and s are known (σ_0 is considered to be known).

If the first equation of (9) is now inserted into the second equation of (10), and if a free constant of integration is chosen such that the portion integrated out at the lower limit vanishes, we obtain

$$\beta(\sigma) = \sqrt{\frac{D}{\pi}}\left\{\int_0^{\tau^*} \frac{s e^{-s\tau}}{\sqrt{\tau}}d\tau + \frac{e^{-s\tau^*}}{\sqrt{\tau^*}}\right\}\left\{1 - \frac{v(\sigma_1)y(\sigma_1)}{v(\sigma^*)y(\sigma^*)}\right\}\Bigg|_{\tau^*=\tau_0^*}^{\infty} +$$

$$+ \frac{1}{2}\sqrt{\frac{D}{\pi}}\int_{\tau_0^*}^{\infty}\frac{e^{-s\tau^*}}{\tau^{*3/2}}\left\{1 - \frac{v(\sigma_1)y(\sigma_1)}{v(\sigma^*)y(\sigma^*)}\right\}d\tau^* \qquad (3.2\text{-}11)$$

After the limits are assigned, all that remains of the first term is

$$\sqrt{\frac{D}{\pi}}\int_0^{\infty}\frac{s e^{-s\tau^*}}{\sqrt{\tau^*}}d\tau^* \equiv \sqrt{sD}$$

because $\sigma_1 = 0$ for $\tau^* = \infty$ (cf. definition of τ^* by the third equation in (9) and curve $I(\sigma)$ in Fig. 1), making the second brace equal to 1, and because $\sigma_1 = \sigma^*$ for $\tau^* = \tau_0^*$, making the second brace equal to zero. Remaining is /47

$$\beta(\sigma) - \sqrt{sD} + \frac{1}{2}\sqrt{\frac{D}{\pi}}\int_{\tau_0^*}^{\infty}\frac{e^{-s\tau^*}}{\tau^{*3/2}}\left\{1 - \frac{v(\sigma_1)y(\sigma_1)}{v(\sigma^*)y(\sigma^*)}\right\}d\tau^* \qquad (3.2\text{-}12)$$

With the dimensionless variables

$$S = \frac{\sigma}{l_c}; \quad Y = \frac{y}{l_c}; \quad V = \frac{v}{l_c}; \quad \Theta = \tau^*\frac{v_c}{l_c}$$

$$\omega = \sqrt{\frac{s\,l_c}{v_c}}; \quad B(S) = \beta(\sigma)\sqrt{\frac{l_c}{D\,v_c}} = \frac{Sh(S)}{Pe^{1/2}} \qquad (3.2\text{-}13)$$

$$J(S) = \frac{v_c}{l_c}I(\sigma)$$

and S^*, S_1, S_0, Θ_0 in place of $\sigma^*, \sigma_1, \sigma_0, \tau_0^*$, we finally obtain

---

6) The Peclet number is defined as $P_e = Re \cdot Sc = \frac{l_c v_c}{D}$ for mass transfer.

from eqn. (12), (9) and (10)

$$B(S) = \frac{Sh(S)}{Pe^{1/2}} = \omega + \frac{1}{2\sqrt{\pi}} \int_{\Theta_0}^{\infty} \frac{e^{-\omega^2\Theta}}{\Theta^{3/2}} \left[1 - \frac{V(S_1)Y(S_1)}{V(S^*)Y(S^*)} \right] d\Theta$$

$$\Theta = J(S) - J(S_1)$$

$$J(S) = \int_{S_0}^{S} \frac{dS}{V(S)}$$

S_0 = The value of S such that (V,Y) attains its maximum value within the range of definition

$S^* = \min [S, S_0]$

$\Theta_0 = \max [0, J(S)]$ [7] (3.2-14)

This gives us a closed system of equations for determining the dimensionless mass transfer coefficient B from V(S), Y(S) and ω. The auxiliary variable S_1 in the first equation can be determined from the second and third equation for given values of Θ and S. /48

Based on a thorough investigation, the following properties of this system could be determined [8]:

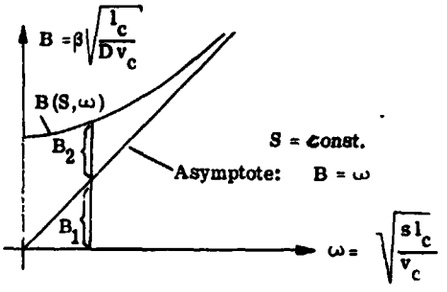

Fig. 3.2-2.

1) B is still a function of ω for given functions Y(S) and V(S) for a given value of S. This function has a horizontal tangent at $\omega = 0$ and an asymptote $B = \omega$ for $\omega \rightarrow \infty$ (see Fig. 2):

$$\left(\frac{\partial B}{\partial \omega}\right)_{\omega=0} = 0 \qquad (3.2\text{-}15)$$

$$\lim_{\omega \rightarrow \infty} B(S,\omega) = \omega \qquad (3.2\text{-}16)$$

Since $B = \omega$, $\beta = \sqrt{Ds}$; the asymptote is therefore the solution given by Danckwerts' theory [25]. The $B(\omega)$ curve exhibits a uniform rise. The B value averaged over the bubble surface $\bar{B}$ also has these properties, of course. /49

---

7) The notation "max [ ]" or "min [ ]" indicates "the largest" and "the smallest" of the variables enclosed by the brackets.

8) The derivations may be found in the Appendix (Chap. 10.1 and 10.2).

2) At a constant value of ω, $B(S,\omega)$ varies quadratically about the point at which S = 0, i.e. it has a horizontal tangent at this point.

With S = 0, B cannot be calculated from equation system (14), although the following simple formula may be derived:

$$B(S=0,\omega) = \sqrt{\omega^2 + 2\left(\frac{dV}{dS}\right)_{S=0}} \qquad (3.2\text{-}17)$$

3) At the rear stagnation point,

$$B(S = S_{\text{stagnation point}}, \omega) = \omega \qquad (3.2\text{-}16)$$

A computer program was prepared in cooperation with Dr. J. Waldvogel for solving equation system (14) for given V(S) and Y(S) functions. For a given set of ω values, the program calculates the values of B at various points on the bubble surface (the number of points must be entered), averages them over the surface and also computes the bubble volume, the bubble surface area and the equivalent diameter. The bubble shape and the velocity distribution on the bubble surface may be introduced in the form of either cylindrical or spherical coordinates; the program automatically converts to S and Y coordinates. In addition, bubble shape and velocity distribution may be entered either with mathematical formulae (subroutines) or with tables.

Programming met with a number of difficulties, primarily because the upper limit of the integral in eqn. (14) is infinite and the integrand has a singularity for $\Theta = 0$. This latter difficulty could, of course, be eliminated through the transformation $\Theta = \xi^2$; but even then with $\xi \rightarrow 0$, the bracketed term is reduced to zero and the function preceding it to infinity, which is very unfavorable for a numerical solution. /50

That equation system (14) breaks down at the stagnation points is due primarily to the fact that the function $I(\sigma)$ has logarithmic poles at those points (see Fig. 1).

4. Comparison of the Relations Derived for Bubble Rise with Other Theoretical Solutions /51

The literature dealing with mass transfer contains a number of theoretical or semi-empirical solutions for both rigid and circulating bubbles and liquid drops. Since these solutions have already been extensively compared and summarized [34, 35, 36, 19, 53], they will not be discussed here. We shall simply point out that the solution given in Chap. 3 is only one which allows for the effect of a steady-state field of flow combined with turbulent motion. This solution will be compared with that of Lochiel and

Calderbank [19], because the latter is formulated in very clear and general terms and encompasses a number of solutions already published.

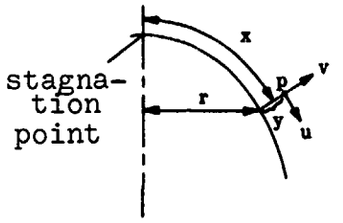

Fig. 4-1.

Lochiel and Cladderbank consider a point P near a rotationally symmetrical body with the coordinates x, y and the respective velocities u, v (cf. Fig. 1[1]).

Under the assumption that the flow boundary layer is significantly and consistently smaller than the radius r, they write the continuity equation in the form

$$\frac{\partial}{\partial x}(uv) + \frac{\partial}{\partial y}(vr) = 0 \qquad (4\text{-}1)$$

and the transport equation in the form

$$u\frac{\partial c}{\partial x} + v\frac{\partial c}{\partial y} = D\frac{\partial^2 c}{\partial y^2} \qquad (4\text{-}2)$$ /52

They then expand u into a series for y = 0, but retain only the first two terms:

$$u = u_o + u_o' y \qquad (4\text{-}3)$$

Equations (1) through (3) are made dimensionless with the flow velocity, the radius of a sphere of equal volume and the difference in concentration between the boundary surface and the flow nucleus; this is designated by an additional subscript 1.

Eqn. (3) is inserted into (1), and v_1 determined from it as a function of the u_{10} and u_{10}' by integration. This result is inserted into eqn. (2), which is then solved for two cases[2]:

a) for

$$u_{10} \ll |u_{10}' \delta_{c1}| \qquad (4\text{-}4)$$

we have

$$\frac{Sh}{Pe^{1/3}} = 0{,}641 \frac{A_s}{A}\left[\int_0^{x_1} \sqrt{u_{10}' r_1}\; r_1\, dx_1\right]^{2/3} \qquad (4\text{-}5)$$

---

1) From now on the notation of these authors will be used.

2) In these equations, the equivalent diameter is the characteristic measurement in Pe and Sh, while in r_1, s_1 and u_{10}' it is the equivalent radius.

b)

$$u_{10} \gg |u_{10}\,\delta_{c_1}| \tag{4-6}$$

we have

$$\frac{Sh}{Pe^{1/2}} = \sqrt{\frac{2}{\pi}}\,\frac{A_s}{A}\left[\int_0^{X_1} u_{10}\,r_1^{\,2}\,dx_1\right]^{1/2} \tag{4-7}$$

In these equations, Sh represents the surface A of the body of rotation whose contour is of length X_1. A_s is the surface area of the sphere of equal volume and δ_{c_1} the dimensionless thickness of the concentration boundary layer. The two solutions differ in that the first term in eqn. (3) is disregarded in the first, and the second term in the second. Case a) corresponds to the rigid surface, case b) to the completely mobile surface. No solution could be derived for the case where both terms in eqn. (3) must be taken into account[3]. /53

In case b) the following equation can be derived for the local mass transfer coefficient from the calculations of Lochiel and Calderback:

$$B(x_1) = \frac{Sh(x_1)}{Pe^{1/2}} = \sqrt{\frac{2}{\pi}}\,\frac{u_{10}\,r_1}{\left[\int_0^{x_1} u_{10}\,r_1^{\,2}\,dx_1\right]^{1/2}} \tag{4-8}$$

Equations (7) and (8) should yield the same results as our solution for $\omega = 0$. This is obviously not the case; but there is definitely a marked similarity in the structure of the formulae: in both cases $Sh/Pe^{\frac{1}{2}}$ is equivalent to an integral formula which is defined by the dimensionless body shape and velocity distribution. Corresponding numerical solutions are compared and discussed in Chap. 5-8. In addition, a curve calculated for bubbles rising in tubes (tube bubbles) according to the theory of Beek and Kramers [18] is shown (see Diagram 16); it can be shown, however, that this theory gives the same result for rising boundary surfaces as eqn. (7)[4].

These deductions define the conditions under which the theory of Lochiel and Calderbank can be applied:

a) From eqn. (1), the thickness of the concentration boundary layer must be uniformly and significantly smaller than the rad radius r (not applicable near the stagnation point);

---

3) Inequalities (4) and (6) were given by the authors in a slightly different form, but we believe this formulation to be the better one.

4) See derivation in Appendix (Chap. 10.3).

b) From eqn. (3), the concentration boundary layer must be thinner than the liquid boundary layer. /54

In the theory presented here, it was assumed that diffusion into a surface element was like that into a unidimensional infinite body. It is implicit in this assumption, however, that the above limitations are true. Also, owing to the "rigid body assumption," the flow within the concentration boundary layer must be something like parallel flow, a property which can be expressed by inequality (6).

If it is assumed by the film theory that the thickness of the concentration boundary layer is D/β, then based on the relation $Sh = B\,Pe^{\frac{1}{2}}$ we can obtain a condition for the Peclet number. Using the same characteristic length and velocity in u_{10} and u'_{10} as in Pe and B, this condition is:

$$Pe \gg \left(\frac{1}{B}\frac{u'_{10}}{u_{10}}\right)^2 \qquad (4\text{-}9)$$

We shall now examine more closely the statement made in the introduction that the solutions obtained -- i.e. eqn. (2.3-17) for bubble formation and eqn. (3.2-14) for bubble rise -- are valid for both the gas and the liquid phases. The previously mentioned conditions must be fulfilled for a rising bubble, including the requirement for a relatively thin concentration boundary layer ($\delta_c \ll d_B$). This layer must also be thin in the case of bubble formation; otherwise, the simplified diffusion equation (eqn. 1.5-4b) could not be used. For bubble rise, this conditions is almost always met in the liquid phase, and on both sides of the gas-liquid interface in the case of bubble formation, regardless of whether or not turbulence is assumed to be present. In bubble formation, a thick boundary layer cannot form due to the very short formation time (in most cases); during bubble rise, the medium diffusing into the liquid is carried away by the liquid flowing about the bubble. /55 A thicker boundary layer could form only in very viscous liquids, in which a bubble would be all but immobile; i.e., in such a case inequality (9) would probably no longer be satisfied.

The situation is different for the gas phase during bubble rise. In laminar flow, a toroidal vortex is formed (cf. Fig. 2); portions located farther from the boundary surface do not simply flow away to be replaced by new ones as in the liquid phase, and there is no convective transfer normal to the streamlines. In this case the material undergoing transfer must advance to the nucleus of the vortex by molecular diffusion. We thus have non-steady state diffusion through a continuously growing "boundary layer"; i.e., our concept of quasi-steady state mass transfer

through a thin concentration boundary layer does not apply. The solutions known from the literature (summarized in [34]) also provide primarily time-dependent formulae for mass transfer in the gas phase.

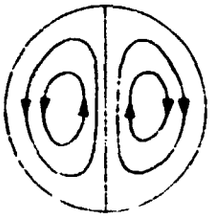

Fig. 4-2. Laminar field of flow within a bubble in steady-state rise.

It might be assumed that our solution must be valid for at least the beginning of the steady-state rise, since the concentration boundary layer is still thin. But this can be true for only a very short time, because the gas which was in contact with the liquid does not mix [illegible] inside the bubble, but "rotates" and again comes into contact with the liquid; during this process it could presumably give up only a small quantity of the previously absorbed diffusing medium to the inner layers. By contrast, our theory presumes that the gas reaching the boundary surface is always in the "core state" corresponding to the mixed state.

The situation is different if the gas in the bubble is turbulent. /56 In this case it may be assumed that a core state and a thin boundary layer are actually present. As statements made in Chap. 8 suggest, however, hydrodynamic turbulence will generally not occur in bubbles rising in the steady-state mode. If, on the other hand, mass transfer in the liquid leads to surface turbulence, this turbulence will be transmitted to the gas phase. The application of our theory to the gas phase therefore appears justified only in a case such as this.

We assumed in Chap. 1.5 that the concentration at the boundary sur[illegible] constant in both phases (see boundary conditions for dif[illegible]l equation (1.5-4b)). This is possible in a physical sens[illegible] if

$$\beta_g \Delta c_g = \beta_{fl} \Delta c_{fl} \tag{4-10}$$

at every point on the bubble surface, for the material flow must be the same on both sides of the interface. From this equation we then obtain

$$\beta_g / \beta_{fl} = \Delta c_{fl} / \Delta c_g = \text{const.} \tag{4-11}$$

It should be stressed that this condition is automatically satisfied if our solution can be applied to both phases and the turbulence -- i.e., ω and s -- is equal in both phases. But this is actually the case for the surface turbulence, since it is produced by the same mechanism in both phases.

Although eqn. (1.1) is a trivial physical condition, it is seldom considered. This is understandable, however, because if Δc_g and Δc_{fl} were to vary along the interface, the problems of mass transfer at the liquid and the gas side of the interface could not be treated separately; and this would very likely lead to considerable mathematical difficulties.

Part II

/57

Calculations and Comparison of Results with Other Theoretical and Experimental Results

5. Ellipsoidal and Spherical Bubbles

/59

5.1. Spheroids in Potential Flow

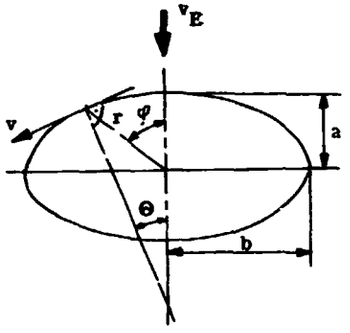

Fig. 5.1-1.

The calculations are performed for spheroids with polar coordinates r and φ. Let us define the eccentricity as

$$E = b/a \qquad (5.1\text{-}1)$$

where a is always half of the axis parallel to the direction of flow. Then, according to Zahm [33], the velocity at the surface can be calculated from the equation

$$v = (1 + k)\, v_B \sin \Theta \qquad (5.1\text{-}2)$$

where k is defined by the following expressions:

a) For oblate spheroids

$$k = -\frac{e\,E^2 - E\,\mathrm{Arcsin}\,(e)}{e - E\,\mathrm{Arcsin}\,(e)} \qquad (5.1\text{-}3)$$

$$e = \sqrt{1 - 1/E^2} = \frac{1}{b}\sqrt{b^2 - a^2} \qquad (5.1\text{-}4)$$

b) For prolate spheroids

/60

$$k = -\frac{\ln\left(\frac{1+e}{1-e}\right) - 2e}{\ln\left(\frac{1+e}{1-e}\right) - \frac{2e}{1-e}} \qquad (5.1\text{-}5)$$

$$e = \sqrt{1 - E^2} = \frac{1}{a}\sqrt{a^2 - b^2} \qquad (5.1\text{-}6)$$

The k values calculated from these equations by Zahm were used in the calculations (cf. Table II in [33]). They are also given in the first row of Table ① as values of 1 + k.

For sin Θ, the equation

$$\sin\Theta = \frac{1}{\sqrt{\frac{E^4}{tg^2\varphi}+1}} = \frac{1}{\sqrt{E^4\,ctg^2\varphi+1}} \tag{5.1-7}$$

can be derived. If we choose

$$l_c = d_B \tag{5.1-8}$$

and

$$v_c = v_B \tag{5.1-9}$$

for the characteristic length and the characteristic velocity, we obtain for the dimensionless shape and velocity distribution

$$R = \frac{r}{d_B} \qquad \sqrt{\frac{1}{\ldots - (E^2-1)\sin^2\varphi}} \tag{5.1-10}$$

$$V = \frac{v}{v_B} = (1+k)\frac{1}{\sqrt{\frac{E^4}{tg^2\varphi}+1}} = (1+k)\frac{1}{\sqrt{E^4\,ctg^2\varphi+1}} \tag{5.1-11}$$

Calculations were performed for various values of E using these functions. The results are summarized in Table ① and Diagrams ② through ⑧. Diagram ③ shows $\bar{B}$ as a function of ω with E as parameter. In qualitative terms, the shape of the curve corresponds to expectations based on the theory. Diagram ② shows the same function with ω as the parameter. It can be readily seen that /61

$$\lim_{b/a\to 0} \bar{B} = \omega \tag{5.1-12}$$

where $b/a \to 0$ corresponds to the case of an infinitely prolate spheroid (constant volume); i.e., an elongated needle in parallel flow. But here, according to eqn. (4.1-7), $f \equiv 0$, so surface renewal is only turbulent, not laminar.

We did not investigate whether the curve for $\omega = 0$ has a vertical or merely a very steep tangent at $b/a = 0$.

The difference between the curve for $\omega = 0$ and the curve calculated by Lochiel and Calderbank [19] -- a difference which increases sharply with the value of b/a -- is surprising. Our solution shows clearly that B rises as the spheroid grows flatter,

while the solution of Lochiel and Calderbank actually indicates a slight drop. The difference with respect to the smaller value is 12% for b/a = 0.5 and 46% for b/a = 3.

Diagrams ④, ⑤ and ⑥ give the curves for b/a = 2, 1 and 0.5, which show the mass transfer coefficients as a function of the angle φ (for simplicity, $B(\varphi)/\overline{B}$ was shown; the values of B are given in a small Table). Also shown is the dimensionless velocity V. As we see, the shape of these curves is strongly dependent on the eccentricity b/a. It is interesting to note that the maxima of the $B/\overline{B}$ curves occur roughly at the point where $V(\varphi)$ has its steepest tangent. The derivative $dv/d\delta$ or the analogous dv/φ thus seems to be the decisive factor in laminar surface renewal, which is responsible for variations in the value of B (cf. eqn. 3.1-2). For a sphere, for example, the surface-current density of characteristic of laminar surface renewal can be calculated from eqn. (3.1-2) as /62

$$\dot{i} = 6 \frac{v_B}{d_B} \cos(\varphi)$$

and the curves in Diagram ⑤ are, up to $\varphi \approx 90^\circ$, very similar to a cosine curve. It is not surprising that the curves flatten as ω increases, since it was already shown in Chap. 3 that B always tends toward the asymptotic value $B = \omega$ as ω increases. The curves $B(\varphi)/\overline{B}$ are shown in Diagram ⑦ for $\omega = 0$ and various eccentricities. It is surprising how "quickly" the sharp maximum of $\varphi = 0$ "slides" into the region of $\varphi \approx 90^\circ$ as the degree of eccentricity increases. The sharp maximum at b/a = 3 is strongly reminiscent of the potential flow about an infinitely thin circular disk, at whose edges infinitely high velocities are developed — which would also mean an infinitely intense transfer of material.

The actual $B(\varphi)$ curves are given in Diagram ⑧ so that they may be compared. The curves derived from the theory of Lochiel and Calderbank [19] are also shown. One can clearly see the effective differences in the magnitude of mass transfer. In both cases shown (b/a = 1 and 2), there is a region near 90° where both solutions are in good agreement. The maxima are located at practically the same point, although our theory leads to much greater maximum values. Striking is the difference in the character of the curves for values greater than approximately 100 ~ 110°. Based on the solution of Lochiel and Calderbank, it can be proved that the curves have a horizontal tangent at both stagnation points; our solution, on the other hand, indicates a horizontal tangent only at the front stagnation point. The rear tangent is extremely steep, probably even vertical. This would explain why the difference between the two solutions becomes more significant as the ellipsoid flattens (cf. Diagram ②). Diagram ⑧ shows, for example, that the differences at the rear point for an oblate spheroid are much greater than for a sphere and are quite significant for

$\varphi = 100 \sim 110^{\circ}$, where the radius is also large; this is a significant factor when mean values are taken over the surface of the bubble. /63

In physical terms, this appreciable difference can probably be explained as follows: When f is negative (i.e., when material is forced away from the boundary surface), our theory does not take into account the fact that this material, which has the concentration of the boundary surface, does not simply disappear, but lingers for a time in the vicinity of the boundary surface. This results in a tendency for the boundary surface concentration to level off, even in layers not adjacent to the boundary surface; i.e., the concentration gradient is sharply reduced, and along with it the diffusion stream. It is intuitively clear that the stream of entrained material at the rear end of an oblate body will be much larger than that of a prolate body. It is likely, therefore, that our theory will show mass transfer coefficients at the rear which are too high, especially in the case of oblate bodies.

Table (9) gives values of $\overline{B}$ for the front half of spheroids for the same values of ω and b/a as in Table (1). Table (10) shows for the same values of ω and b/a the portion of mass transfer at the front half relative to total mass transfer. A sphere with $\omega = 0$ is taken as a characteristic example. In this sphere, 69% of the total mass transfer takes place at the front half. According to Lochiel and Calderbank, this figure is 70.7% — very close to our solution. Based on Diagram (8), however, we can predict that with b/a = 2, the percentage according to Lochiel and Calderbank will be significantly higher, while according to our theory it will fall to 67%.

5.2. Spherical or Spheroidal Bubbles and Drops with Complete Internal Circulation /64

The basic prerequisite for the applicability of our theory to bubbles and drops is that their circulation be unimpeded, i.e. that there be free interfacial flow. But this is not always the case. Very small bubbles and drops behave as rigid spheres, and even the circulation of larger bubbles and drops can be totally or partially prevented by small quantities of surfactants. The latter case obtains when a rigid cap forms on the rear end of a bubble or drop, while the front part remains mobile [36]. Basically, the greater the value of d_B and the smaller the contamination by surfactants, the greater the ease with which circulation within a bubble or drop develops. We shall not pursue the problem of when and to what extent circulation occurs; we shall simply refer to a few places in the literature where this problem is discussed and where additional references may be found [3a, 34, 36].

In cases where circulation is not prevented but is strongly inhibited (e.g. highly viscous drops falling in gases), our theory

is not usually valid[1]. It might well provide a good approximation for rapidly rising bubbles (large Re) and for drops rising or falling in liquids, provided the viscosity of the drop is not substantially greater than that of the liquid medium.

If streamline separation occurs -- which is likely only if circulation is appreciably inhibited or if the velocity is sufficiently high -- our theory can be used in calculating mass transfer only up to the separation point. In the derivations which follow, it is assumed that this case does not obtain.

To be able to apply the results obtained for potential flow, we make the assumption that at every point on the phase boundary surface v is α times greater than the value which would be produced by potential flow at the same velocity of bubble rise. The number α is less than one and location-dependent[2]. Our fundamental relation /65

$$Sh = \overline{B} \cdot Pe^{\frac{1}{2}} \tag{5.2-1}$$

derived from eqn. (1.5-1) or eqn. (3.2-14) then assumes the form

$$Sh = \overline{B} \cdot \alpha^{\frac{1}{2}} \cdot Pe^{\frac{1}{2}} \tag{5.2-2}$$

where the value calculated for potential flow is to be substituted for $\overline{B}$. This procedure is not possible if α is "very small," lest condition (4-6) be violated. There are various possible means of determining α. If we assume that surface forces are not a factor, a simple consideration of dimensional aspects will reveal that α can be dependent only on Re, ρ_i/ρ_o and μ_i/μ_o.

$$\alpha = f(Re, \rho_i/\rho_o, \mu_i/\mu_o) \quad 3) \tag{5.2-3}$$

Conkie and Savic [35] provide the following theoretically derived formula for spherical bubbles or drops in the case $Re = v_B \cdot d_B/\nu_o > 1$:

---

1) The more precise conditions for the applicability of the theory were discussed in Chap. 4.

2) Various researchers have already worked from this hypothesis (see, for example, [35,36]. It is not strictly true, as the theoretical calculations of Chao [38] show, but it seems to be fairly good approximation.

3) Here, Re is the "outer" Reynolds number calculated with μ_o and ρ_o.

$$\alpha = a \cdot Re\left(\frac{\mu_o}{\mu_i}\right)^2 \left[\sqrt{1 + \frac{b}{Re}\left(\frac{\mu_i}{\mu_o}\right)^2} - 1\right] \quad 4) \qquad (5.2\text{-}4)$$

according to which α is dependent only on $(\mu_o/\mu_i)\sqrt{Re}$. This relation was derived from a balance of energy which is "destroyed" by dissipation within the body. An arbitrary substitution was made for the interior of the body by Hill's field of flow, which is free of frictive forces but subject to rotative forces (see [37]), and some arbitrary assumptions regarding the boundary layer and tangential stresses were made, based more on mathematical expediency than physical observation. In addition, ρ_i appears in eqn. (3) but not in eqn. (4); there would thus seem to be a number of reasons for doubting the correctness of this equation. 166

For large value of $(\mu_o/\mu_i)\sqrt{Re}$, Conkie and Savic give the following relation as an asymptotic approximation to eqn. (4):

$$\alpha = 1 - \frac{53.3}{Re}\left(\frac{\mu_i}{\mu_o}\right)^2 \quad 5) \qquad (5.2\text{-}4a)$$

which can be used approximately from the point at which $(\mu_o/\mu_i)\sqrt{Re} = 50$ (cf. Fig. 3 in [35]).

Griffith gives an experimentally determined curve for $\alpha^{\frac{1}{2}}$ as a function of $(\mu_o/\mu_i)\sqrt{Re}$ (Fig. 3 in [36]), which is lower in the region $1 < (\mu_o/\mu_i)\sqrt{Re} < 30$ than eqn. (4). But since this curve was not determined from direct measurements, but on the strength of the formula

$$Sh = 2 + 1.13\,\alpha^{\frac{1}{2}}\,Pe^{\frac{1}{2}} \qquad (5.2\text{-}5)$$

from measured values of Sh, it cannot be accepted without reservation. It can be used at best in conjunction with this formula.

By different means, a seemingly more satisfactory solution can be obtained, but one which is correct only for α values not too

---

4) The authors give for the constants a and b the values a = 0.0094 and b = 213; but these values are incorrect. Accurate calculations yield the values a = 0.01044 and b = 191.5. For large argument values, this function approaches the value (a·b)/2, which must be one. The incorrect constants provide a somewhat higher value; as a result, one is reached with $(\mu_o/\mu_i)\sqrt{Re} = 220$.

5) The constant in the second term is derived from eqn. (4) with the aid of the binomial series as b/4, which, with the correct value of b, would yield 47.88.

different from one. Chao [38] made the assumption that the velocity distribution near the interface differs little from the inviscid solution[6] in the case of spherical bubbles and high Reynolds numbers, and has determined the differences with perturbation calculations. Lochiel and Calderbank [19] have adopted his computational method with a slightly modified boundary condition and calculated mass transfer according to their own theory using the velocity distribution obtained; in this way they derived the formula /67

$$Sh = 1{,}13 \left[1 - \frac{2 + 3\left(\frac{\mu_i}{\mu_o}\right)}{1 + \left(\frac{\varrho_i \mu_i}{\varrho_o \mu_o}\right)^{1/2}} \frac{1{,}45}{Re^{1/2}} \right]^{1/2} Pe^{1/2} \qquad (5.2\text{-}6)$$

[7]

For a sphere in potential flow, the theory of Lochiel and Calderbank gives us[8]

$$Sh = 1.13\ Pe^{\frac{1}{2}} \qquad (5.2\text{-}7)$$

By comparing eqn. (2) and (1) with eqn. (6) and (7), we obtain for α the formal relation

$$\alpha = 1 - \frac{2 + 3\frac{\mu_i}{\mu_o}}{1 + \left(\frac{\varrho_i \mu_i}{\varrho_o \mu_o}\right)^{1/2}} \frac{1{,}45}{Re^{1/2}} \qquad (5.2\text{-}8)$$

the structure of which corresponds to eqn. (3). /68

---

6) Potential flow, outside Hill flow subject to rotative forces inside.

7) $Re = v_B \cdot d_B / \nu_o$; the formula is valid for the outer side of the interface for high Re and thin concentration boundary layers.

8) The same formula has already been presented by Boussinesq [41]; it is valid for the outer side of the interface if the concentration boundary layers are thin.

Hadamard [39] and Rybczynski [40] have calculated the external and internal velocity fields for the creeping movement (Re < 1) of a viscous sphere in a viscous liquid. Based on their solutions,

$$\alpha = \frac{\mu_o}{3(\mu_i + \mu_o)} = \frac{1}{3(\frac{\mu_i}{\mu_o} + 1)} \qquad (5.2\text{-}9)$$

According to this equation, the values of α must be between 0 and 1/3. If it is inserted into eqn. (2) along with the value 1.13 for $\overline{B}$ (obtained from eqn. (7)), this leads to the equation

$$Sh = 0{,}652 \left(\frac{\mu_o}{\mu_i + \mu_o}\right)^{1/2} Pe^{1/2} \qquad 9) \qquad (5.2\text{-}10)$$

Solutions of this type have also been presented by other authors, with only slight variations in the constant (Geddes [44], Ward et al. [11, 45], Griffith [42]). Their agreement with experimental results appears to be satisfactory [11].

Although all these equations were derived for a sphere, they are applied also to spheroids in the absence of a better solution.

To provide some concrete examples, values of α calculated from eqn. (8) and (4a) for air bubbles in water are given in Table 1. The values for d_B and v_B correspond to the first three bubbles in Table 9-1.

TABLE 5.2-1. AIR BUBBLES IN WATER AT 20°C /69

d_B [cm]	v_B [cm/s]	Re	α acc. to eqn. (8)	$\sqrt{\alpha}$ acc. to eqn. (8)	$\frac{\mu_o}{\mu_i}\sqrt{Re}$	α acc. to eqn. (4a)
0.05	6	29.7	0.455	0.675	300.5	0.9994
0.1	14.6	144.6	0.753	0.869	662.5	0.9999
0.5	23.0	1139	0.912	0.955	1860	0.99998

9) This formula is valid for Re < 1 and a thin concentration boundary layer for the outer phase of the interface.

While eqn. (4a) supplies improbably high α values, the values derived from eqn. (8) seem plausible. The number for $d_B = 0.05$ cm is probably incorrect, because eqn. (8) is valid only for high Reynolds numbers if α is not too different from one.

In view of the theoretical precepts on which the equations discussed here are based, and in view of the numerical examples given above, it appears that eqn. (9) can be recommended for low Reynolds numbers, and eqn. (8) for high Reynolds numbers, while the correctness of eqn. (4) -- intended to be valid over a wide range of Re [35] -- is a matter of some doubt. Further clarification of this point would, of course, require experimental verification, which would be possible only with the aid of refined measurement techniques.

6. Cylindrical Bubbles Rising in Vertical Tubes ("Tube Bubbles") /70

If bubbles rising in tubes are large enough relative to the diameter of the tube, they assume a more or less cylindrical shape: the front end is spherical and the rear end is flat. For simplicity, such bubbles will henceforth be referred to as "tube bubbles." Since the shape and the velocity profile at the surface of such bubbles have already been the object of a great deal of theoretical and experimental work [1, 14, 15, 16, 17], we shall cite only those results which are necessary for our calculations.

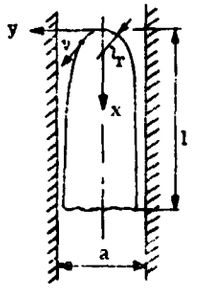

Fig. 6-1. Shape of the tube bubble.

The bubble shape is shown in Fig. 1. It is spherical on top and widens to approach the wall of the tube toward the bottom. The bubble contour relative to the diameter of the tube is independent of this diameter and of the length of the bubble. Van Heuven and Beek [13] have established an arc with the radius

$$r = 0.35\ a \qquad (6\text{-}1)$$

for the upper part of the bubble, and an hyperbola for the lower part, tangent to the circle and asymptotic to the wall of the tube. With a as the characteristic length, we thus obtain for the bubble contour (X and Y are dimensionless coordinates): /71

$$Y = \sqrt{0.7\,X - X^2} \qquad (6\text{-}2)$$

$$Y = \frac{0,7 \cdot \sqrt{2} - 1,245}{4(X + 0,15)} + 0,5 = -\frac{0,063762\ 62665}{X + 0,15} + 0,5 \qquad (6\text{-}3)$$

with the point of contact given as

$$X = 0.35\ (1 - 1/\sqrt{2}) = 0.10251\,26267 \qquad (6\text{-}4)$$

Of course, this is a somewhat simplified representation of the bubble shape, but these equations are precise enough for our calculations. Davis and Taylor [1] and Dumitrescu [14] suggest slightly different equations, but the difference is quite small in practical terms. A much more precise analysis of the bubble shape and velocity profile in the liquid may be found in the study by Kouremenos [16].

Regarding the velocity profile at the interface, it is assumed that the surface forces and the viscosity forces are negligible, which is generally true in most practical cases. But then if we consider Bernouill's equation and the fact that the pressure within the bubble is constant, we are lead to the simple relation

$$v = \sqrt{2\ gx} \tag{6-5}$$

The characteristic velocity is

$$v_c = \sqrt{2\ ga} \tag{6-6}$$

so:

$$v = \sqrt{X} \tag{6-7}$$

The calculations were made with equations (2), (3), (4) and (7) for various values of 1/a; mass transfer at the flat rear surface of the bubble was ignored. The results are summarized in Table (11) and shown graphically in Diagrams (12) and (13). Also given in Table (11) in dimensionless form are the equivalent diameter, surface area and volume of the bubble. Corresponding to the chosen characteristic length and characteristic velocity, /72

$$B = \beta \sqrt[4]{\frac{a}{2g}} \tag{6-8}$$

and

$$\omega = \sqrt{s} \sqrt[4]{\frac{a}{2g}} \tag{6-9}$$

Since all the bubbles have the same contour and the same velocity profile, regardless of bubble length, the local value of B is independent of bubble length. The local B values are given in Table (14) as a function of X and ω and shown graphically in Diagram (15). It can also be shown that the distribution of B values has the following property:

$$\lim_{X \to 0} B(X, \omega) = \omega \tag{6-10}$$

In qualitative terms, the diagrams correspond to our expectations. In Diagram (16), $\overline{B} \cdot F^*$ is shown as a function of 1/a, together with points plotted by van Heuven and Beek [13] and the theoretical curve computed by Beek and Kramers [18]. The curve

for ω = 0 is consistently ca. 16% higher than that of Beek and Kramer.

This diagram is discussed in greater detail in Chapter 8.

7. Large Spherical Cap Bubbles

/73

When a bubble attains a certain volume, it assumes the form of a spherical cap in an unperturbed liquid (see, for example, [1], [4], [9] and [20]). According to investigations by Tadaki and Maeda [9], this occurs whenever

$$Re \cdot M^{0.23} > 16.5^{1)} \qquad (7\text{-}1)$$

$$M = (g \cdot \mu_{fl}^4)/(\rho_{fl} \cdot \sigma^3)$$

where all bubbles are similar and have an eccentricity E = b/h = 3.5, corresponding to an angle $\Theta = 59.5^\circ$ (cf. Fig. 1). Other authors [2, 5] have assumed a mean angle of $\Theta = 50^\circ$, based on the classic investigations by Davis and Taylor [1], who found values for Θ between 46° and 64°. But such measurements are subject to a certain degree of error for the following reasons:

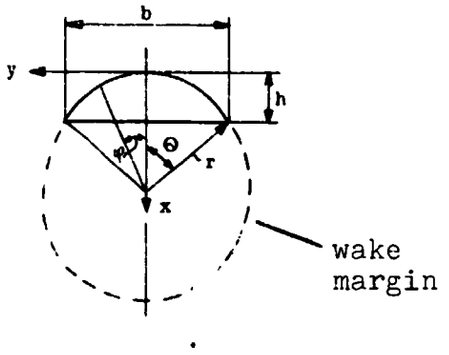

Fig. 7-1. The shape of a large bubble.

a) As we shall see, the contour is theoretically not a precise circular arc; also, the rounded rim at the separation point makes the determination of r certain. /74

b) Any slight fluctuations in shape (which are very common) will automatically result in a pronounced scatter of Θ values determined from still photographs[2)].

---

1) Based on eqn. (9-4) and the value of r/d_B given in Tab. 17 for $\Theta = 60^\circ$, the diameter d_B = 1.75 cm in water at 20°C.

2) Cross-sectional photographs of large CO_2 bubbles in water show significant fluctuations in bubble shape [7]. Although the side photographs made by Davis and Taylor [1] of air bubbles in nitrobenzene suggest that these bubbles have more stable shapes, no relationship can be found between the measured values of Θ and the volume of the bubble.

It is not very important, incidentally, that the angle Θ be precisely known for mass transfer calculations, because the error in the measured values is much greater than the differences between the theoretical curves computed for various values of Θ (cf. Diagram (20)).

As has been pointed out by a number of researchers (viz. [1] and [5]), spherical cap bubbles are given a full spherical shape by a wake region (cf. Fig. 1). The exact structure of the wake region not known, but the research work of Collins [5, 6] strongly suggests that this region consists of a large toroidal vortex. Baird and Davidson [2] have observed that in the absorption of CO_2 bubbles in water, large bubbles of this type exhibit a mass transfer coefficient which decreases with time, while that of smaller bubbles ($d_B < 2.5$ cm) is constant. They tried to explain this behavior by theorizing that the large bubbles are trailed by a closed wake region which is gradually saturated, while the dead zone of smaller bubbles is repeatedly renewed. This explanation is lent support by the investigations of Calderbank and Lochiel [7]; these researchers made overhead photographs of CO_2 bubbles rising in water and obtained very irregular cross-sections in the range 1.4 cm $\leq d_B \leq$ 1.8 cm, suggesting extreme fluctuations in bubble shape. Of course, under such conditions a stable dead zone is improbable.

Cross-sectional photographs of bubbles with $d_B > 2.4$ cm show much milder irregularities, and Calderbank and Lochiel have even reported that these bubbles are stable spherical caps (they made no observations in the range 1.8 cm $\leq d_B \leq$ 2.4 cm). Since the flow about these large bubbles is inhibited neither by frictive forces nor surface tensions, the flow about the bubble/wake sphere should, in the case of stable wake eddies, correspond to the potential flow about a spherical body. The velocity distribution on the bubble surface would then be /75

$$v = 1.5 \cdot v_B \cdot \sin \varphi \qquad (7\text{-}2)$$

On the other hand, Bernoull's equation is valid, and if we allow for the fact that the pressure is constant within the bubble, we obtain from this equation the relation

$$v = \sqrt{2\,gx} = \sqrt{2\,gr\,(1 - \cos\varphi)} \qquad (7\text{-}3)$$

If the velocity of rise

$$v_B = 2/3\ (\sqrt{g \cdot r}) \qquad (7\text{-}4)$$

determined theoretically by Davis and Taylor is inserted into eqn. (2), we find that the difference between this velocity and eqn. (2) is practically negligible up to $\varphi = 20^\circ$, and amounts to no more than about 10% with $\varphi = 50^\circ$. Nevertheless, an obvious contradiction is involved here, and it is hardly proper to arbitrarily switch from eqn. (2) to eqn. (3) when making mass transfer calculations.

The answer to this questions is found in a study by Collins [5], in which a perturbation calculation is used to show that the bubble contour is not a true circle, but deviates from a true circle only slightly[3]. This means that eqn. (2) is only an approximation, while eqn. (3) is exact and even independent of bubble shape (e.g., the velocity profile was also $v = \sqrt{2\,gx}$ for the tube bubbles discussed in Chap. 6). Because eqn. (2) deviates from eqn. (3) to a much greater degree than the bubble contour from a circular arc, we shall use eqn. (3) for mass transfer calculations, while continuing to describe the bubble contour as a circular arc. /76

This information may be put into more explicit terms by saying:

The bubble will assume that shape for which the velocity prescribed for the surface by eqn. (3) is produced by the potential flow about the bubble and the wake region.

From eqn. (4) or (4a) we obtain

$$Fr = \frac{v_B^2}{g \cdot r} = \text{const.} \tag{7-5}$$

Because the shape and velocity of rise of these bubbles are determined solely by inertial and gravitational forces, Fr is the only dimensionless factor. According to the theoretically determined equation shown above, Fr has a constant value, which means that all the bubbles should be similar in shape. That most researchers assume a constant, though not always the same, value for θ in their theoretical calculations is thus completely justified from a dimensional standpoint.

The mass transfer calculations were performed for $\vartheta = 20^\circ$, 30°, 40°, 50° and 60°. Using the characteristic variables

$$l_c = d_B \qquad v_c = \sqrt{2\,g\,d_B} \tag{7-6}$$

and

we obtain for the dimensionless bubble contour and velocity distribution

$$Y = \sqrt{2\,(r/d_B)\,X - X^2} \tag{7-7}$$

$$V = \sqrt{X} \tag{7-8}$$

---

3) The calculations lead to

$$v_B = 0.652\sqrt{g \cdot \bar{r}} \tag{7-4a}$$

as the second approximation instead of eqn. (4), where $\bar{r}$ is the mean radius of curvature of the bubble contour.

and for B and ω /77

$$B = \frac{\beta}{\sqrt{D}} \sqrt[4]{\frac{d_B}{2g}} \qquad (7\text{-}9)$$

$$\omega = \sqrt{8} \sqrt[4]{\frac{d_B}{2g}} \qquad (7\text{-}10)$$

The results of the calculation are summarized in Table (17) and Diagrams (18), (19) and (20), where only mass transfer at the front surface is taken into consideration -- primarily because the velocities at the flat lower surface are unknown[4]. In Table (17), $\overline{B}$ is given as a function of θ and ω, together with some data on bubble geometry[5]. This time the local value of B was not shown as a function of X, because the variation is very small (about 14% at $\theta = 60^{\circ}$); in addition, the shape of the curves is similar to that for tube bubbles (cf. Diagram (15)). The curve derived from the theory of Lochiel and Calderbank has also been drawn into Diagram (18); the curve for $\omega = 0$ is about 24-26% higher than that of Lochiel and Calderbank over the entire calculated range, although the results for the tube bubble would lead one to expect a difference no greater than about 16%. Diagram (20) is discussed in more detail in Chapter 8.

8. Comparison of Results Derived in This Study for Bubbles in Steady-State Rise with Some Experimental Results Known from the Literature and with Other Theoretical Solutions /78

Diagrams (16) and (20) present some data taken from the literature, together with curves derived from our theoretical solutions and those of other authors. All data are based on the absorption of CO_2 bubbles in water, i.e. on a process in which mass transfer in the liquid phase is the only factor to be considered.

The curves computed for bubbles rising in tubes are compared with measurements made by van Heuven and Beek [13] in Diagram (16). The plotted points and the theoretical curve calculated by the authors according to Beek and Kramers [18] were taken from Fig. 10

---

4) Because a dead zone is generally characterized by significantly smaller velocities than the external flow, one would expect less mass transfer at the lower part of the bubble; and while turbulence in the wake region could increase this exchange, most researchers assume that almost all mass transfer takes place at the front surface.

5) Since it can be proved mathematically that

$$\lim_{\theta \to 0} \overline{B} = \omega \qquad (7\text{-}11)$$

the curves were added to Diagram (18) up to $\theta = 0$, although this case is not physically possible.

in [13][1]; only the ordinates had to be recalculated by an appropriate factor. Since the diameter of the tube used in these experiments was only 0.48 or 0.238 cm, there was certainly no turbulence present, so the curve for $\omega = 0$ should be valid. Although the points of the curve exhibit a pronounced scatter, they seem to be more in agreement with the theoretical curve derived by Beek and Kramers [2]. The curve for $\omega = 0$ is consistently ca. 16% higher than this curve.

It should be pointed out that van Heuven and Beek have determined experimentally that the phase boundary on the lower part of the front surface either stagnates or flows very slowly; by ignoring this portion and considering the bubble length to be the true length minus the stagnating portion, they have achieved good agreement with the theoretical curve. If the complete bubble length is considered, the points are shifted to the right and thus fall below the two theoretical curves (cf. Fig. 5 in [13]). Under conditions such as these, it is questionable to compare these experimental results with the theoretical curves, because the basic assumption for both theoretical solutions was that surface tension and viscosity were not a factor. If a portion of the surface is rigid or very highly retarded, surface tension gradients must be present, and these are likely to influence the velocity at points where the phase boundary is still mobile. Thus, the uncertainty in experimental results is probably greater than the difference between the two theoretical solutions. On might say, however, that they confirm the accuracy of both theories in terms of order of magnitude[3]. /79

Some results from the literature regarding the absorption of CO_2 bubbles in water [2, 7, 8] are presented in Diagram 20, along with various theoretical curves. Data gathered by Baird [8] and Calderbank and Lochiel [7] were taken from Fig. 7 of the latter article. The points found by Baird and Davidson [2] are from Fig. 5 of their paper, but they had to be recalculated because these

---

1) Due to the small scale, only abscissa values were taken from Fig. 10. Since Fig. 5 has a larger scale and contains the same plotted points (which are only shifted somewhat in the direction of the abscissa w.r.t. Fig. 10), the ordinate values and coordinates of the theoretical curve were taken from Fig. 5.

2) It can be shown that the theoretical solution of Beek and Kramers [18] and of Lochiel and Calderbank [19] are identical for freely rising rotationally symmetrical surfaces (see Appendix, Chap. 10.3).

3) There is another reason why the experimental results yield smaller values for $\bar{B}$ than theoretical solutions: Enrichment occurs in the liquid film surrounding the bubble, which lowers the concentration gradient; but B was calculated with the original gradient. Estimates show that such an effect is likely in the experiments of van Heuven and Beek.

authors relate $\bar{\beta}$ to the surface area of the equal-volume sphere.

The points in Diagram (20) indicate values of $\bar{\beta}$ relative to the total surface area of the spherical cap bubble, while the theoretical curves apply only to the front surface. Three curves were plotted for $\Theta = 67.4^{\circ}$ ($E = b/h = 3$), because this value was found experimentally by Calderbank and Lochiel[4], and one curve for $\Theta = 50^{\circ}$, because this is the value used by Baird and Davidson. /80

The diffusivity was calculated according to Spalding [21] for $\vartheta = 20^{\circ}$ C; D was found to equal 18.10^{-5} cm^2/s. Curve "d" was taken directly from Fig. 7 of lit. [7]. It was computed using the velocity profile defined by eqn. (7-2), the authors using their own measured values for v_B (reduced velocity of rise due to proximity of tube wall). The surprisingly large scatter exhibited by the measured values does not permit a clear interpretation of the results, although a few conclusions can be drawn:

If one of the theoretical curves "a", "b", "c" or "d" were correct for purely laminar flow, and if turbulence were exerting a particular influence on the transfer of material, then all the plotted points would have to lie considerably above the curve in question. Since this is not the case in any of the four curves, it can be concluded that these experiments were not influenced to a significant degree by turbulence. While there are two groups of curves which lie somewhat above "c" and "d", Calderbank and Lochiel [7] cite some reasons for this, which will now be discussed.

Calderbank and Lochiel explain the experimental results and the position of curve "d" as follows:

a) Their plotted points in the range 1.4 cm $\leq d_B \leq$ 2 cm lie above curve "d", because this is a transition zone in which the bubble is not yet a stable spherical cap, but exhibits large, irregular fluctuations in shape[5] which increase mass transfer, particularly at the lower end of the bubble.

---

4) Their column had a diameter of only 4", making effects of the tube wall noticeable. This led not only to a reduction in the velocity of rise -- also pointed out by the authors themselves -- but apparently to greater bubble curvature, resulting in a larger angle Θ.

5) Values for the diameter at which the bubbles are spherical caps in water at 20° C are given in the literature as $d_B = 1.7 \sim 1.8$ cm [3,4], and the value calculated in Chap. 7 from eqn. (7-1) verifies this data. In reality, of course, there is a gradual transition from the unstable spheroid to the stable spherical cap.

b) Their points are also higher than curve "d" in the region above $d_B = 2.8$ cm. They attribute this to the perturbations caused at the lower surface of the cap by the smaller bubbles observed in the wake region. /81

c) The rest of the points lie below curve "d" because this curve applies only to the front surface, while the $\overline{\beta}$ points apply to the entire surface of the spherical cap bubble.

Since the bubbles are rising in an otherwise still liquid, turbulence can be produced only by the motion of the bubble itself. Moreover, the front surface is dominated by potential flow, so that there are no tangential stresses which could produce turbulence. Only in the wake region or in the adjacent free boundary layer can such stresses arise. It can therefore be assumed that either curve "a" or curve "c" (Θ given as 67.4°) applies to the front surface of the bubble. Smaller $\overline{\beta}$ values may be expected for the lower surface of the bubble, provided turbulence is minimal, since the velocities are smaller in the wake region. Point c) of the preceding paragraph tends to support this reasoning. If we set aside the two groups mentioned under a) and b) as special cases, the following estimation may be made for the scatter region of the remaining points[6]:

If it is assumed that there is no transfer of material at the bubble floor, the points plotted for the front surface would have to be raised by about 90%. Most would then lie above "a". For the center of the scatter region to fall roughly on curves "a" and "b", $\overline{\beta}$ on the bubble floor would have to be about 36% of the $\overline{\beta}$ value of the front surface; and for it to fall roughly on curve "c", $\overline{\beta}$ on the bubble floor would have to be about 66% of the $\overline{\beta}$ value of the front surface.

Although this estimation does not indicate whether curve "a" or "c" is the better one for the front surface, it does tell us that $\overline{\beta}$ on the bubble floor is considerably smaller than $\overline{\beta}$ on the front surface. This means that there are no significant turbulence effects on the bubble floor. In this case, therefore, the hope that experimental results could be better explained by /82 the introduction of a turbulence-dependent variable ω is in vain. If an appreciable turbulence effect is at all present, it will be of roughly the same magnitude as the scatter of the measured values. The large spherical cap bubbles are, incidentally, the very type of bubble for which a turbulence effect would seem most likely. It does not appear worthwhile, therefore, to introduce a turbulence variable such as ω when dealing with bubbles in steady-state rise[7].

---

6) A spherical cap with $\Theta = 60^\circ$ was assumed for the calculations.

7) To my knowledge, no researcher has considered it necessary to make allowance for turbulence in bubbles in steady-state rise. It was done here because our theory is based on a generalization of a formation theory in which turbulence plays a large role.

Still, an interesting conclusion can be drawn from the theory presented here which lends support to the experimantal observation that there is no marked turbulence effect in bubbles in steady-state rise. This conclusion is discussed in detail in Chapter 9. The situation is different, of course, if surface turbulence occurs, for it is well known that this type of turbulence can increase mass transfer to a significant degree. The applicability of our theory to this phenomenon is discussed in Chap. 11.

As for the laminar solution ($\omega = 0$), we have seen that our theory yields higher transfer coefficients than the theory of Lochiel and Calderbank [19] -- 12-46% higher for a spheroid [8], 16% for a cylindrical tube bubble, and 24-26% for a spherical cap. The investigated experimental results for tube bubbles and spherical cap bubbles (Diagrams (16) and (20)) suggest that our theory leads to transfer coefficients which are too high, although this is not certain. In any case, the theory of Lochiel and Calderbank [19] is recommended as the better theory because it has a better physical foundation. It is derived from the steady-state transport equation, in which allowance is also made for the convective terms. Our theory is based on the unsteady-state unidimensional diffusion equation, where the effects of bubble shape and velocity at the interface are taken into account by the laminar surface-renewal model. While this model may seem to be a plausible assumption, it cannot be derived from physical laws, and it contains an assumption which has no counterpart in reality: that a surface element is comprised of still smaller surface elements of varying age, and that at each of these elements the concentration distribution normal to the phase boundary surface is exclusively dependent on age, i.e. remains unaffected by the concentration distribution above an adjacent element. Another weakness of this theory is that it is valid only for sliding boundary surfaces and breaks down completely in the case of rigid or "strongly retarded" boundary surfaces. By contrast, the theory of Lochiel and Calderbank permits a steady transition from mobile to rigid boundary surfaces. /83

Under these circumstances it is not worthwhile to compare our results further with those from the literature. We shall, however, point out two studies which contain mass transfer data for drops and bubbles [10, 11, 12], and two others in which additional references may be found [3a, 22].

9. Theoretical Results Concerning the Influence of Turbulence on Mass Transfer for Bubbles in Steady-State Rise /84

According to eqn. (3.2-15),

---

8) Possible reasons for the relatively large discrepencies in the case of oblate spheroids were discussed in Chap. 5.1.

$$\left(\frac{\partial B}{\partial \omega}\right)_{\omega=0} = 0 \qquad (9\text{-}1)$$

which can also be seen from the calculated sets of curves (cf. Diagrams (3), (13) and (19)). Since B is the dimensionless mass transfer coefficient and ω is a dimensionless turbulence parameter, the meaning of this equation can be formulated as follows:

Minor turbulence has no significant effect on mass transfer.

To clarify what is meant by "minor turbulence," Table 1 gives some data on bubbles rising in water. Bubble dimensions were chosen according to Grassmann's Diagram 10.11.5 in such a way that the assumed sliding of the phase boundary would be possible and that the dimensions would fall into different characteristic areas. Bubbles 1 and 2 are spherical, bubble 3 is spheroidal[1], and bubbles 4 through 6 are spherical caps. The v_B values given in column 4 were calculated either by the formulae in [4] or according to Collins [5]:

Bubbles 1 and 2:
$$v_B = 0{,}33\, g^{0{,}76} \left(\frac{\rho_{fl}}{\mu_{fl}}\right)^{0{,}52} \left(\frac{d_B}{2}\right)^{1{,}28} \qquad (9\text{-}2)$$

Bubble 3:
$$v_B = 1{,}35 \sqrt{\frac{\sigma}{\rho_{fl}\,(d_B/2)}} \qquad (9\text{-}3)$$

Bubbles 4, 5 and 6:
$$v_B = 0{,}652 \sqrt{g\,\bar{r}}\ ^{2)} \qquad (9\text{-}4)$$ /86

The last equation is the corrected equation of Collins [5]; the equation of Davis and Taylor [1] also given in [4] is of a similar form, except that the factor on the left-hand side is slightly different. For simplicity, Θ was assumed to equal 60° for bubbles 4 through 6 (half the stress angle of the spherical cap), because this value is almost identical to that indicated by Tadaki and Maeda [9] ($E = 3.5$, $\Theta = 59.5^\circ$). Since potential flow was assumed, the ω values given in column 5 were taken from Diagrams (3) and (19). We can than calculate s from the relations

$$s = \omega^2 \frac{v_B}{d_B} \qquad \text{(bubbles 1-3)} \qquad (9\text{-}5)$$

$$s = \omega^2 \sqrt{\frac{2g}{d_B}} \qquad \text{(bubbles 4-6)} \qquad (9\text{-}6)$$

---

1) Path of bubble rise helical or zig-zag; this should have been allowed for in Table 9-1 by a corresponding increase in v_B, but was not for the sake of simplicity.

2) $\bar{r}$ signifies the mean radius of curvature, because the bubbles are not true spherical caps according to Collins' calculations.

TABLE 9-1. GAS BUBBLES IN PURE WATER AT 20° C
Characteristic Parameters of Turbulent Surface Renewal for Bubbles of Various Dimensions for the Case of a 5% or 10% Increase in the Mass Transfer Coefficient

[When two numbers appear in the same square, the top number refers to 5%, the bottom number to 10%.]

/85

***)

1	2	3	4	5	6	7	8	9
Charakteristische Bezeichnung →					"Turbulente Erneuerung"	"Laminare Erneuerung"	"Erneuerungsverhältnis"	"Spezifische turbulente Erneuerung"
No. ↓ Shape	d_B [cm]	E	v_B [cm s^{-1}]	ω	s [s^{-1}]	v_B/d_B [s^{-1}]	$s\frac{d_B}{v_B}$	$1-e^{-s\,d_B/v_B}$
1 ○	0,05	1	6,01	0,45 0,65	24,3 50,8	120,2	0,202 0,423	0,183 0,344
2 ○	0,1	1	14,55	" "	29,4 61,3	145,5	" "	" "
3 ○	0,5	1,5 *)	23,03	0,50 0,73	11,5 24,5	46,06	0,250 0,532	0,221 0,4125
4 ⌓	2,5	≈3,5	31,1	0,37 **) (0,555) 0,535 (0,802)	3,835 8,01	12,44	0,308 0,644	0,265 0,474
5 ⌓	5		44,0	" "	2,71 5,66	8,80	" "	" "
6 ⌓	7,5	"	53,9	" "	2,213 4,63	7,19	" "	" "

Key

*) This value of E was computed to simplify the calculation, although E could also be calculated according to Tadaki and Maeda [9].

**) ω was defined as $\sqrt{s\ \sqrt[4]{d_B/2g}}$ for spherical cap bubbles and as $\sqrt{s\ d_B/v_B}$ for spherical and spheroidal bubbles. If the ω values for spherical cap bubbles are recalculated for the latter definition, the numbers in parentheses are obtained (eqn. (4) and the r/d_B value for $\theta = 60^\circ$ given in Tab. 17 were used for recalculation).

***) Commas in tabulated material are equivalent to decimal points.

Col. 1: Characteristic Notation
Col. 6: "Turbulent Renewal"
Col. 7: "Laminar Renewal"
Col. 8: "Renewal Ratio"
Col. 9: "Specific Turbulent Renewal"

The variables given in columns 6 through 9 have the following physical significance:

s: The new surface produced by turbulent vortices per unit of time and surface (surface renewal rate).

v_B/d_B: Indicates the number of times the bubble travels the length of its equivalent diameter in one unit of time. This parameter is to a certain extent characteristic of the laminar surface renewal rate, although it is probably not a single-value coefficient, a point which will be discussed later.

$s \frac{d_B}{v_B}$: Characteristic parameter for the ratio of turbulent to laminar surface renewal (only to the extent, of course, that v_B/d_B is characteristic of laminar surface renewal). /87

$1 - e^{-s\frac{d_B}{v_B}}$: Portion of the surface which is renewed in the time d_B/v_B by turbulent vortices; i.e. in the time required for the bubble to travel the length of its equivalent diameter[3].

In Table 1 these parameters are identified with names in quotation marks. These names are intended to express that which is characteristic of the corresponding parameter; but since they are used only in conjunction with this table, they will always be in quotation marks when referred to. The numerical values in the Table provide the following information:

1.) To achieve a particular percentage increase in the mass transfer coefficient, a certain value of ω is required for each bubble type which increases slightly with bubble eccentricity (the values adjusted to fit the same definition).

2.) "Turbulent renewal" and "laminar renewal" vary over the investigated range of diameters by more than a factor of 10.

3.) The "renewal ratio" and the "specific turbulent renewal" which is determined by it vary little; they increase slightly with increasing eccentricity. This is, incidentally, a direct consequence of point 1.), since if ω is defined as $\sqrt{s \cdot d_B/v_B}$, the "renewal ratio" is equal to ω^2 (cf. footnote ** in the Table).

---

3) It is clear from eqn. (2.1-12) that a surface of age τ^* has only one component $\exp(-s\tau^*)$ which was not yet renewed since its creation by turbulent vortices. Since we are regarding the bubble surface in one instant as completely new, after time $\tau^* = d_B/v_B$ only the component $\exp(-s \cdot d_B/v_B)$ will not be renewed.

These facts make it likely that a particular ratio must exist between turbulent and laminar renewal in order to achieve a, say, 10% increase in mass transfer through turbulence, regardless of bubble dimensions.

This statement seems so plausible in a physical sense that one might wonder why it is not strictly true, i.e. why the dimensionless parameters in columns 5, 8 and 9 are not constant for different bubble shapes. I believe that the answer lies primarily /88
in the fact that v_B/d_B is a parameter which provides only a very crude characterization of laminar surface renewal. A better parameter would probably be surface current density $\dot{f}$ (cf. eqn. (3.1-2)) or the value $\bar{\dot{f}}$ averaged over the surface. In this case, the quotient $s/\bar{\dot{f}}$ would have to be used in place of $s \cdot d_B/v_B$, and defined as

$$\omega = \sqrt{s/\bar{\dot{f}}} \qquad (9\text{-}7)$$

Unfortunately, however, this definition also involves certain complications, since taking the average of $\dot{f}$ is meaningful only at that part of the bubble where $\dot{f} \geq 0$[4], while $\bar{B}$ is calculated by taking the average over the entire surface. In spherical and spheroidal bubbles, $\dot{f} \geq 0$ on only half the surface, while in spherical cap bubbles $\dot{f}$ is positive everywhere (calculations involved the front surface only, with no allowance made for the fact that there is a stagnation point at the separation point). On this basis, therefore, only those bubbles for which $\dot{f}$ is positive over an equal portion of the surface can be compared. Let us take bubbles 2 and 3 as examples. When we consider "specific turbulent renewal," we see that, in order to increase the mass transfer coefficient by 5%, 18.3% of the surface of bubble 2 must be renewed by "turbulent renewal" in the time required for the bubble to travel the length of its own equivalent diameter; this figure is 22.1% for bubble 3. In order to achieve the same effect, therefore, the "specific turbulent renewal" must be greater for bubble 3; i.e., if v_B and d_B were equal, s itself would have to be greater. If the assertion made in the last paragraph is more valid than the figures in Table 1 would indicate, and $\dot{f}$ is actually a better parameter for laminar surface renewal than v_B/d_B, it follows that $\bar{\dot{f}}$ must be greater for bubble 3 than for bubble 2. To test this, the values of $\bar{\dot{f}}$ would have to be calculated for both cases; but due to the complex mathematical derivations involved, this was not done. The somewhat speculative observations made in this paragraph are thus intended as a guide for a possible interpretation.

---

4) The value of $\dot{f}$ averaged over the entire bubble surface must be equal to zero, because exactly as much new surface must be created as old surface is lost.

The principal purpose of this Chapter was to clarify our theory on turbulence effects with the aid of a concrete example. The 5% or 10% increase in mass transfer assumed in Table 1 is not usually noticeable due to the large scatter of measured values. Yet this small increase requires a ca. 20-40% "specific turbulent renewal" (cf. column 9), i.e. relatively high values. The reason for this can be readily explained on the basis of the mathematical solution obtained. Let us examine the diagram in Fig. 3.2-2, where B is shown schematically as a function of ω (see examples calculated for $\overline{B}(\omega)$ in Diagrams (3), (13) and (19)). The ordinate B of any point is comprised of two lengths B_1 and B_2, where B_1 is the ordinate value of the asymptote $B = \omega$, corresponding to Danckwert's solution $\beta = \sqrt{s \cdot D}$. We reach this solution with our model if we assume that, while a turbulent surface renewal is present, the bubble itself is unperturbed, i.e. B_1 is the purely turbulent component of B, while B_2 designates an additional increase in mass transfer by laminar surface renewal. B_2 is largest for $\omega = 0$, and approaches zero as ω increases. The effects of laminar and turbulent surface renewal on mass transfer are therefore not additive. When turbulent renewal appears, the effect of laminar renewal is first reduced to the same degree, and only when turbulence strengthens will the effect of turbulent surface renewal become predominant.

/89

In order to better illustrate the turbulence intensity required for an appreciable increase in mass transfer, we shall examine bubble 3 from Table 1. To increase mass transfer at this bubble by 10%, the turbulence must renew about 40% of the entire bubble surface within the short time of $d_B/v_B \approx 0.02$ sec (cf. column 7). This appears to be a very intense turbulence. If we also consider that according to our model the surface renewal required should be produced by small vortices (i.e. at least small with respect to d_B), and that according to Levich [24] the small vortices have little chance of reaching the surface due to the damping effect of surface forces, it seems very unlikely that hydrodynamic turbulence could have an effect on mass transfer in bubbles of this size. Turbulence is much more likely to be a factor in the case of very large bubbles, such as those formed by an underwater explosion. The situation is different for surface turbulence, which will be discussed in Chap. 11.

If the results obtained are put into a somewhat more general form, we might say:

/90

When intense laminar surface renewal occurs -- e.g., in the case of large, rapidly rising bubbles -- small, irregular surface fluctuations have no effect on mass transfer.

Here we are speaking of smaller surface instabilities not necessarily produced by turbulent vortices, such as capillary waves or other local oscillations. The above assertion is based on the following reasoning: Small fluctuations produce no

significant perturbation in the field of streamline flow, but only a local expansion and contraction of the surface, by which new surface is continuously created and old surface vanishes. The increased mass transfer which may result will be maximal when the newly created surface has the concentration of the liquid core (which is not likely). This, however, is a case of surface renewal which can be described just as well by s as renewal by turbulent eddies; therefore, the model can be applied. Should the fluctuations grow larger, the field of flow surrounding the bubble will also be perturbed, in which case mass transfer could be significantly increased. For example, cross-sectional photographs of large CO_2 bubbles in water ($d_B \approx 2.5$ cm) show irregularities amounting to about 10% of the cross-sectional diameter [7], while no appreciable increase in the mass transfer coefficient can be determined. On the other hand, smaller bubbles which undergo extreme fluctuations in shape exhibit a distinct increase in the mass transfer coefficient (see bubbles in range $1.4 \leq d_B \leq 2$ cm in Fig. 7 of [7], or in Diagram (20)).

In conclusion, it should be mentioned that there are a number of theories in the literature which account for turbulence with the aid of a more or less complicated model of surface renewal [25-32]. The effect of small eddies (small relative to the concentration boundary layer) is often taken into account by an "eddy diffusivity" which increases with the distance from the phase boundary and is added to the diffusion coefficient for molecular diffusion; a model of this type can also be combined with a surface renewal model [30]. There have also been a number of attempts to relate the parameters of a model (s in our theory) /91
to such hydrodynamic parameters as viscosity, surface tension and dissipation [30, 24, 23]. The theory presented in this paper is unique in that it accounts for both turbulent and laminar surface renewal. Our theory predicts a constant value of 0.5 for the exponent in the often-used power relation

$$\beta \sim D^n$$

This value is usually accurate for rising and circulating bubbles (for which our theory was developed), although the exponent generally varies between 0.5 and 1. A number of the models mentioned so far permit such a variation of the exponent.

10. Appendix /92

10.1. Some Properties of the System of Equations (3.2-14)

Differentiating with respect to ω, we obtain from the first equation in (3.2-14)

$$\frac{\partial B}{\partial \omega} = 1 - \frac{\omega}{\sqrt{\pi}} \int_{\Theta_0}^{\infty} \frac{e^{-\omega^2\Theta}}{\Theta^{1/2}} \left[1 - \frac{V(S_1)\,Y(S_1)}{V(S^*)\,Y(S^*)} \right] d\Theta \qquad (10.1\text{-}1)$$

which, with the relation

$$K = 1 - \frac{V(S_1)\,Y(S_1)}{V(S^*)\,Y(S^*)} \qquad (10.1\text{-}2)$$

can be written as

$$\frac{\partial B}{\partial \omega} = 1 - \frac{\omega}{\sqrt{\pi}} \int_{\Theta_0}^{\infty} \frac{e^{-\omega^2 \epsilon}}{\Theta^{1/2}} K \, d\Theta \qquad (10.1\text{-}3)$$

The produce VY will always have its maximum at S*. This follows from the equation defining S* (fifth equation in (3.2-14)), in which it was implicit that V·Y has only one maximum. This is a meaningless restriction, however, since for physical reasons V(S) and Y(S) should each have a first uniformly rising and then uniformly falling curve (cf. Fig. 3.2-1). If this were not the case, there would probably be separation at some point, and the calculation could not be carried out beyond the separation point in any event. We thus have for K

$$0 \leqslant K \leqslant 1 \qquad (10.1\text{-}4)$$

In addition, K will be uniform within the limits of integration, a fact which becomes clear when we consider that

a) If $S < S_0$, Θ varies from $\Theta_0 = 0$ to ∞, while S_1 varies from S to zero, and

b) if $S > S_0$, Θ varies from $\Theta_0 > 0$ to ∞, while S_1 varies from S_0 to zero.

/93

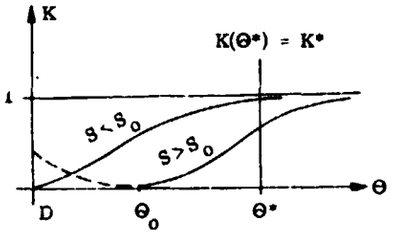

Fig. 10.1-1.

These two cases are shown in Fig. 1. For $S \leq S_0$, K would trace the broken line shown in the Figure between zero and Θ_0, a line which, however, lies outside the region of integration. In any case, we can see that K has a horizontal tangent at Θ_0 ($\Theta_0 > 0$!). For $S < S_0$, on the other hand, the initial tangent will not be horizontal.

Since K can never be greater than 1, it follows from the first equation in (3.2-14) that the second term vanishes for $\omega \to \infty$; we thus have

$$\lim_{\omega \to 0} B(S,\omega) = \omega \qquad (10.1\text{-}5)$$

Thus, for a given value of S, the curve $B(\omega)$ has an asymptote

which passes through zero and has an incidence angle of 45° (cf. Fig. 3.2-1). This curve must also rise uniformly, since an increase in turbulence (ω) cannot result in a reduction in the mass transfer coefficient (B). We thus have for $\partial B/\partial \omega$

$$\frac{\partial B}{\partial \omega} \geq 0 \tag{10.1-6}$$

which can be proved mathematically with eqn. (3). Introducing /94
the symbol

$$\text{Int} = \frac{\omega}{\sqrt{\pi}} \int_{\Theta_o}^{\infty} \frac{e^{-\omega^2\Theta}}{\Theta^{1/2}} K \, d\Theta \tag{10.1-7}$$

it follows from eqn. (3) that

$$\text{Int} \leq 1 \tag{10.1-8}$$

If we choose a value Θ^* such that

$$\Theta^* > \Theta_o \tag{10.1-9}$$

and designate the corresponding value of K as K* (it does not matter whether S is greater than or less than S_o), we may write (cf. Fig. 1)

$$\text{Int} \geq \frac{\omega K^*}{\sqrt{\pi}} \int_{\Theta^*}^{\infty} \frac{e^{-\omega^2\Theta}}{\Theta^{1/2}} d\Theta = \frac{\omega K^*}{\sqrt{\pi}} \int_{0}^{\infty} \frac{e^{-\omega^2\Theta}}{\Theta^{1/2}} d\Theta - \frac{\omega K^*}{\sqrt{\pi}} \int_{0}^{\Theta^*} \frac{e^{-\omega^2\Theta}}{\Theta^{1/2}} d\Theta \tag{10/1-10}$$

Allowing ω to tend to zero, there follows

$$\lim_{\omega \to 0} \text{Int} \geq \lim_{\omega \to 0} \frac{\omega K^*}{\sqrt{\pi}} \int_{0}^{\infty} \frac{e^{-\omega^2\Theta}}{\Theta^{1/2}} d\Theta - \lim_{\omega \to 0} \frac{\omega K^*}{\sqrt{\pi}} \int_{0}^{\Theta^*} \frac{e^{-\omega^2\Theta}}{\Theta^{1/2}} d\Theta \tag{10.1-11}$$

The second member on the right-hand side must vanish, because $\Theta^{\frac{1}{2}}$ yields a finite value when integrated between zero and Θ^*. We are therefore left with

$$\lim_{\omega \to 0} \text{Int} \geq \lim_{\omega \to 0} \frac{\omega K^*}{\sqrt{\pi}} \int_{0}^{\infty} \frac{e^{-\omega^2\Theta}}{\Theta^{1/2}} d\Theta = K^* \tag{10.1-12}$$

Since Θ^* can be arbitrarily chosen, the maximum value of K* is /95
1 (cf. Fig. 1), so

$$\lim_{\omega \to 0} \text{Int} \geq 1 \tag{10.1-13}$$

which together with eqn. (8) leads to

$$\lim_{\omega \to 0} \text{Int} \equiv 1 \qquad (10.1\text{-}14)$$

Inserted into eqn. (3), this yields

$$\boxed{\lim_{\omega \to 0} \frac{\partial B}{\partial \omega} = 0} \qquad (10.1\text{-}15)$$

As we approach the rear stagnation point, Θ_0 tends to ∞, which is immediately evident from the third equation in (3.2-10) and the shape of $I(\sigma)$ in Fig. 3.2-1. In this way the integral in the third equation of (3.2-14) vanishes, and we obtain

$$B(S = S_{\text{stagnation point}}, \omega) \equiv \omega \qquad (10.1\text{-}16)$$

10.2. An Approximation Formula for $B(S,\omega)$ for Small Values of S[1)]

At point S = 0, the function B(S) is expanded into a power series, of which only the first two members are preserved. To do this, the first three equations of system (3.2-14) are used:

$$B(S) = \omega + \frac{1}{2\sqrt{\pi}} \int_0^\infty \frac{e^{-\omega^2\Theta}}{\Theta^{3/2}} \left[1 - \frac{V(S_1)\,Y(S_1)}{V(S)\;Y(S)} \right] d\Theta \qquad (10.2\text{-}1)$$ /96

$$\epsilon = J(S) - J(S_1) \qquad (10.2\text{-}2)$$

$$J(S) = \int_{S_o}^{S} \frac{dS}{V(S)} \qquad (10.2\text{-}3)$$

Since $S < S_0$ for small values of S, the lower limit of integration in eqn. (1) was set equal to zero, and S substituted at once for S* in the brackets (cf. eqn. system (3.2-14)). The brackets are expanded into a power series of Θ after $V(S_1)Y(S_1)$ are first expanded. Designating the inverse function of $J(S)_1$ as J^{-1}, it follows from eqn. (2) that

$$S_1 = J^{-1}\left\{ J(S) - \Theta \right\} \qquad (10.2\text{-}4)$$

A general function $g(S_1)$ can then be expanded into a power series of $-\Theta$ as follows:

---

1) The derivation which follows was suggested by Dr. J. Waldvogel.

$$g(S_1) = g\left[J^{-1}\left\{J(S) - \Theta\right\}\right] = \sum_{k=0}^{\infty} \frac{(-\Theta)^k}{k!} b_k \qquad (10.2\text{-}5)$$

where

$$b_k = \frac{\partial^k}{\partial(-\Theta)^k} g\left[J^{-1}\left\{J(S) - \Theta\right\}\right]\Bigg|_{-\Theta = 0} \qquad (10.2\text{-}6)$$

With the substitution

$$u = J(S) - \Theta \qquad (10.2\text{-}7)$$

eqn. (6) can be written as /97

$$b_k = \frac{d^k}{du^k} g\left[J^{-1}(u)\right] \left(\frac{\partial u}{\partial(-\Theta)}\right)^k \Bigg|_{u = J(S)} \qquad (10.2\text{-}8)$$

Since according to eqn. (7), $\partial u/\partial(-\Theta)$,

$$b_k = \frac{d^k}{du^k} g\left[J^{-1}(u)\right] \Bigg|_{u = J(S)} \qquad (10.2\text{-}9)$$

From this equation we recognize the recursion formula

$$b_{k+1} = \frac{d}{d(J(S))} b_k \qquad (10.2\text{-}10)$$

If we first differentiate with respect to S, eqn. (10) becomes

$$b_{k+1} = \frac{d}{dS}(b_k) \cdot \frac{dS}{d(J(S))} = \frac{db_k}{dS}\left[\frac{d(J(S))}{dS}\right]^{-1} \qquad (10.2\text{-}11)$$

From eqn. (3) we obtain

$$\frac{d}{dS} J(S) = \frac{1}{V(S)} \qquad (10.2\text{-}12)$$

which leads to

$$b_{k+1} = V(S) \frac{d}{dS} b_k \,. \qquad (10.2\text{-}13)$$

when inserted into eqn. (10). According to eqn. (2), $S_1 = S$ for $\Theta = 0$; it thus follows from eqn. (5) that

$$b_o = g(S) \qquad (10.2\text{-}14)$$

Due to the axial symmetry of the bubble, V(S) and Y(S) must be antisymmetrical functions, which can thus be formulated as: /98

$$V(S) = a\,(S - bS^3 + \ldots) \tag{10.2-15}$$

$$Y(S) = S - cS^3 + \ldots \tag{10.2-16}$$

With $g(S_1) = V(S_1)Y(S_1)$, and dividing by $V(S)Y(S)$, it follows from eqn. (5) that

$$\frac{V(S_1)Y(S_1)}{V(S)\,Y(S)} = \sum_{k=0}^{\infty} \frac{(-1)^k \Theta^k}{k!} \frac{b_k}{V(S)Y(S)} \tag{10.2-17}$$

From equations (13) through (16), we obtain for the first coefficients of the series

$$b_0 / \left\{ V(S)\,Y(S) \right\} = 1$$

$$b_1 / \left\{ V(S)\,Y(S) \right\} = 2a \left[1 - (2b + c)\,S^2 + \ldots \right]$$

$$b_2 / \left\{ V(S)\,Y(S) \right\} = 4a^2 \left[1 - 3(2b + c)\,S^2 + \ldots \right]$$

From these coefficients, we can recognize the law

$$b_k / \left\{ V(S)\,Y(S) \right\} = (2a)^k \left[1 - (2^k - 1)(2b + c)\,S^2 + \ldots \right] \tag{10.2-18}$$

which can be easily proved by complete induction. Inserting eqn. (18) into eqn. (17) and that into eqn. (1), we obtain

$$B(S) = \omega + \frac{1}{2\sqrt{\pi}} \int_0^{\infty} \frac{e^{-\omega^2\Theta}}{\Theta^{3/2}} \left[1 - \sum_{k=0}^{\infty} \frac{(-1)^k \Theta^k}{k!} (2a)^k \left[1 - (2a)^k (2^k - 1)(2b+c)S^2 + \ldots \right] \right] d\Theta \tag{10.2-19}$$

Only the first two members of the infinite series are considered; for k = 0, these members yield the value 1, which cancels with the 1 before the summation sign. We can thus write

$$B(S) \approx \omega + \frac{1}{2\sqrt{\pi}} \int_0^{\infty} \frac{e^{-\omega^2\Theta}}{\Theta^{3/2}} (-1) \sum_{k=1}^{\infty} \frac{(-1)^k \Theta^k}{k!} (2a)^k \left[1 - (2^k - 1)(2b+c)S^2 \right] d\Theta \tag{10.2-20}$$

/99

The integration is by parts:

$$B(S) \approx \omega + \frac{1}{2\sqrt{\pi}} \sum_{k=1}^{\infty} \frac{(-1)^{k+1}(2a)^k}{k!} \left[1 - (2^k - 1)(2b+c)S^2 \right] \int_0^{\infty} e^{-\omega^2\Theta} \Theta^{k-3/2}\, d\Theta \tag{10.2-21}$$

From this we first calculate the integral together with several of the factors present:

$$\frac{1}{2\sqrt{\pi}} \frac{(-1)^{k+1}}{k!} \int_0^{\infty} e^{-\omega^2\Theta} \Theta^{k-3/2}\, d\Theta = \frac{1}{2\sqrt{\pi}} \frac{(-1)^{k+1}}{k!} \frac{1}{\omega^{2k-1}} (k-3/2)!$$

Since $(k-3/2)! = \Gamma(k - \frac{1}{2})$, the following expression can be derived for $(k - 3/2)!$ with the aid of the functional equation $\Gamma(x + 1) = x \cdot \Gamma(x)$:

$$(k-3/2)! = \Gamma(k-1/2) = (k-3/2)(k-5/2) \ldots\ldots 3/2 \cdot 1/2 \cdot \Gamma(1/2) = (k-3/2)(k-5/2) \ldots\ldots 3/2 \cdot 1/2 \cdot \sqrt{\pi}$$

Inserted into the above equation and somewhat rearranged, this leads to

$$\frac{1}{2\sqrt{\pi}} \frac{(-1)^{k+1}}{k!} \int_0^\infty e^{-\omega^2\Theta} \Theta^{k-3/2} \, d\Theta = (-1)^k \frac{\omega}{\omega^{2k}} \frac{(k-3/2)(k-1/2)\ldots\ldots 3/2 \cdot 1/2 \cdot (-1/2)}{k!}$$

By multiplying each factor above the second fraction bar by (-1), $(-1)^k$ can be eliminated:

$$\frac{1}{2\sqrt{\pi}} \frac{(-1)^{k+1}}{k!} \int_0^\infty e^{-\omega^2\Theta} \Theta^{k-3/2} \, d\Theta = \frac{\omega}{\omega^{2k}} \frac{1/2\,(-1/2)\,(-3/2)\ldots\ldots(1/2-k+1)}{k!} =$$

$$= \binom{1/2}{k} \frac{\omega}{\omega^{2k}} \qquad (10.2\text{-}22) \qquad (10.2\text{-}22)$$

Inserting this into eqn. (21) and removing the brackets, we obtain /100

$$B(S) \approx \omega + \sum_{k=1}^{\infty} (2s)^k \binom{1/2}{k} \frac{\omega}{\omega^{2k}} - \sum_{k=i}^{\infty} (2^k-1)(2b+c)S^2(2a)^k \binom{1/2}{k} \frac{\omega}{\omega^{2k}} \qquad (10.2\text{-}23)$$

Summation may begin from k = 0 instead of k = 1 and the equality sign omitted, since ω appears in the first sum and zero the second for k = 0.

$$B(S) \approx \omega \sum_{k=0}^{\infty} \binom{1/2}{k} \left(\frac{2a}{\omega^2}\right)^k - \omega(2b+c)S^2 \sum_{k=0}^{\infty} (2^k-1) \binom{1/2}{k} \left(\frac{2a}{\omega^2}\right)^k =$$

$$= \omega \sum_{k=0}^{\infty} \binom{1/2}{k} \left(\frac{2a}{\omega^2}\right)^k - \omega(2b+c)S^2 \left[\sum_{k=0}^{\infty} \binom{1/2}{k} \left(\frac{4a}{\omega^2}\right) - \sum_{k=0}^{\infty} \binom{1/2}{k} \left(\frac{2a}{\omega^2}\right)^k \right] \qquad (10.2\text{-}24)$$

Since according to the binomial series

$$\sum_{k=0}^{\infty} \binom{1/2}{k} u^k = \sqrt{1+u} \qquad (10.2\text{-}25)$$

there follows

$$B(S) \approx \omega\sqrt{1+\frac{2a}{\omega^2}} - \omega(2b+c)S^2\left[\sqrt{1+\frac{4a}{\omega^2}} - \sqrt{1+\frac{2a}{\omega^2}}\right]$$

which leads to

$$\boxed{B(S) \approx \omega^2 + 2a - S^2(2b+c)\left\{\sqrt{\omega^2+4a} - \sqrt{\omega^2+2a}\right\}} \qquad (10.2\text{-}26)$$

Since according to eqn. (15)

$$a = \left(\frac{dV}{dS}\right)_{S=0} \qquad (10.2\text{-}27)$$ /101

it follows from eqn. (24) that

$$\boxed{B(S=0) = \sqrt{\omega^2 + 2\left(\frac{dV}{dS}\right)_{S=0}}} \qquad (10.2\text{-}28)$$

10.3. Identity of the Theoretical Solutions Given by Beek and Kramers [18] and by Lochiel and Calderbank [19] for Mass Transfer at a Sliding Boundary Surface

Beek and Kramers give the following formula for the total material flow at a sliding boundary surface (their eqn. (36)):

$$\phi = 2c_o\sqrt{\frac{D}{\pi}}\left[\int_0^{\tau_e}\left(\frac{dA}{d\tau}\right)^2 d\tau\right]^{1/2} \qquad (10.3\text{-}1)$$

where c_o is the difference in concentration between the boundary surface and the liquid core and A is the total exchange surface up to point x (cf. Fig. 4-1)[1]. τ is defined as

$$\tau = \int_0^{\frac{dx}{u_o}} \qquad (10.3\text{-}2)$$

(their eqn. (18)) and τ_e is the value of τ corresponding to the maximum value of x. The fact that eqn. (2) yields $\tau = \infty$ for $x \neq 0$

---

1) From now on the notation of Lochiel and Calderbank will be used, as in Chap. 4.

(cf. Chap. 3.2) is apparently disregarded here, although this is not important if eqn. (1) is transformed such that x appears as the variable of integration (this is suggested by the authors themselves). From eqn. (2), /102

$$d\tau = \frac{dx}{u_o} \tag{10.3-3}$$

and from the geometry in Fig. 4-1,

$$dA = 2\pi\, r\, dx = 2\pi\, r\, u_o\, d\tau \tag{10.3-4}$$

Dividing eqn. (1) by $A \cdot c_o$ and substituting from eqn. (4) and (5) for $dA/d\tau$ and τ, we obtain

$$\beta = \frac{\phi}{A \cdot c_o} = \frac{2}{A}\sqrt{\frac{D}{\pi}}\left[\int_0^{x_e} (2\pi r u_o)^2 \frac{dx}{u_o}\right]^{1/2} \tag{10.3-5}$$

Making this equation dimensionless with the equal-volume sphere $(d_B/2)$ and with the free stream velocity (v_B), and using the subscript 1 to designate a parameter as dimensionless, we obtain, after a few transformations,

$$Sh = \sqrt{\frac{2}{\pi}}\,\frac{A_s}{A}\left[\int_0^{x_{1e}} u_{10}\, r_1^2\, dx_1\right]^{1/2} \cdot Pe^{1/2} \tag{10.3-6}$$

Here, $A_s = d_B^2\,\pi$ (surface area of the equal-volume sphere), $Sh = \beta \cdot d_B/D$ and $Pe = v_B \cdot d_B/$. Eqn. (6) is identical to eqn. (4-7), since $X_1 = x_{1e}$.

11. A Comment on Surface Turbulence /103

It is well known that surface turbulence occurs whenever mass transfer leads to the formation of a layer whose surface tension is greater than that of the mixture in the liquid core (e.g. in the rectification of binary mixtures, when the component transferring to the liquid has the greatest surface tension). Since this layer is unstable, it contracts at different points and vanishes in the interior of the liquid, accompanied by the explosive surge of "fresh" liquid to the surface[1].

---

1) See also lit. [49], especially pages 44-51, where some additicnal references are cited and discussed.

The model of turbulent surface renewal used in this study is especially suitable for the description of this type of turbulence, since in this case the turbulence develops directly at the surface, and one need not wonder whether and how many "vortices" reach the interface. Here the parameter s is very closely related to the actual physical process and has a less hypothetical character than in the case of hydrodynamic turbulence. The only departure from reality is that s characterizes infinitely small eddies, while the "eruptions" at an interface are actually of a measurable magnitude. We recommend that s be determined on the basis of mass transfer experiments as a means of characterizing the intensity of surface turbulence. Such an experiment might be organized as follows:

Mass transfer would be measured in two cases for very large bubbles in steady-state rise, and $Sh/Pe^{-0.5}$ would be determined on the basis of the measurements (according to eqn. (5.2-2), $Sh/Pe^{-0.5} = \alpha^{0.5}\bar{B}$):

1.) For the case in which the identity of the surface turbulence is to be determined ($\alpha^{0.5}\bar{B}_1$);

2.) For a different case, in which no surface turbulence occurs ($\omega = 0$), but the bubble has the same shape, size and velocity of rise as before ($\alpha^{0.5}\bar{B}_2$).

If, for example, $\alpha^{0.5}\bar{B}_1$ is 40% greater than $\alpha^{0.5}\bar{B}_2$, and if the bubble is a spheroid with eccentricity b/a = 1.5, the value /104 $\bar{B} = 1.527$ taken from Diagram ② for b/a = 1.5 and $\omega = 0$ is increased by 40% and the value of ω is read at this point, from which s can then be calculated. To improve interpolation, additional curves for constant values of ω may be drawn into this diagram, based on Table ①. The advantage of this procedure is that the error in the curve for $\omega = 0$ (as compared with the more accurate solution of Lochiel and Calderbank) is largely eliminated[2].

Of course, another possible means of determining the intensity of surface turbulence would be to bring completely still gas into contact with completely still liquid for a certain period of time, determine β from mass transfer measurements, and calculate s from Danckwert's equation $\beta = \sqrt{D \cdot s}$. Whether one or both of the experiments proposed here could be performed with sufficient accuracy is another matter.

---

2) Frank [48] and especially Anderes [49] have measured the increase in mass transfer caused by surface turbulence for a number of mass systems. These measurements were made on irregular bubbles which formed at a nozzle and then rose only a short distance.

If we compare the numerical examples in Chap. 9 of the intensity of surface renewal required to produce a particular increase in mass transfer in rapidly rising bubbles (cf. esp. p. 54), we see that at points where mass transfer is markedly increased by surface turbulence (see [49]), the intensity of the surface renewal must be very high. This statement is an important qualitative result of our theory.

Summary /105

A mathematical model was formulated for heat and mass transfer in bubbles which form at a nozzle and than rise in an otherwise still liquid. The hydrodynamics of the flow were assumed to be known, and their effect as a result of combined laminar and turbulent surface renewal was taken into account. The exchange process was considered in three phases: (1) bubble formation, (2) transition period, and (3) quasi-steady state bubble rise. A mathematical solution was derived for the first and third phases on the basis of similar assumptions, and indications as to how to estimate the exchange process in the transition period were presented. In the absence of any theoretical or experimental results regarding bubble formation, with which this theory could be compared, and in view of the fact that a numerical solution would have involved complicated computer programming, solutions for rising bubbles were worked out only for the following cases: spheroids in potential flow, cylindrical bubbles rising in tubes, and large spherical cap bubbles. The calculations were carried out in dimensionless form, and the results were summarized in tables and diagrams. A comparison of these results with experimental results from the literature regarding the absorption of CO_2 bubbles in water, as well as with the theoretical solutions presented by Lochiel and Calderbank for rotationally symmetrical bodies in laminar flow, led to the following results:

1.) The influence of turbulence on the exchange process in bubbles in steady-state rise cannot be determined experimentally. It is either negligible or lies within the range of error. For this reason a theoretical consideration of turbulence would seem to be unnecessary.

2.) In agreement with the above results, it was determined by purely theoretical means that only intense turbulence will appreciably increase the mass transfer coefficient; a small degree of turbulence has practically no effect. In addition, numerical data were presented regarding the degree of surface renewal needed to achieve a particular percentage increase in the transfer coefficient for several characteristic cases. /106

3.) Based on qualitative considerations, it was concluded from the theoretical model that small, irregular interfacial fluctuations (not necessarily the result of turbulence) will likewise have no effect on mass transfer in the case of rapidly rising

bubbles. Experimental results from the literature seem to confirm this conclusion.

4.) For purely laminar flow, this theory yielded mass transfer coefficients which were 12-46% higher than the theoretical solutions of Lochiel and Calderbank in the cases investigated. Although it is not entirely clear, based on an analysis of experimental results, which theory is superior, the theory of Lochiel and Calderbank is recommended because it a) has a better physical foundation and b) is mathematically simpler.

It was determined that the proposed model is especially suitable for the description of surface turbulence, which is known to be capable of significantly increasing mass transfer. Two theoretical possibilities were suggested for determining the intensity of the surface renewal caused by surface turbulence by means of this theory.

TABLE (1): SPHEROID*)

$\overline{B}$ as a Function of ω and E

1+k	1,209	1,305	1,5	1,803	2,118	2,428	2,742
F^n	3,382	3,227	3,142	3,238	3,441	3,684	3,944
Shape							
ω \ E	1:2	1:1,5	1	1,5	2	2,5	3
0	1,055	1,192	1,349	1,527	1,645	1,720	1,772
0,1	1,059	1,196	1,352	1,530	1,648	1,723	1,775
0,2	1,071	1,187	1,362	1,539	1,657	1,731	1,784
0,5	1,154	1,262	1,430	1,601	1,717	1,791	1,844
1	1,422	1,510	1,653	1,807	1,916	1,989	2,041
1,5	1,795	1,863	1,979	2,113	2,212	2,280	2,330
2	2,223	2,276	2,370	2,483	2,571	2,634	2,681
3	3,150	3,184	3,250	3,332	3,401	3,451	3,490
4	4,113	4,138	4,187	4,250	4,306	4,346	4,378
5	5,091	5,110	5,150	5,200	5,247	5,279	5,304
10	10,05	10,05	10,07	10,10	10,13	10,14	10,14

$\overline{B} = \bar{\beta}\sqrt{\frac{d_0}{D \cdot v_0}}$ $\omega = \sqrt{\frac{s \cdot d_0}{v_0}}$ $E = b/a$ 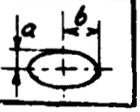

*) Commas in tabulated material are equivalent to decimal points.

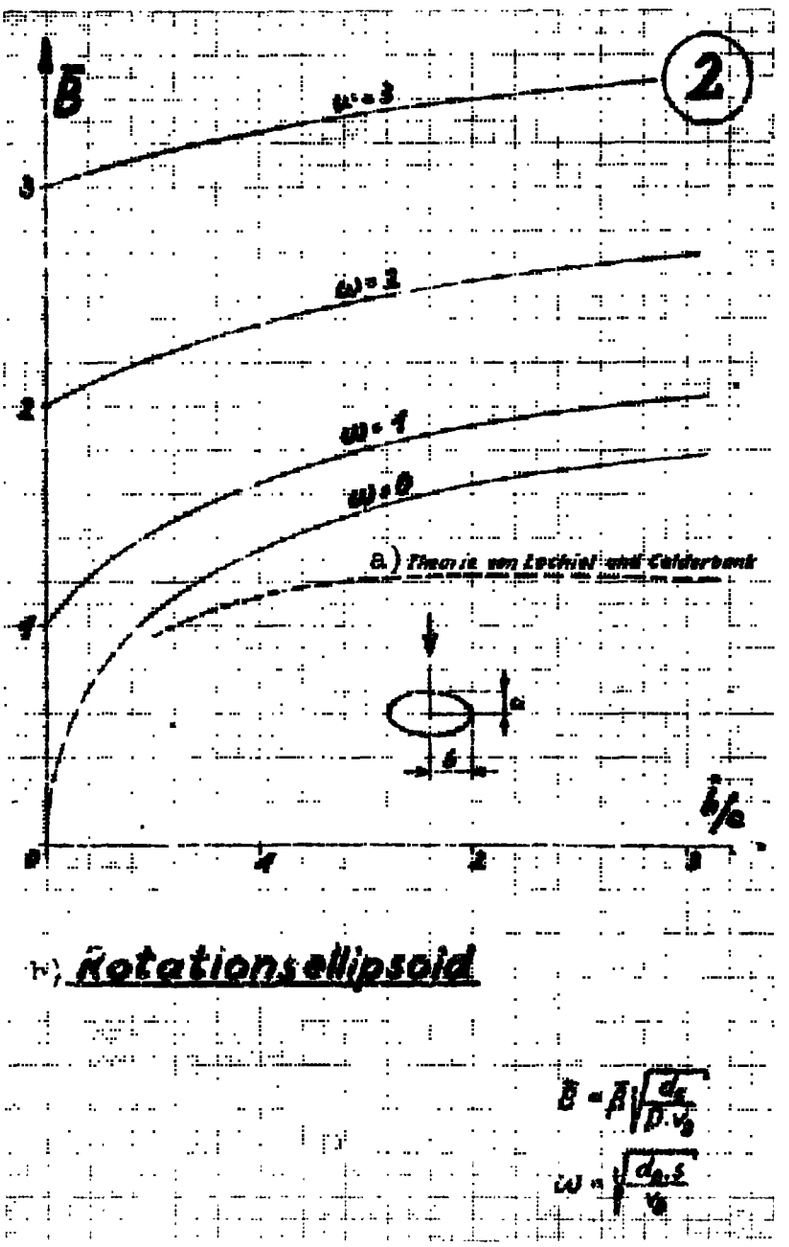

Key: a) Theory of Lochiel and Calderbank
b) Spheroid (Ellipsoid of Revolution)

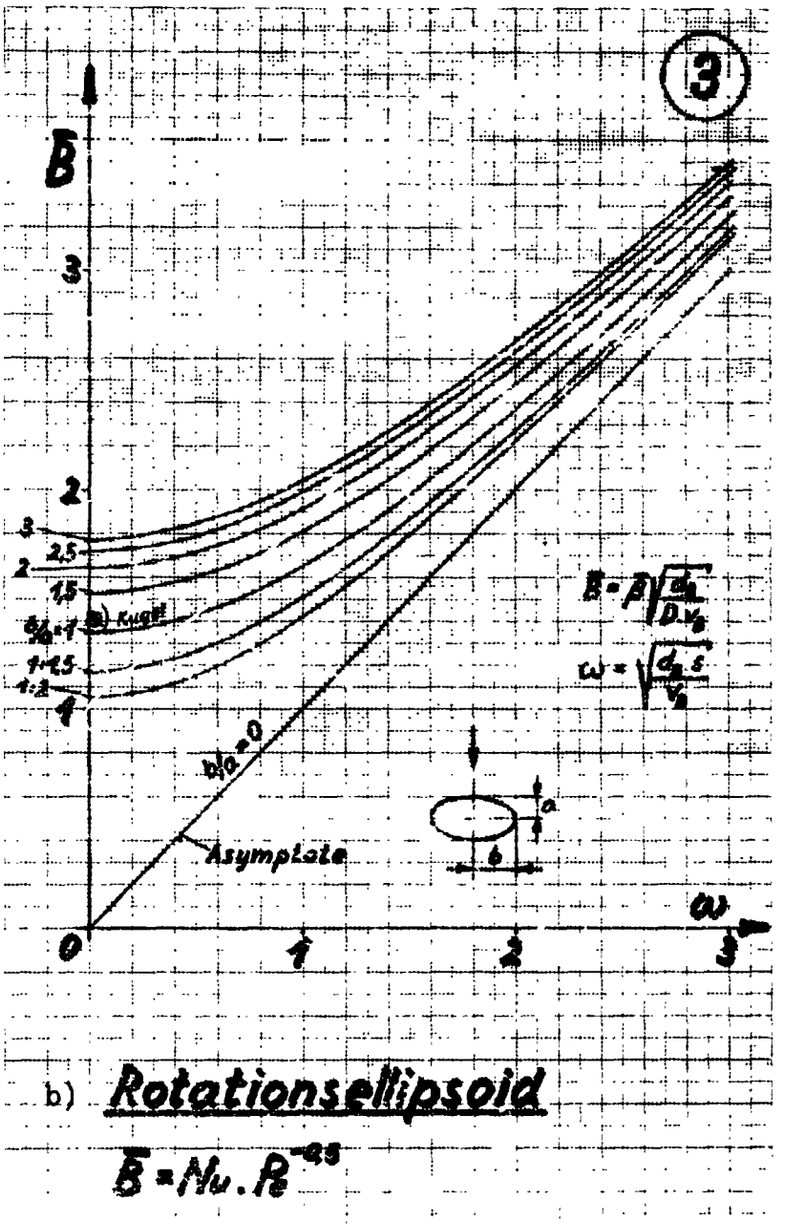

Key: a) Sphere
b) Spheroid

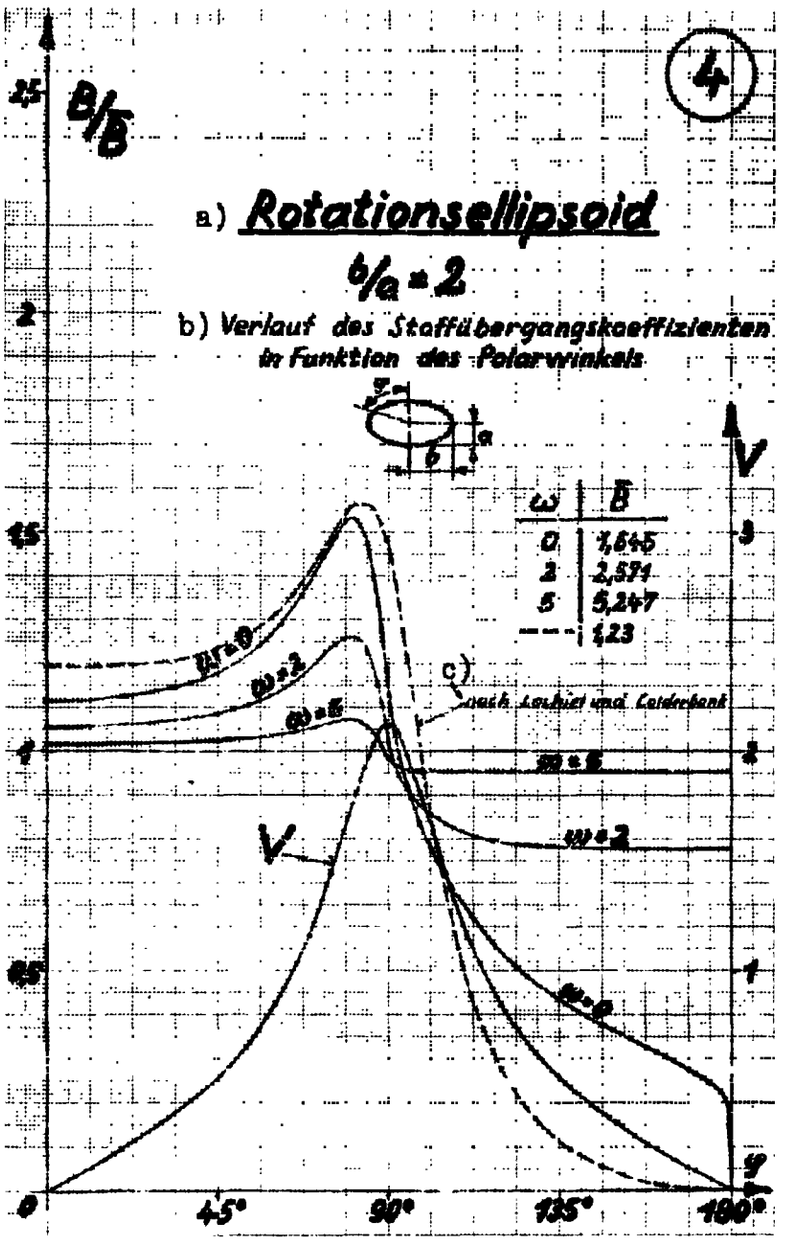

Key: a) Spheroid

b) Mass transfer coefficient as a function of polar angle

c) According to Lochiel and Calderbank

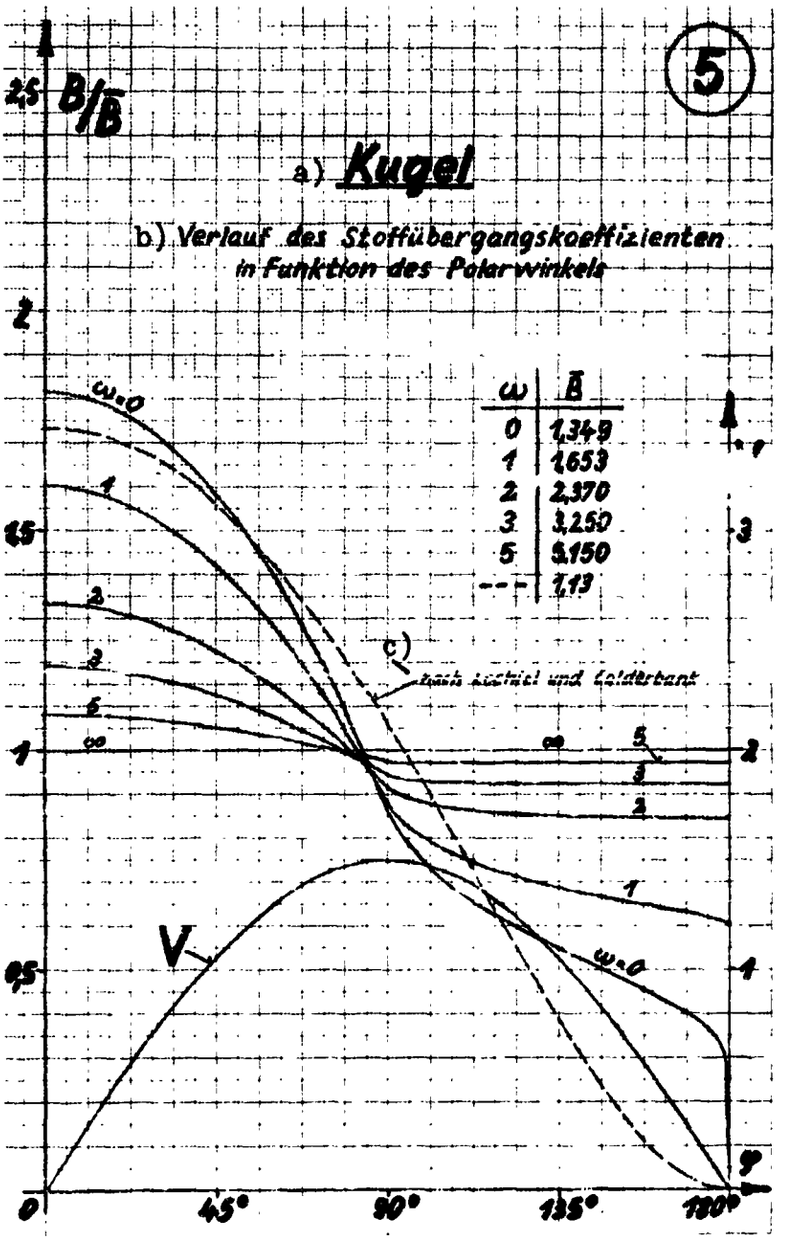

Key: a) Sphere

b) Mass transfer coefficient as a function of polar angle

c) According to Lochiel and Calderbank

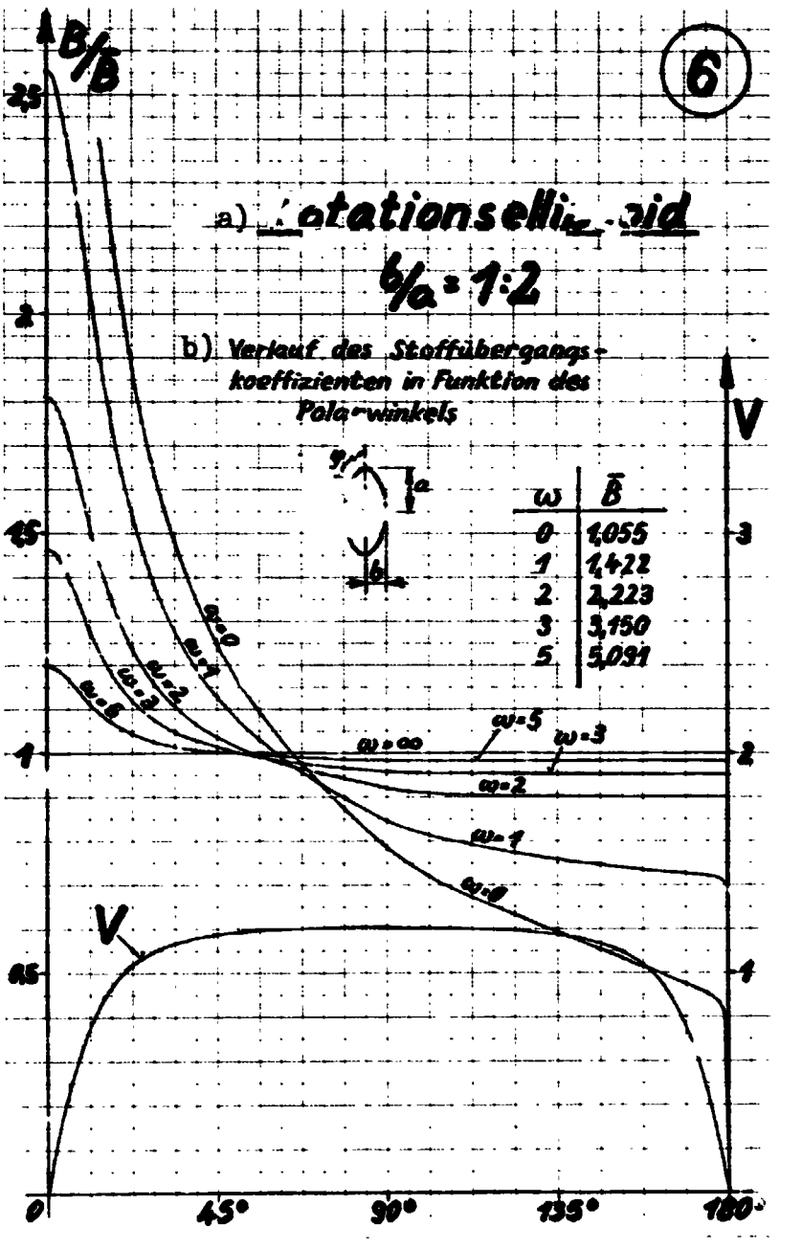

Key: a) Spheroid
b) Mass transfer coefficient as a function of polar angle

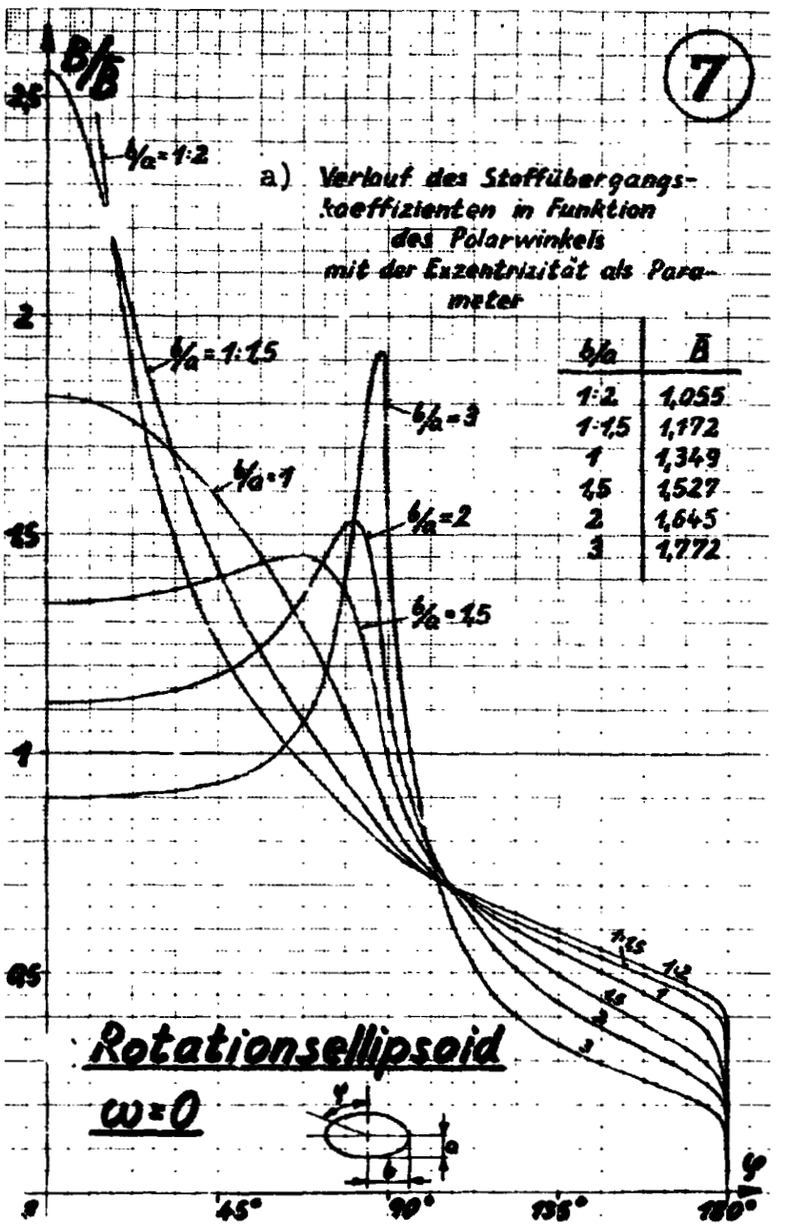

Key: a) Mass transfer coefficient as a function of polar angle with eccentricity as parameter

b) Spheroid

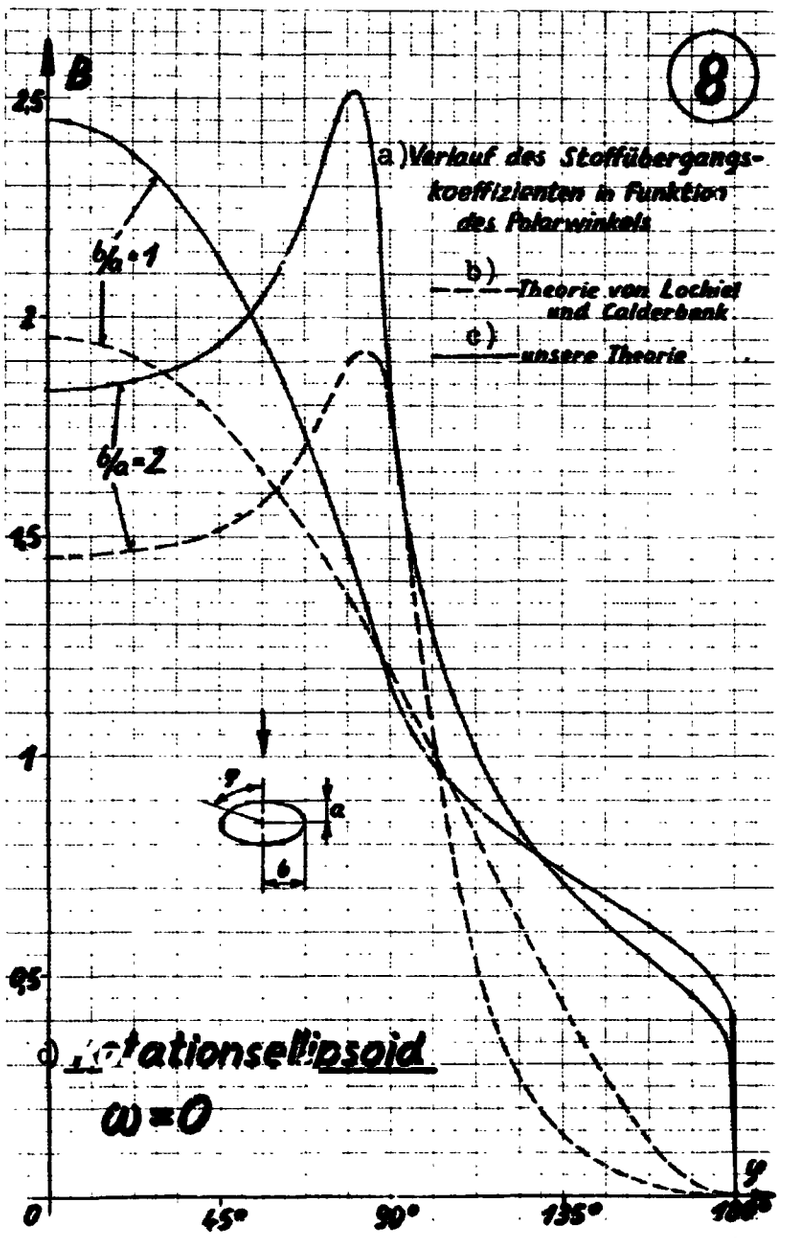

Key: a) Mass transfer coefficient as function of polar angle

b) Theory of Lochiel and Calderbank

c) Our theory

d) Spheroid

TABLE (9): SEMI-SPHEROID*)

$\overline{B}$ as a Function of ω and E

1+k	1,209	1,305	1,5	1,803	2,118	2,428	2,742
F*	1,691	1,614	1,571	1,619	1,721	1,842	1,992
ω \ E	1:2	1:1,5	1	1,5	2	2,5	3
0	1,472	1,632	1,862	2,077	2,205	2,298	2,325
0,1	1,475	1,634	1,865	2,080	2,209	2,301	2,327
0,2	1,484	1,642	1,872	2,087	2,214	2,288	2,335
0,5	1,546	1,699	1,923	2,135	2,263	2,338	2,386
1	1,752	1,889	2,097	2,301	2,428	2,506	2,558
1,5	2,060	2,178	2,363	2,554	2,679	2,758	2,813
2	2,436	2,535	2,697	2,872	2,992	3,071	3,129
3	3,296	3,367	3,489	3,632	3,738	3,814	3,872
4	4,222	4,277	4,372	4,489	4,580	4,649	4,704
5	5,178	5,222	5,299	5,396	5,474	5,536	5,588
10	10,09	10,11	10,15	10,20	10,24	10,28	10,31

$\bar{B} = \bar{\beta}\sqrt{\frac{d_B}{D \cdot v_B}}$ $\quad \omega = \sqrt{\frac{s \cdot d_B}{v_B}}$ $\quad E = b/a$ 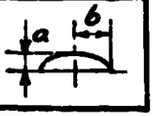

Here, d_B is the equivalent diameter of the entire spheroid.

*) Upper part; commas in the Table are equivalent to decimal points.

TABLE (10): SPHEROID*)

Transfer at Upper Half
Relative to Total Transfer:

$\bar{B}_a$:(2$\bar{B}$) as a Function of ω and E

ω \ E	1:2	1:1,5	1	1,5	2	2,5	3
0	0,698	0,696	0,690	0,680	0,670	0,662	0,656
0,1	0,696	0,695	0,690	0,680	0,670	0,662	0,655
0,2	0,693	0,692	0,687	0,678	0,668	0,661	0,654
0,5	0,690	0,693	0,680	0,667	0,659	0,653	0,647
1	0,616	0,625	0,634	0,637	0,633	0,630	0,627
1,5	0,574	0,585	0,595	0,604	0,606	0,605	0,604
2	0,548	0,557	0,569	0,578	0,582	0,583	0,584
3	0,523	0,529	0,537	0,545	0,550	0,553	0,555
4	0,513	0,517	0,522	0,528	0,532	0,535	0,537
5	0,509	0,511	0,514	0,519	0,522	0,524	0,527
10	0,502	0,503	0,504	0,505	0,505	0,507	0,508

$\bar{B}=\bar{\beta}\sqrt{\frac{d_e}{D \cdot v_e}}$ $\quad \omega=\sqrt{\frac{s \cdot d_e}{v_e}}$ $\quad E=b/a$ 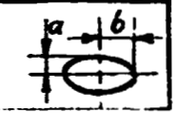

B_a is $\bar{B}$ for the upper half.

*) Commas in the Table are equivalent to decimal points.

TABLE (11) : TUBE BUBBLE*)

$\bar{B}$ as a Function of ω and 1/a

d_B^*	0,6793	0,9515	1,2870	1,5168	1,6969	1,8494
F^*	1,1647	2,5123	5,4042	8,3930	11,424	14,479
V^*	0,1641	0,4511	1,1163	1,8271	2,5582	3,301
ω \ 1/a	0,5	1	2	3	4	5
0	1,284	1,108	0,9317	0,8371	0,7758	0,7313
0,1	1,288	1,112	0,9360	0,8426	0,7816	0,7375
0,2	1,297	1,125	0,9506	0,8587	0,7989	0,7558
0,5	1,374	1,209	1,048	0,9658	0,9132	0,8758
1	1,616	1,479	1,348	1,287	1,249	1,223
1,5	1,959	1,846	1,746	1,700	1,672	1,654
2	2,361	2,267	2,188	2,153	2,131	2,117
3	3,249	3,182	3,127	3,103	3,088	3,078
4	4,189	4,138	4,096	4,077	4,066	4,059
5	5,152	5,110	5,079	5,062	5,053	5,047
10	10,077	10,055	10,039	10,031	10,027	. ..
20	20,038	20,027	20,019	20,016	20,013	20,012

$$\bar{B} = \frac{\beta}{\sqrt{D}} \sqrt[4]{\frac{a}{2g}} \qquad \omega = \sqrt{3} \sqrt[4]{\frac{a}{2g}}$$

$$d_B^* = \frac{d_B}{a} \qquad F^* = \frac{F}{a^2} \qquad V^* = \frac{V}{a^3}.$$

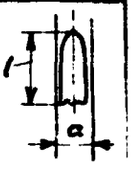

*) Commas in the Table are equivalent to decimal points.

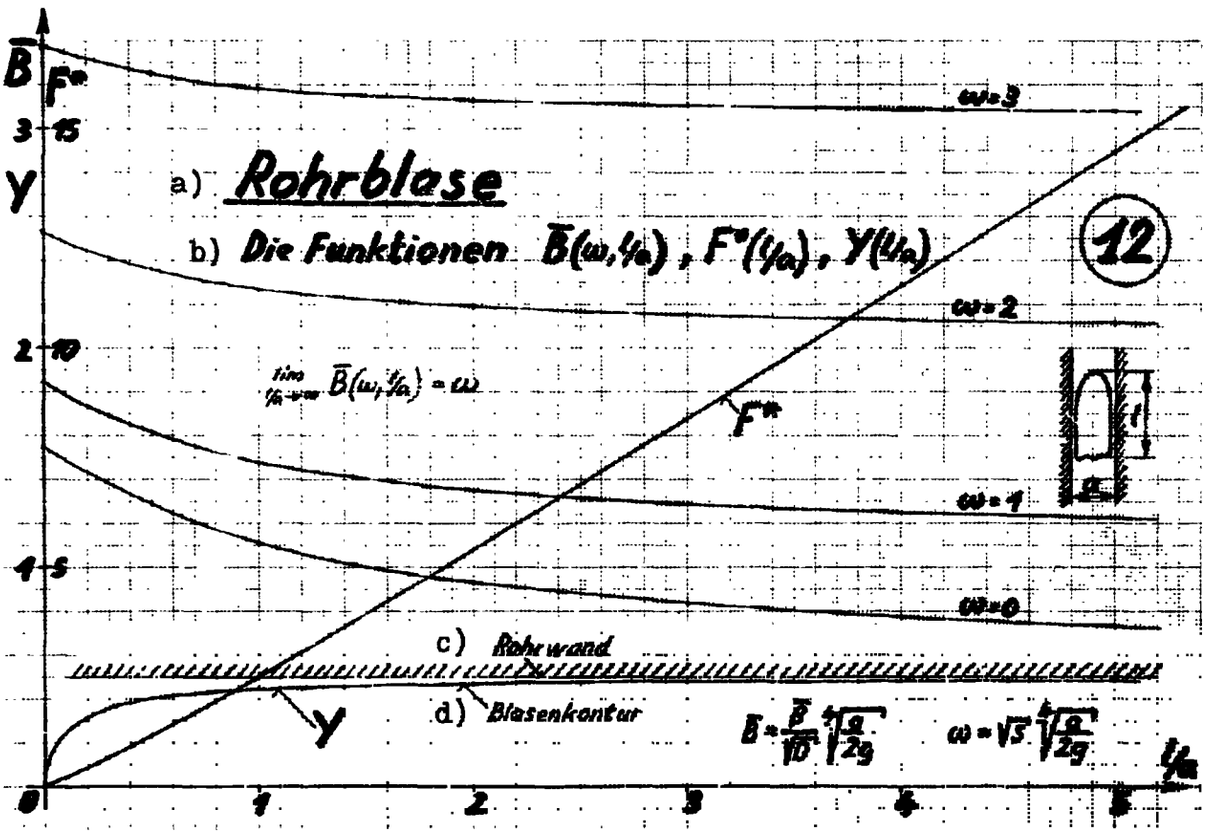

Key: a) Tube Bubble
b) The Functions $\bar{B}$(,l/a), etc.
c) Wall of tube
d) Bubble contour

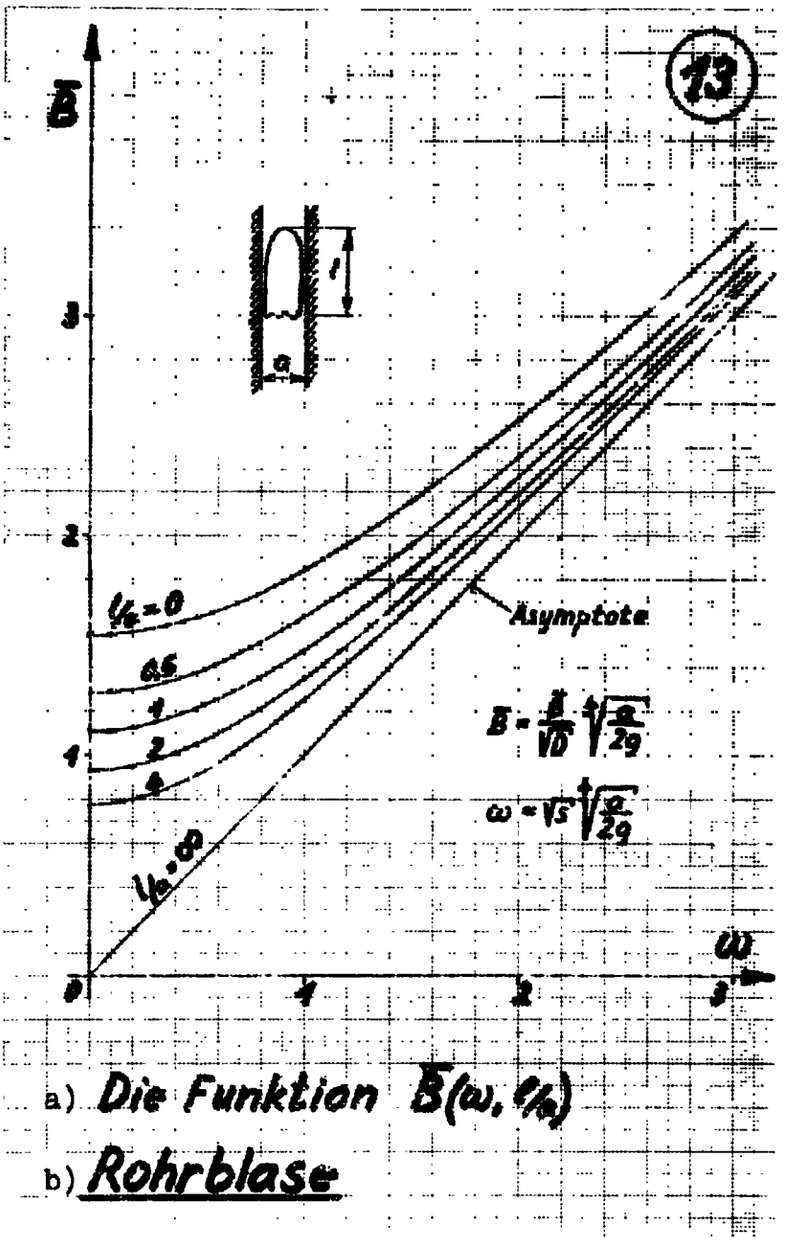

Key: a) The Function $\bar{B}(\omega, l/a)$
b) Tube Bubble

TABLE (14): TUBE BUBBLE*)

B as a Function of ω and x/a

x/a \ ω	0	0,5	1	2	3	4	5
0	1,546	1,625	1,841	2,528	3,375	4,288	5,234
0,125	1,420	1,503	1,731	2,443	3,310	4,236	5,190
0,25	1,278	1,368	1,609	2,353	3,241	4,182	5,146
0,375	1,160	1,256	1,512	2,287	3,192	4,144	5,116
0,5	1,092	1,173	1,442	2,239	3,160	4,120	5,096
0,75	0,9506	1,062	1,352	2,183	3,122	4,092	5,080
1	0,8716	0,9909	1,297	2,152	3,101	4,076	5,061
1,5	0,7921	0,9038	1,234	2,118	3,078	4,059	5,047
2	0,7096	0,8511	1,198	2,099	3,066	4,049	5,040
2,5	0,6655	0,8148	1,173	2,087	3,058	4,043	5,035
3	0,6318	0,7879	1,156	2,078	3,052	4,039	5,031
3,5	0,6053	0,7670	1,143	2,072	3,048	4,036	5,029
4	0,5833	0,7500	1,133	2,066	3,044	4,033	5,027
4,5	0,5645	0,7360	1,125	2,062	3,041	4,031	5,025
5	0,5489	0,7241	1,118	2,059	3,039	4,029	5,023

$$B = \frac{\beta}{\sqrt{D}} \sqrt[4]{\frac{a}{2g}} \qquad \omega = \sqrt{s} \sqrt[4]{\frac{a}{2g}}$$

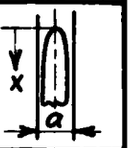

*) Commas in the Table are equivalent to decimal points.

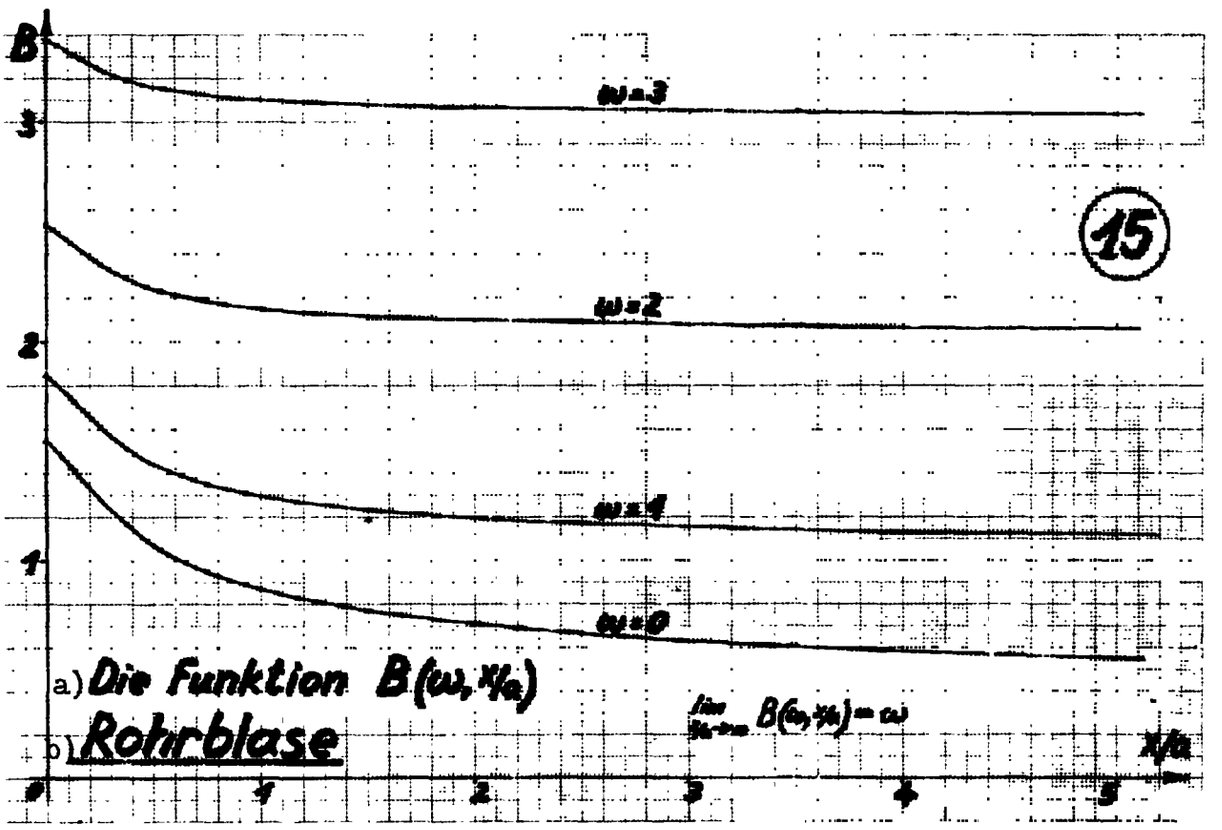

Key: a) The Function B(ω,x/a)
b) Tube Bubble

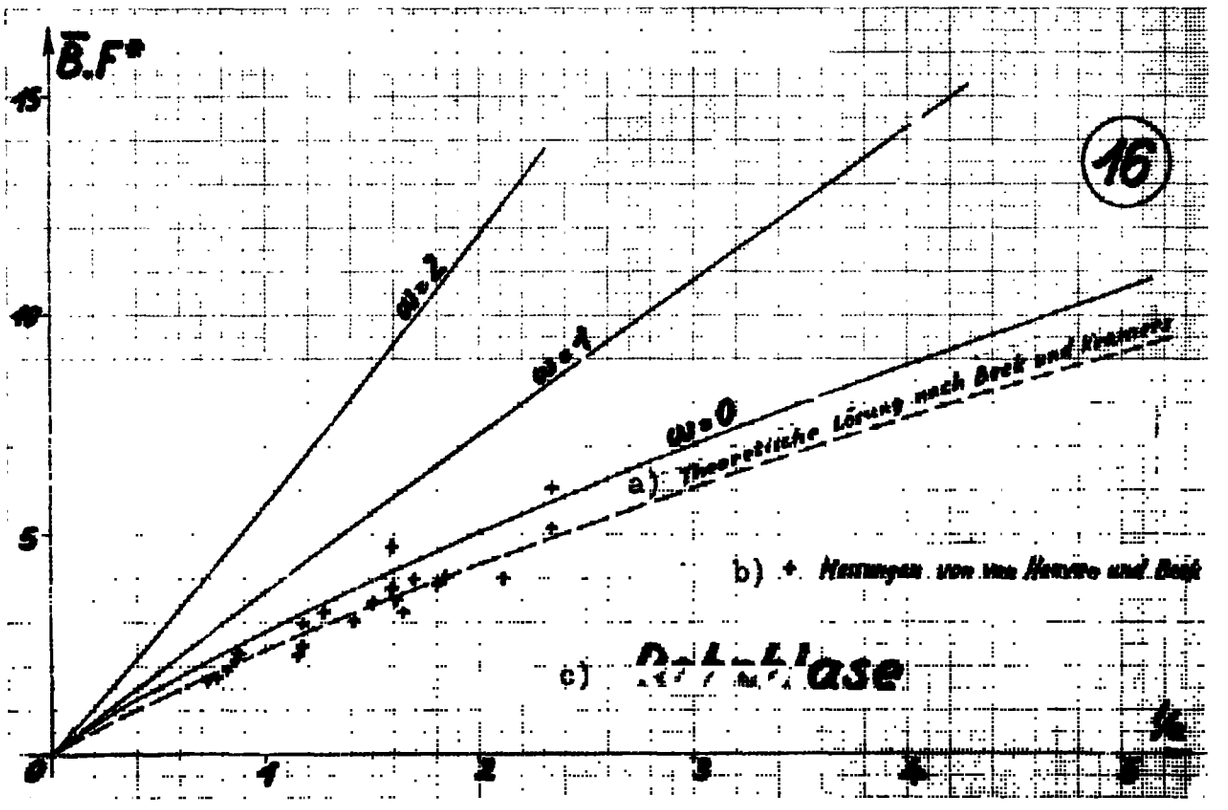

Key: a) Theoretical solution according to Beek and Kramers

b) Measurements by van Heuven and Beek

c) Tube Bubble

TABLE (17): SPHERICAL CAP*)

$\bar{B}$ as a Function of and θ

F^*	4,919	3,834	3,260	2,918	2,707
h/d_0	0,2193	0,2859	0,3484	0,4073	0,4642
r/d_0	3,603	2,134	1,489	1,140	0,9283
ω \ θ	20°	30°	40°	50°	60°
0	0,8597	0,9699	1,049	1,105	1,143
0,1	0,8635	0,9751	1,054	1,110	1,147
0,2	0,8807	0,9903	1,068	1,123	1,160
0,5	0,9926	1,091	1,162	1,212	1,246
1	1,319	1,392	1,448	1,488	1,515
1,5	1,728	1,785	1,829	1,860	1,881
2	2,176	2,222	2,257	2,282	2,298
3	3,120	3,152	3,177	3,194	3,206
4	4,091	4,115	4,134	4,148	4,156
5	5,073	5,093	5,108	5,119	5,126
10	10,037	10,047	10,054	10,060	10,063
20	20,018	20,023	20,027	20,030	20,032

$$\bar{B} = \frac{\beta}{\sqrt{D}} \sqrt[4]{\frac{d_0}{2g}} \qquad F^* = F/d_0^2 \qquad \omega = \sqrt{s} \cdot \sqrt[4]{\frac{d_0}{2g}}$$

*) Commas in the Table are equivalent to decimal points

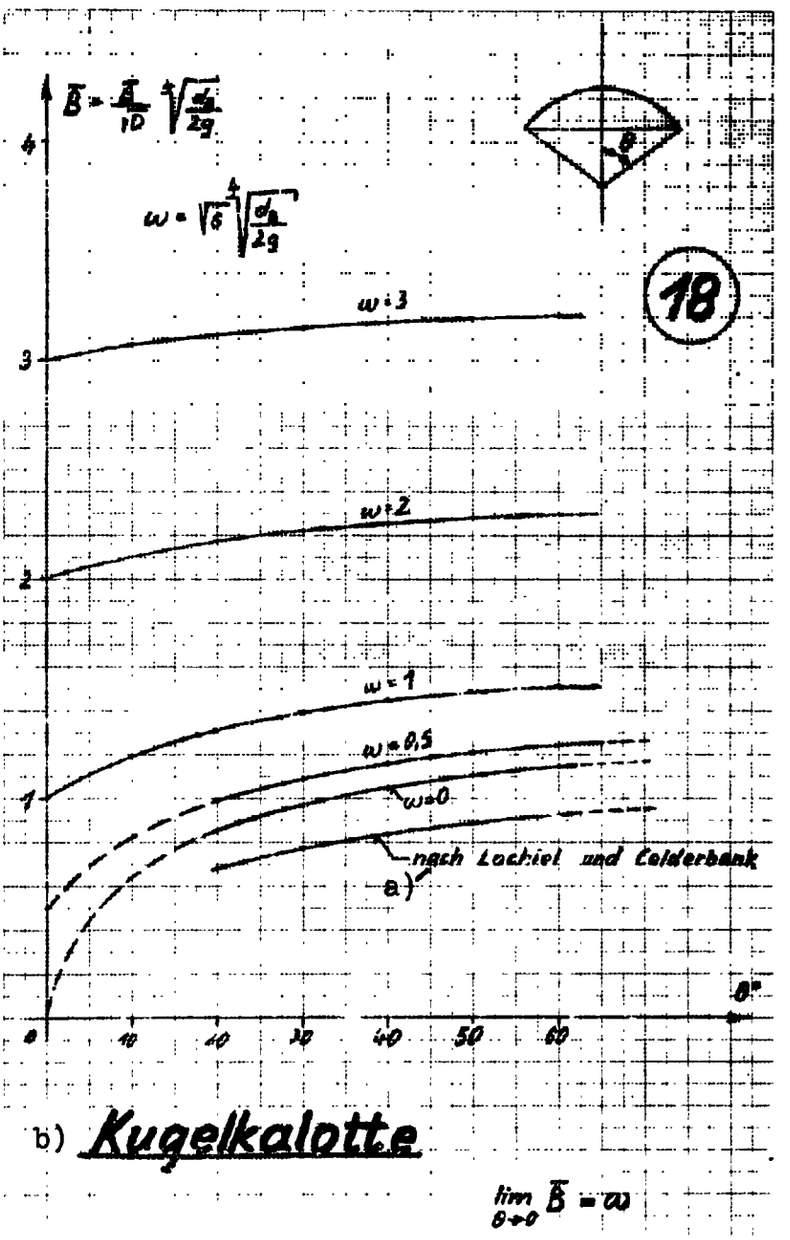

Key: a) Acc. to Lochiel and Calderbank

b) Spherical Cap

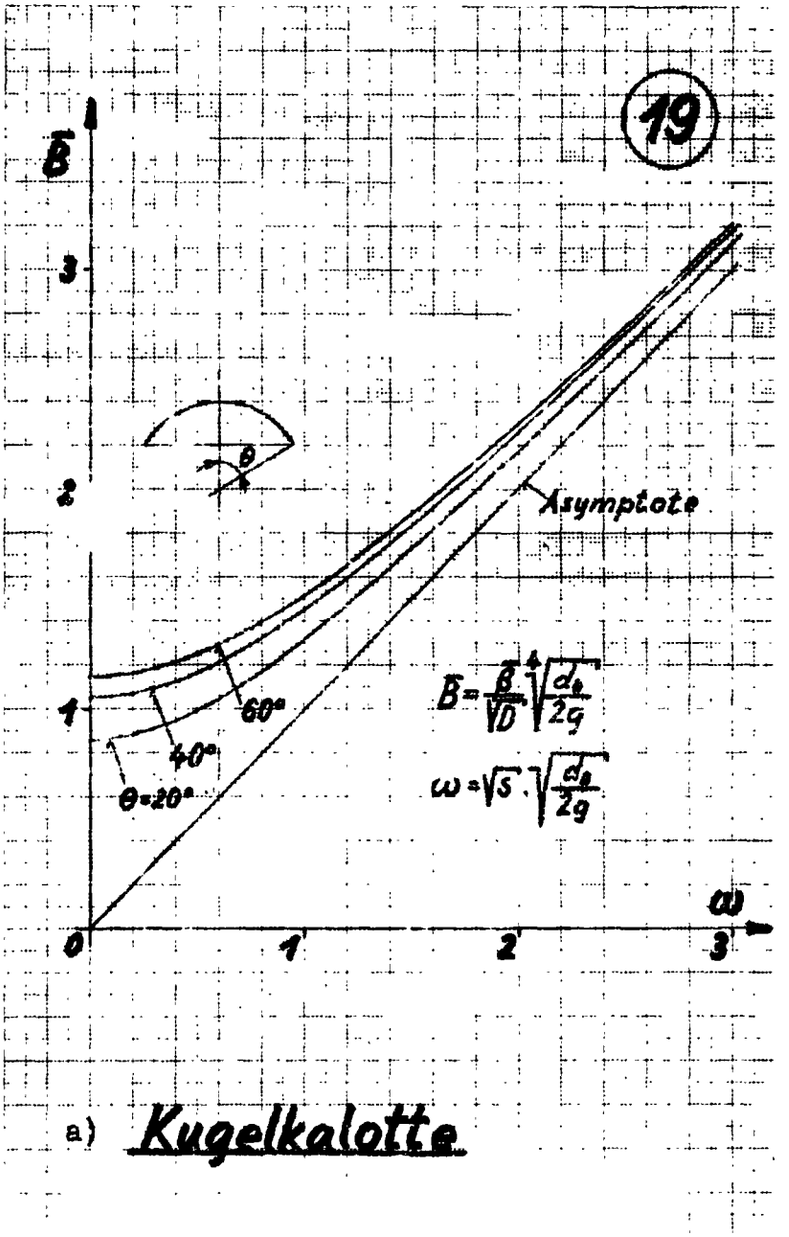

Key: a) Spherical Cap

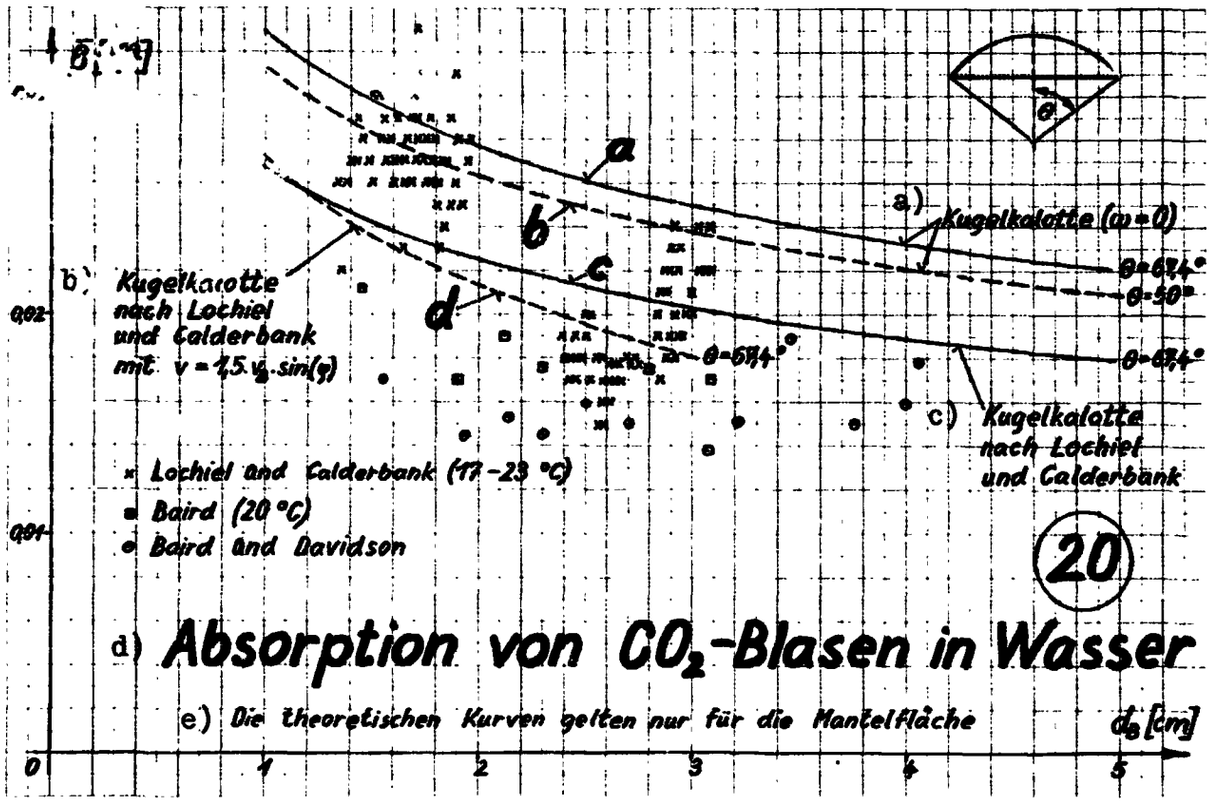

Key:
a) Spherical cap
b) Spherical cap according to Lochiel and Calderbank with $v = 1.5 \cdot v_B \cdot \sin(\varphi)$
c) Spherical cap according to Lochiel and Calderbank
d) Absorption of CO_2 bubbles in Water
e) The theoretical curves are valid only for the front surface.

REFERENCES

1. Davis, R. M. and Taylor, G. J., "The Mechanics of Large Bubbles Rising Through Extended Liquids and Through Liquids in Tubes," Proc. Roy. Soc., A200, 375 (1950).

2. Baird, M. H. J. and Davidson, J. F., "Gas Absorption by Large Rising Bubbles," Chem. Eng. Sci., 17, 87-93 (1962).

3. Valentin, F. H. H., "Absorption in Gas-Liquid Dispersions. Some Aspects of Bubble Technology, E. & F. N. Spon Ltd., London, 1967, p. 16.

3a. Ibid, Chap. 4.

4. Grassmann, P., Physikalische Grundlagen der Chemie-Ingenieur-Technik [Physical Foundations of Chemical Engineering Technology], H. R. Sauerlaender & Co., Aarau/Frankfurt am Main, § 10.11 and § 10.12.

4a. Ibid., § 10.13.

5. Collins, R., "A Second Approximation for the Velocity of a Large Gas Bubble Rising in an Infinite Liquid," J. Fluid Mech., 25, 469 (1966).

6. Collins, R., "Structure and Behaviour of Wakes Behind Two-Dimensional Air Bubbles in Water," Chem. Eng. Sci., 20, 851 (1965).

7. Calderbank, P. H. and Lochiel, A. C., "Mass Transfer Coefficients, Velocities and Shapes of Carbon Dioxide Bubbles in Free Rise Through Distilled Water," Chem. Eng. Sci, 19, 485-503 (1964).

8. Baird, M. H. J., Ph.D. Thesis, University of Cambridge, 1960.

9. Tadaki, T. and Maeda, S., "On the Shape and Velocity of Single Air Bubbles Rising in Various Liquids," Chem. Eng. Japan, 4, 254-264 (1961).

10. Hammerton, D. and Garner, F. H., "Gas Absorption from Single Bubbles," Trans. Instn. Chem. Engrs., 32, supplement (1954).

11. Ward, D. M., Trass, O. and Johnson, A. J., "Mass Transfer From Fluid and Solid Spheres at Low Reynold Numbers," Can. Jour. of Chem. Eng., 164-168 (August 1962).

12. Leonard, J. H. and Houghton, G., "Mass Transfer and Velocity of Rise Phenomena for Single Bubbles," Chem. Eng. Sci., 18, 133-142 (1963).

13. van Heuven, Y. W. and Beek, W. J., "Gas Absorption in Narrow Gas Lifts," Chem. Eng. Sci., 18, 377-390 (1963).

14. Dumitrescu, D. T., "Streamline Flow About an Air Bubble in a Vertical Tube " [in German], Z. angew. Math. Mech., 23, 139-149 (1943).

15. White, E. T. and Beardmore, R. H., "The Velocity of Rise of Single Cylindrical Air Bubbles Through Liquids Contained in Vertical Tubes," Chem. Eng. Sci., 17, 351-361 (1962).

16. Kouremenos, D., "On the Streamline Flow of Single Cylindrical Gas Bubbles Rising in Vertical Tubes" [in German], Ph.D. Thesis no. 3939, Eidgenoessische Technische Hochschule, Zurich, 1966.

17. Zukoski, E. E., "Influence of Viscosity, Surface Tension and Inclination Angle on Motion of Long Bubbles in Closed Tubes," J. Fluid Mechanics 25/4, 821-837 (1966).

18. Beek, W. J. and Kramers, H., "Mass Transfer with Change in Interfacial Area," Chem. Eng. Sci., 16, 909-921 (1962).

19. Lochiel, A. C. and Calderbank, P. H., "Mass Transfer in the Continuous Phase Around Axisymmetric Bodies of Revolution," Chem. Eng. Sci., 19, 471-484 (1964).

20. Siemes, W., "Gas Bubbles in Liquids; Part II: The Rise of Gas Bubbles in Liquids" [in German], Chem. Ing. Techn., 26, 614-630 (1954).

21. Spalding, D. B., Connective Mass Transfer, Edward Arnold Pub. Ltd., London, 1963, p. 139.

22. L'Ecuyer, M. R. and Murthy, S. N. B., "Energy Transfer from a Liquid to a Gas Bubble Forming at a Submerged Orifice," NASA TN D-2547.

23. Dobbins, W. E., "BOD and Oxygen Relationships in Streams," J. San. Engng. Div., Proc. A.S.C.E., 90, SA 3, 53, 1964.

24. Levich, V. G., Physicochemical Hydrodynamics, Chap. XII, § 135 136, Prentice Hall, Engelwood Cliffs, N.Y., 1962.

25. Danckwerts, P. V., "Significance of Liquid-Film Coefficient in Gas Absorption," Ind. Eng. Chem., 43, 1460 (1951).

26. Toor, H. L. and Marchello, J. M., "Film Penetration Model for Mass and Heat Transfer," A. J. Ch. E. Jour., 4, 97 (1958).

27. Harriott, P., "A Random Eddy Modification of the Penetration Theory," 17, 149 (1962).

28. Ruckenstein, E., "A Note Concerning Turbulent Exchange of Heat or Mass with a Boundary," Chem. Eng. Sci., 7, 265 (1958).

29. Ruckenstein, E., Chem. Eng. Sci., 18, 233 (1963).

30. King, C. J., "Turbulent Liquid Phase Mass Transfer at a Free Gas-Liquid Interface," Ind. Eng. Chem. Fundamentals, 5, 1 (1966).

31. Dobbins, W. E., Biological Treatment of Sewage and Industrial Wastes, Reinhold Pub. Corp., New York, N.Y., 1956, p. 141.

32. Hanratty, T. J., "Turbulent Exchange of Mass and Momentun with a Boundary," A. I. Ch. E. Jour., 2, 359 (1956).

33. Zahm, A. F., "Flow and Drag Formulas for Simple Quadrics," Report 253, Nat. Advis. Comm. for Aeronautics, Washington, 517, 1926.

34. Sideman, S. and Shabtai, H., "Direct Contact Heat Transfer Between a Single Drop and an Immiscible Liquid Medium," The Canadian Jour. of Chem. Eng., 107 (June 1964).

35. Conkie, W. R. and Savic, P., "Calculation of the Influence of Internal Circulation in a Liquid Drop on Heat Transfer and Drag," Report No. MT-23, Nat. Res. Council of Canada, Ottawa, 22 October 1953.

36. Griffith, R. M., "Mass Transfer from Drops and Bubbles," Chem. Eng. Sci., 12, 198 (1960).

37. L. M. Milne-Thomson, Theoretical Hydrohynamics, The MacMillan Company, N. Y., 1960, p. 554.

38. Chao, B. T., "Motion of Spherical Gas Bubbles in a Viscous Liquid at Large Reynolds Numbers," The Physics of Fluids 5/1, 69 (1962).

39. Hadamard, J., "Mouvement permanent lent d'une sphere liquide et visqueuse dans un liquide visqueux," C. R. Acad. Sci. Paris, 152, 1735 (1911).

40. Rybczynski, W., "On the Advancing Movement of a Liquid Sphere in a Viscous Medium" [in German], Bull. Int. Acad. Sci. Cracovie, 40-46, 1911.

41. Boussinesq, J., J. Math., 6, 285 (1905).

42. Griffith, R. M., "The Effect of Surfactants on the Terminal Velocity of Drops and Bubbles," Chem. Eng. Sci., 17, 1057, (1962).

43. Savic, P., Rep. No. MT-22, Division of Mech. Engng., Nat. Research Council of Canada, 31 July 1953.

44. Geddes, A. P., Trans. A. I. Ch. E., 42, 79 (1946).

45. Bowman, C. W., Wand, D. M., Johnson, A. I. and Trass, O., "Mass Transfer from Fluid and Solid Spheres at Low Reynolds Numbers," Canad. Jour. of Chem. Eng., 39, 9 (1961).

46. Schulte-Vieting, H. J., "Heat and Mass Transfer Between Steam Bubbles and Liquid in Oxygen-Nitrogen Mixtures" [in German], Dissertation, Frankfurt am Main, 1954; excerpt in Chem. Eng. Techn., 27, 507-512 (1955).

47. Grossmann, U., Dissertation ETH No. 2396 (1955); excerpt in Chem. Ing. Tech., 28, 107 (1956).

48. Frank, A., "Heat and Mass Transfer Between a Steam Bubble and Liquid in N_2-O_2 Mixtures" [in German], Dissertation ETH No. 2827 (1958).

49. Anderes, G., "The Dependence of Mass Transfer Between Steam Bubbles and Liquid on the Direction of Transfer and the Properties of the Liquid" [in German], Dissertation ETH No. 3101 (1960).

50. Wyss, E., "Determination of Heat and Mass Transfer Between a Steam Bubble and Liquid for Water vs. Water Vapor + Inert Gases" [in German], Dissertation ETH No. 3234 (1962).

51. Lochiel, A. C., Ph.D. Thesis, University of Edinburgh, 1963.

52. Higbie, R., "The Rate of Absorption of a Pure Gas into a Still Liquid During Short Periods of Exposure," Trans. Am. Inst. Chem. Engrs., 31, 365 (1935).

53. Pritchard, C. L. and Biswas, S. K., "Mass Transfer from Drops in Forced Convection," British Chem. Engng., 12, 879-885 (1967).

54. Teiriki Tadaki and Siro Maeda, "Some Considerations on Surface Renewal Theory," Chem. Eng. Japan, 2, 233-237 (1964).

55. Siemens, W., "Gas Bubbles in Liquids; Part I: The Formation of Gas Bubbles at an Upward-Directed Orifice" [in German], Chem. Ing. Techn., 26, 479-496 (1954).

ABOUT THE AUTHOR

3 October 1934	born in Budapest
1941-1949	attended public school in Hungary
1949-1953	attended humanistic Gymnasium in Budapest
	final examination 1953
1953-1956	student, Department of Mechanical Engineering of the Technische Hochschule, Budapest
1957-1959	student, Dept. of Mechanical Engineering of the Eidgenoessische Technische Hochschule, Zurich
Jan 1960-Feb 1964	research engineer at the hydrodynamics laboratory of the Brown Boveri Co., Baden
	Oct 1962-July 1963 leave of absence for advanced studies in applied mechanics at the Imperial College of Science and Technology in London, leading to the academic title D. I. C.
Feb 1964-May 1966	assistent to Prof. O. Zweifel, ETH, chair for apparatus in transportation and construction engineering
May 1966-present	assistent to Prof. Dr. P. Grassmann, ETH, Institute for Caloric Apparatus, Low-Temperature Technology and Research Techniques.